A Koiter-Newton arclength method for buckling-sensitive structures

A Koiter-Newton arclength method for buckling-sensitive structures

Proefschrift

ter verkrijging van de graad van doctor
aan de Technische Universiteit Delft,
op gezag van de Rector Magnificus Prof.dr.ir. K.C.A.M. Luyben,
voorzitter van het College voor Promoties,
in het openbaar te verdedigen op vrijdag 19 july 2013 om 10.00 uur

door

Ke Liang

Bachelor of Aircraft Design Engineering,
Northwestern Polytechnical University, Xi'an, China
geboren te Luoyang, China.

Dit proefschrift is goedgekeurd door de promotoren:
Prof.dr. Z. Gürdal

Copromotor: Dr. M.M. Abdalla

Samenstelling promotiecommissie:

Rector Magnificus:	voorzitter
Prof. dr. Z. Gürdal	Technische Universiteit Delft, promotor
Dr. M.M. Abdalla	Technische Universiteit Delft, copromotor
Prof. dr. ir. M.J.L. van Tooren	Technische Universiteit Delft
Prof. dr. A.V. Metrikine	Technische Universiteit Delft
Prof. dr. V.V. Toropov	University of Leeds
Prof. dr. V.V. Vasiliev	Russian Academy of Sciences
Prof. dr. Q. Sun	Northwestern Polytechnical University

Keywords: Buckling/Imperfection/Geometric Nonlinearity/Path-following/
Koiter-Newton Approach/Reduced Order Model/Finite Elements.

ISBN 978-94-6203-387-0

Printed by: Wöhrmann Print Service, Zutphen, the Netherlands

Dedicated to my parents and Xiaxia

Forewords

I have worked as a Ph.D. researcher in the Department of Aerospace Structures and Computational Mechanics at Faculty of Aerospace Engineering, TUDelft for a period of three years. At the completion of this thesis, first, I would like to thank my promoter Prof.dr. Z. Gürdal who provided me with patient guidance and unflinching encouragement during my research. Even now, I remember the first email that I sent to him to apply to become, if possible, a guest Ph.D researcher in his group and his warm response. Then, many thanks to my daily supervisor Dr. Mostafa Abdalla, who offered me constructive advices and timely critiques on my work and also constantly encourage me to conduct my research independently.

I would also like to thank my supervisor Prof. Sun Qin in China. He taught me how to become a researcher when I started my Ph.D study, and additionally he has continued to provide valuable support to me during my time abroad. I would like to thank the China Scholarship Council, for giving me a one-year scholarship. The research leading to these results has also received funding from the European Communitys Seventh Framework Programme ([FP7/2007-2013]) under grant agreement $n^0$282522. Thank yous to my DESICOS project partners, Prof. Richard.Degenhardt (from DLR), Dr. Mark.W.Hilburger (from NASA) and the others, all of whom have given me many suggestions and advices, that have improved my research work.

Many thanks to Ir. Jan Hol, Dr. Roeland De Breuker, Dr. Martin Ruess and Dr. Christos Kassapoglou, good partners for any project. Thanks to Laura, who gave me so much help on the administrative issues and kept me sane. I also want to thank Miranda Aldham-Breary for teaching me a pure English and reviewing the text carefully. Thanks to Ir. Daniël Peeters and Dr. Roeland De Breuker for translating some parts of my thesis into Dutch. My last, but not least thanks to all of my office colleagues. It has been a great pleasure working with so many helpful and nice colleagues in the AeS group. During my studies at Delft, I have been very lucky to make many good friends. Thank you all for lighting up my life here.

Moreover, I thank all the committee members for kindly agreeing to devote time and effort in judging and giving precious opinions to this thesis.

Finally, this thesis is specially dedicated to my parents and my love Xiaxia Shen for their unconditional love. Without their support, I could not have come this far.

Summary

Thin-walled structures, when properly designed, possess a high strength-to-weight and stiffness-to-weight ratio, and therefore are used as the primary components in some weight critical structural applications, such as aerospace and marine engineering. These structures are prone to be limited in their load carrying capability by buckling, while staying in the linear elastic range of the material. Buckling of thin-walled structures is an inherently nonlinear phenomena. When the material stays within its linear elastic range, the source of the nonlinearity is purely geometric. Thus, the analysis of nonlinear response of structures, especially thin-walled structures which are buckling sensitive, is important for determining their load carrying capability. For this reason, structural geometric nonlinearities are increasingly taken into account in engineering design. Nowadays, with the expanding computational power of modern computers nonlinear finite element analysis using commercial software is becoming the standard technique used to obtain the nonlinear response of complex structures, however, the repeated analyses that are needed in the design phase are still computationally intensive, in terms of the computation time required to run large models, even for modern computers. For this reason, reduced order techniques that reduce the problem size are attractive whenever repetitive analyses are required, such as in design optimization.

Research on reduced order modeling of the nonlinear response of structures has attracted much attention from researchers. Some analytic techniques constitute very powerful tools for reducing the number of degrees of freedom (DOFs) in a nonlinear system, such as the Rayleigh-Ritz techniques and perturbation techniques. These two reduced basis techniques can be implemented in both analytical and numerical contexts, and due to the modeling versatility of the finite element method (FEM), most researchers prefer to reconstruct them within the FEM context, referred to as reduction methods. There are two families of reduction methods which can be recognized. The first family consists the path-following reduction methods which are based on some analytic techniques to reduce the number of DOFs in the full model and are able to trace the entire nonlinear equilibrium path of structures automatically, while they may find difficulties in the presence of buckling. Koiter reduction methods belong to the second family, and they are very good at handling the buckling sensitive cases due to the use of Koiter's classical initial postbuckling theory, but the Koiter perturbation approach also limits the validity of these methods to a small range around the bifurcation point. The focus of the research reported in this thesis therefore is to find ways to synthesize the advantages of current reduction methods and obtain a new reduced basis path-following approach.

In this thesis, a new approach called the Koiter-Newton (K-N) is presented for the

numerical solution of a class of elastic nonlinear structural analysis problems. The method combines ideas from Koiter's initial post-buckling analysis and Newton arc-length methods to obtain an algorithm that is accurate over the entire equilibrium path of structures and efficient in the presence of buckling and/or imperfection sensitivity.

The proposed approach is performed in a step by step manner to trace the entire equilibrium path, as is commonly used in the classical Newton arc-length method. In every expansion step, the approach works by combining a prediction step using a nonlinear reduced order model (ROM) based on Koiter's initial postbuckling expansion with a Newton arc-length correction procedure. This nonlinear prediction provided by the reduced order model is much better compared to linear predictors used by the classical Newton-Raphson method, thus allowing the algorithm to use fairly large step sizes.

The basic premise behind the proposed approach is the use of Koiter's asymptotic expansion from the beginning rather than using it only at the bifurcation point in contrast to the traditional Koiter approaches. In each asymptotic expansion, the force space is reduced by the span of a set of perturbation loads that are chosen to excite the possible buckling branches. According to the stability of the equilibrium point, at which the asymptotic expansion is applied, different ways for selecting the perturbation loads are proposed. The proposed selection rules guarantee that the expansion step of the proposed approach can be applied at any point along the equilibrium path.

The proposed technique requires derivatives of the element load vectors with respect to the degrees of freedom up to the third order. This is two orders more than what is traditionally needed for Newton's method. To facilitate differentiation, nonlinear elements based on the element independent co-rotational frame are applied in the Koiter-Newton analysis. Automatic differentiation is used to find the derivatives of the co-rotational frame with respect to element degrees of freedom. In this way, full nonlinear kinematics are taken into account when constructing the reduced order model.

In some cases, the nonlinear in-plane rotations of structures can be neglected, although the rotations of the normals to the mid-surface are finite. In such cases, Von Kármán kinematics, which ignore some nonlinear items in the Green's stain-displacement relations, possess an acceptable accuracy compared with the full nonlinear kinematics. Hence, the Koiter-Newton approach is also implemented based on Von Kármán kinematics to achieve a better computational efficiency.

Various numerical examples of beam and shell models are presented and used to

evaluate the performance of the method. The Koiter-Newton analyses using the co-rotational kinematics and the Von Kármán kinematics are accurate and more computational efficient, compared with the results obtained using ABAQUS which adopts a full nonlinear analysis. The improved efficiency demonstrated by the Koiter-Newton technique will open the door to the direct use of detailed nonlinear finite element models in the design optimization of next generation flight and launch vehicles.

Samenvatting

Dunwandige structuren hebben een hoge sterkte-gewicht en stijfheid-gewicht verhouding als ze goed ontworpen zijn en worden daarom gebruikt als primaire constructies in bepaalde gewicht-kritische toepassingen zoals lucht-en ruimtevaart of zeevaart technologie. Deze structuren zijn beperkt in hun krachtdragende capaciteit door knik terwijl het materiaal nog in het linear-elastische bereik is. Knik van dunwandige structuren is een inherent niet-lineair fenomeen. Als het materiaal binnen zijn lineair-elastische gebied blijft, is de bron van de niet-lineariteit puur geometrisch. De analyse van niet-lineaire structuren is dus belangrijk om hun krachtdragende capaciteit te berekenen, zeker bij dunwandige structuren, die knikgevoelig zijn. Dit is de reden dat er meer en meer rekening gehouden wordt met structureel geometrische niet-lineariteit. Door de steeds toenemende rekenkracht van moderne computers worden niet-lineaire eindige elementen analyses tegenwoordig de standaardtechniek om de niet-lineaire respons van complexe structuren te berekenen. Echter, de hoeveelheid analyses die nodig zijn in de ontwerpfase zijn erg rekenintensief voor grote structuren en vragen dus veel tijd, zelfs op moderne computers. Hierdoor zijn lagereorde technieken die de grootte van het probleem reduceren erg aantrekkelijk wanneer meerdere analyses nodig zijn, zoals in ontwerpoptimalisatie.

Het lagere-orde modelleren van de niet-lineaire respons van structuren is al vaak onderzocht. Sommige analytische technieken vormen erg krachtige manieren om het aantal vrijheidsgraden in een niet-lineair systeem te reduceren, zoals Rayleigh-Ritz en perturbatietechnieken. Deze twee basistechnieken kunnen zowel in een analytische als in een numerieke context geïmplementeerd worden, en door de flexibiliteit die de eindige elementen methode biedt, verkiezen de meeste onderzoekers om ze te implementeren in de eindige elementen context. Hieraan wordt gerefereerd als reductiemethodes. Er kunnen twee soorten reductiemethodes onderscheiden worden. De eerste soort bestaat uit de evenwichtspadtracerende reductiemethodes die gebaseerd zijn op analystische technieken om het aantal vrijheidsgraden in een volledig model te reduceren en in staat zijn om automatisch het volledige niet-lineaire evenwichtspad van de structuur te bepalen, terwijl ze soms falen bij knikverschijnselen. Koiter reduceermethodes behoren tot de tweede soort en zijn erg goed in het berekenen van knikgevoelige structuren door het gebruik van Koiter's klassieke initiële postknik theorie. Maar de Koiter perturbatiemethode limiteert de geldigheid van deze methodes tot een kleine omgeving rond het vertakkingspunt. De focus van het onderzoek in deze thesis ligt daarom op het vinden van manieren om de voordelen van de huidige reduceermethodes te combineren en het vinden van een nieuwe evenwichtspadtracerende reductiemethode.

In deze thesis is een nieuwe methode voor het numeriek oplossen van een klasse

van niet-lineaire structurele analyse problemen geponeerd. Deze methode wordt Koiter-Newton (K-N) genoemd. De methode combineert ideen van Koiter's initiële post-knik analyse en Newton's booglengte methode om een algoritme te bekomen dat accuraat is over het hele evenwichtspad van de structuren en efficient is als knik en/of imperfectiegevoeiligheid aanwezig zijn.

Het hele evenwichtspad wordt stap voor stap gereconstrueerd, zoals het gewoonlijk wordt gedaan in de klassieke Newton booglengte methode. Voor elke nieuwe stap is er een voorspellende stap, die gebruik maakt van het niet-lineaire lagere-orde model gebaseerd op Koiter's initiële post-knik expansie, en die gevolgd wordt door een Newton booglengte correctie. Deze niet-lineaire voorspelling door het lagere-orde model is veel beter vergeleken met lineaire voorspellers gebruikt in de klassieke Newton-Raphson methode en laat het algoritme dus toe een redelijk grote stapgrootte te gebruiken.

De basis van de voorgestelde methode is het gebruik van Koiter's asymptotische expansie van in het begin, dit in tegenstelling tot de klassieke Koiter methode waarbij het enkel wordt gebruikt bij het vertakkingspunt. In iedere asymptotische expansie is de kracht-ruimte gereduceerd door een set van kleine krachten die mogelijk knikvormen kunnen veroorzaken. Volgens de stabiliteit van het evenwichtspunt, waar de asymptotische expansie is toegepast, zijn er verschillende manieren voorgesteld om die kleine krachten te selecteren. De voorgestelde selectieprocedures garanderen dat de uitbreidingsstap van de voorgestelde methode toegepast kan worden op elk punt langs het evenwichtspad.

De voorgestelde techniek heeft de eerste, tweede en derde afgeleides van de krachtenvectoren van elk elementent naar de vrijheidsgraden nodig. Dit zijn twee afgeleides meer dan wat normaal nodig is voor Newton's methode. Om de afleiding te vereenvoudigen zijn niet-lineaire elementen gebaseerd op het elementonafhankelijke meedraaiende referentiekader toegepast in de Koiter-Newton analyse. Om de afgeleides van het meedraaiende referentiekader naar de vrijheidsgraden te vinden is automatische afleiding gebruikt. Op deze manier is rekening gehouden met volledige niet-lineaire kinematica terwijl het lagere-orde model wordt opgesteld.

In bepaalde gevallen kunnen de niet-lineaire rotaties in het vlak van de structuur genegeerd worden, ook al zijn de verdraaiingen van de loodrechten tot het middenoppervlak eindig. In deze gevallen heeft de Von Krmn kinematica, die sommige niet-lineaire delen in de rekrelaties van Green negeert, een aanvaardbare nauwkeurigheid. Daarom is de Koiter-Newton methode ook gemplementeerd gebaseerd op de Von Krmn kinematica om een betere rekenefficintie te bereiken.

Verschillende numerieke voorbeelden van balk en schaal-modellen zijn beschreven en

gebruikt om de prestaties van de methode te evalueren. De Koiter-Newton analyse die gebruik maakt van de co-rotationele kinematica en de Von Krmn kinematica is nauwkeurig en efficinter qua rekentijd vergeleken met de resultaten van ABAQUS die een volledige niet-lineaire analyse gebruikt. De verbeterde efficintie aangetoond door de Koiter-Newton techniek zal het mogelijk maken om direct gebruik te maken van gedetailleerde niet-lineaire eindige elementen modellen in de optimalisatie van de volgende generatie vlieg- en lanceervoertuigen.

Contents

List of Figures

List of Tables

Chapter 1

Introduction

1.1 Background and motivation

Nonlinear static analysis of structures is an essential step of the design of flight vehicles and is important for many practical situations, for example, it is crucial to carry out a nonlinear static analysis when the displacements and/or rotations of a structure that is being designed are large. Even more important for flight vehicles is the case where a structure, or some of its components, are prone to buckling.

Thin-walled structures which constitute the main structural components for the bodies of flight vehicles are prone to static buckling instabilities due to their favorable strength-to-weight ratio together with their slenderness. The form of such structures often makes buckling strength the key design criterion of a design process [1], and often, at the onset of buckling, the stress level remains much lower than the yield stress. In many cases, it is crucial to assess the load carrying capability of a structure at which buckling occurs as well as the behavior of the structure beyond that buckling point. In addition, many shell type structures exhibit unstable post-buckling behavior and are highly sensitive to geometric or load imperfections [2, 3]. In the presence of buckling, such structures may exhibit high out-of-plane displacements, compared to wall thickness, which cause geometrically nonlinear structural responses. Therefore, geometrically nonlinear analysis of new structures during the design process is essential for this class of structures to obtain realistic modeling of the engineered and product [4].

Chapter 1

In recent years, nonlinear structural analysis of static and dynamic problems has become the focus of research efforts [5]. This is largely due to the emphasis placed by manufactures and contractors on realistic modeling and accurate analysis of critical structures [6]. Traditionally, there have been two major approaches to this problem. One is to use the finite element (FE) method based incremental-iterative procedures. This is the most popular technique used in industrial and research applications. Nowadays, the size of the detailed finite element model used by customers and companies is steadily growing, and the nonlinearities of the structural behavior are increasingly taken into account even in the early stages of the design. In spite of recent advances in computer hardware and the significant increases in the speed and capacity of present-day computers, the repeated solution in time of large nonlinear system of equations stemming from a FE discretization to reproduce the nonlinear behavior of a general structure is still a computationally heavy task [7, 8]. For this reason, approach two which is an asymptotic method that can significantly reduce the number of degrees of freedom using some classical analytic or semi-analytic techniques has begun to attract more attention from researchers working in the field of nonlinear structural analysis.

Some analytic techniques, such as the Rayleigh-Ritz technique and the perturbation technique, can be used to reduce the number of degrees of freedom in an analysis. The deformation modes of various components are described in terms of simple analytic functions resulting in a small system of nonlinear equations to be solved. Moreover, exact bifurcation analysis is usually easy to perform including initial post-buckling analysis. Initial post-buckling analysis describes the behavior of the structure in the immediate vicinity of the buckling point. As such it is invaluable in its ability to provide the analyst with a quick qualitative assessment of the post-buckling behavior of a structure. As to be expected, the semi-analytic approach is orders of magnitude faster than nonlinear finite element analysis. This is demonstrated by the following quote, taken from a recent design study: "The efficiency of ...[semi-analytic] analysis methods and models permits global optimization of a stiffened panel concept for less computer time than typically required for a single non-linear finite element analysis." However, analytic or semi-analytic methods are only applicable for simple geometries and more often than not simplified boundary conditions and loading.

The challenge is to synthesize the best aspects of both approaches. It is desirable to discretize fairly general structures in a finite element environment while at the same time greatly reducing the computational effort to make it viable for optimization purposes. In the nonlinear structural analysis, most of the reduction methods that have been proposed are hybrid procedures which combine contemporary finite element method and classical asymptotic method.

In the recent years two main families of reduction methods implemented in a finite element environment have been recognized. The first family consists of reduction methods that work in combination with path-following techniques. Through the updating of the basis vectors and correcting the results these methods can be used to trace the nonlinear structural equilibrium path automatically. The selection of basis vectors is critical and the accuracy of the method is sensitive to this selection. In addition, these methods often use path derivatives in the expansion, which causes difficulties near the bifurcation points. For this reason these methods may not be suitable for handling some buckling sensitive cases.

Another family of reduction methods is based on Koiter's celebrated initial post-buckling theory and numerically performs Koiter's asymptotic expansion at the bifurcation point. Recently, work at the Aerospace Structures group at Delft University of Technology [7, 8] has focused on the development of this kind of physics-based reduced order models. Several orders of magnitude reduction in model size is possible using this approach. The method has been implemented in a finite element environment and applied to moderately complex structures, unstiffened shells and stiffened panels, and is currently available in an open-loop format. The model is reduced and the validity of the reduced model is found only in a small range near the bifurcation point. There is no further link between the original finite element model and the reduced order model. Thus, the range of validity of the approximate model needs to be assessed by comparing it to a full finite element analysis. This situation greatly limits the applicability of the new approach.

To achieve greater applicability, a combination of Koiter's analysis and the Newton arc-length method is proposed in this thesis [9]. In this Koiter-Newton approach, a reduced order model (ROM) is constructed based on Koiter's theory in every step, which is used to make an initial nonlinear prediction of the response of the structure. Compared with traditional Newton methods which use the linear prediction, a larger step size can be achieved using the Koiter-Newton approach due to this better nonlinear prediction provided by the ROM, see Fig. 1.1. In addition, this nonlinear prediction can also detect and trace the buckling branch accurately in the presence of buckling, as shown in Fig. 1.1. The exact unbalanced force residual at the new predicted point is calculated using the full finite element model. Then in a corrector phase, this residual is driven to zero in a manner similar to that used in traditional Newton arc-length methods. This correction procedure can be presented by the small red arrow in Fig. 1.1. As the solution proceeds to higher and higher load levels, the quality of the ROM are assessed, based on the norm of force residuals, and if needed the ROM is updated to reflect changes in structural stiffness and load distribution. The proposed approach can trace the entire nonlinear equilibrium path based on the reduction method automatically and will significantly improve the efficiency of nonlinear static finite element analysis by incorporating informa-

tion from Koiter's analysis while retaining the complete generality usually associated with finite element modeling. This improved efficiency will open the door for the direct use of detailed nonlinear finite element models in the design optimization of next generation flight and launch vehicles [10, 11]. The basic characteristics of the current proposed Koiter-Newton approach are shown in Fig. 1.2.

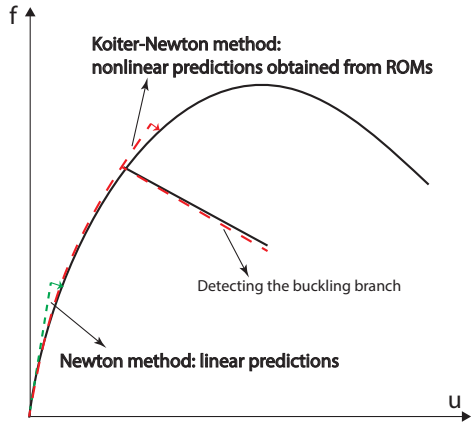

Figure 1.1: Path-following strategy of the Koiter-Newton approach, compared with Newton methods

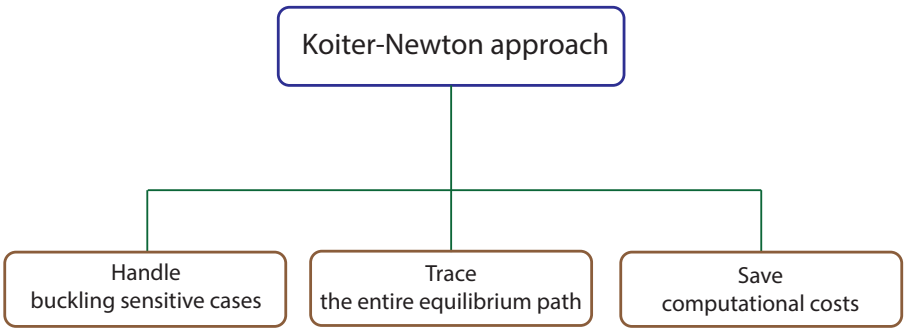

Figure 1.2: Basic characteristics of the proposed Koiter-Newton approach

In recent years, a lot of effort has been made by several research groups to apply asymptotic techniques in finite element context for nonlinear structural analysis, and this will be discussed, along with some involved specific issues, in the following section. Based on this discussion, the research objectives for the present research

will be formulated in the subsequent section.

1.2 Literature review

A brief review of the relevant literature of interest for the research presented in this thesis work is presented in this section with the reduction methods for nonlinear structural analysis forming the focal point of the discussion. The three main topics dealt with in this section, are: path-following techniques in buckling analysis, path-following reduction methods and Koiter reduction methods. Comparison of the current reduction methods is also discussed.

1.2.1 Path-following techniques in buckling analysis

It is necessary to obtain the nonlinear relationship between the applied loads and the structural responses in engineering. Once the nonlinear response curve of a structure is plotted, the buckling point can be easily achieved from the curve, and then the load carrying capability is gained. The buckling points in nonlinear structural elasticity can be classified into limit points λ_c and bifurcation points λ_s [12], as shown in Fig. 1.3. For limit points, whether they belong to a snap-through type or a snap-back type [13], the path-following scheme to compute the regular equilibrium points successively on the equilibrium path are sufficient for the computational stability analysis. For bifurcation points, a branch detection technique can be used for switching into the postbuckling path of a structure [12].

To trace the equilibrium path and also obtain the buckling characteristics of a structure, many researchers [14, 15] have tried to use some analytical techniques to do the geometrically nonlinear analysis. While, for the structures with complicated geometries and boundary conditions, analytical methods face difficulties to gain the solutions of these nonlinear system of equations. To solve these difficulties many numerical solutions have been proposed for such nonlinear system of equations by researchers [16, 17, 18]. Nowadays, nonlinear equilibrium equations of structures are usually solved by using the traditional Newton-Raphson method together with an incremental/iterative solution technique [19, 20]. While, this method is computationally very expensive in the case of nonlinear analysis of the structures with complex and serious nonlinear behavior. In addition, the Newton-Raphson method always diverges when passing the limit points of a structure. The reason is that

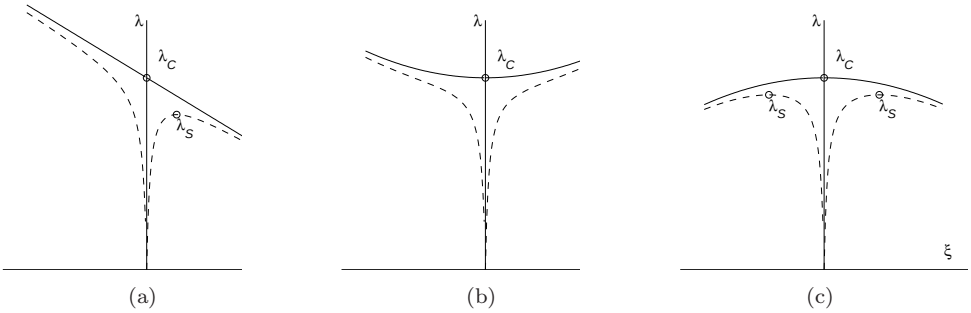

Figure 1.3: Koiter's theory: load-deflection curves [7]. (a) non-symmetric structure (b) symmetric stable (c) symmetric unstable

a simple load control or displacement control will fail if the nonlinear response of a structure exists both the snap-through and snap-back phenomenons. In order to trace the equilibrium paths through all types of limit points in the response, the arc-length methods proposed by Riks [21, 22],Wempner [23] or Crisfield [24] are commonly employed. In the arc-length methods, an auxiliary constraint equation is applied together with the general Newton-Raphson iteration during solving the equilibrium equations. Considerable research [25, 26, 27] has been done to set up such an auxiliary constraint equation, and different similar methods have been derived from the different choices of this auxiliary equation. In these methods, both the displacement and the load are controlled during the iterations, hence these arc-length based methods are possible to pass the limit points with snap-through or snap-back. While, in the case of highly nonlinear behavior state, they still suffer from passing the limit points of structures. Based on the arc-length methods, the normal flow algorithm appeared in the literature as early as 1981, by Georg [28]. In Ragon and Gürdal's paper [19], they compared the relative efficiencies of the Riks/Wempner, Crisfield, and normal flow solution algorithms for tracking nonlinear equilibrium paths of structures, and found that the normal flow algorithm performs better when dealing with the severe nonlinearities of structures. It has been verified that this algorithm has advantages in terms of computational efficiency and numerical robustness [12, 29, 30, 31], and it is now a well known in numerical analysis.

1.2.2 Path-following reduction methods

A nonlinear finite element analysis based on the path-following technique is still not economically feasible for large complex structures with thousands of degrees of

freedom despite the capabilities of present day computers. Hence, the application of a hybrid approach which can combines contemporary finite elements and classical analytic approximations has attracted more attentions [32, 33, 34, 35, 36]. The techniques for reducing the degrees of freedom in a FE environment are referred to as reduction methods. Such a global-local approach can preserve the modeling versatility inherent in the FE method and also reduce the number of degrees of freedom using some classic approximations [35].

As discussed in section 1.1, there are two main families of reduction methods. The first family consists of reduction methods that work in combination with path-following techniques. Another family of reduction methods is based on Koiter's celebrated initial post-buckling theory. In this subsection, the first family of reduction methods, the path-following reduction methods, will be discussed. Through updating the reduced order model and correcting the results, these methods can be used to trace the nonlinear structural equilibrium path automatically.

Actually, a nonlinear system of equilibrium equations can be used to present the nonlinear response of a discretized structure. Then, a reduced nonlinear system of equations with considerably fewer unknowns is constructed using some asymptotic techniques to replace the original equilibrium equations of the structure [37]. The Rayleigh-Ritz and perturbation techniques are two major asymptotic techniques used to reduce the number of degrees of freedom in a nonlinear analysis. The Rayleigh-Ritz technique expresses the displacement using a linear combination of global approximation functions or basis vectors, while the perturbation technique uses power series with respect to a certain parameter to express the displacement. According to the different asymptotic techniques adopted for reducing the number of degrees of freedom in the finite element model, the path-following reduction methods can be classified as Rayleigh-Ritz reduced path-following methods [38, 39, 35, 40] and perturbation reduced path-following methods [41, 42].

As discussed above, in the Rayleigh-Ritz reduced path-following methods, the deformation of a structure is presented by some known modes, such as basis vectors or global RayleighRitz approximation functions, and the number of these known modes is usually much smaller than the total number of degrees of freedom of the original FE model [37]. Hence, the effectiveness of the reduction method depends largely on the proper selection of these basis vectors such that their combination may give the correct deformation of the structure, and the ease with which they can be generated without incurring a large amount of computational overhead. For this purpose, various choices for approximation functions were proposed in the literature. Similar to the modal superposition technique, Nagy [38] selected the first few buckling modes to represent the prebuckling nonlinear behavior of structures. The first linear and subsequent nonlinear solution vectors at consecutive steps were adopted by Almroth

et al. [39]. Noor et al. [35] chose a nonlinear solution and its path derivatives of ascending order commonly used in the static perturbation technique as the basis vectors. Recently Chan and Hsiao [40] have considered nonlinear solutions and the correction vectors generated during a nonlinear iteration step for this purpose. In their work, an implicit reduction technique is proposed where only the displacement corrections are evaluated in the reduced system while the residual forces are calculated in the full system as usual, thus enabling the method to be applicable to materially and geometrically nonlinear problems. For Rayleigh-Ritz reduced path-following methods, the selection of basis vectors is crucial and the accuracy of these methods are very sensitive to this selection. In addition, the path derivatives [35] are often applied in the expansion as the basis vectors, and it will make the algorithm divergent near the bifurcation/limit points. Hence, these methods may not be suitable for handling some buckling sensitive cases.

The perturbation reduced path-following methods are generated based on the analytical perturbation techniques [43, 44, 45, 46, 47]. For these methods, the nonlinear branch is expanded in the form of power series with respect to a path parameter. The principle of these methods is to determine some terms of the series by solving a recursive set of linear problems which yields an approximate analytical representation of the solution branch. A perturbation technique is also a good means to use to build up an efficient Ritz basis to be used in a Ritz reduction technique, as proposed and tested by Noor and Peters [35]. In order to settle the difficulty of computing more than the first few terms of the series, due to the growing complexity of the problems to be solved, Damil and Potier-Ferry [48, 49] have proposed an asymptotic-numerical method which permits one to compute a large number of terms of a perturbation series using very classical programming techniques and little computational time. They considered the bifurcation branches in their original algorithm [41] which is based on the asymptotic numerical method (ANM) and Padé approximants by giving two choices for the control parameter a (Signorini expansion and bifurcation-type expansion). Based on this method, Azrar [50, 41] has obtained the post-buckling branch of elastic plates and shells. Cochenlin [42] has extended it to any generic nonlinear solution branch, and showed that with a proper choice of the perturbation parameter the series have a finite radius of convergence which is not necessarily small. Based on Potier-Ferry's works Boutyour [51] detected the bifurcation point using two manners. One manner is to analyze the poles of the Padé approximants, and another one is to evaluate a bifurcation indicator which is well adapted to ANM along the computed solution branch. In addition, there are many other very relevant possibilities for choices of path parameters, see Lopez [52] and especially Mottaqi et al [53]. For the current perturbation reduced path-following methods, in the case of buckling, the expansion parameter needs to be changed to trace the buckling branches. Hence, it is not convenient for the current perturbation reduced path-following methods to achieve automations in the presence of buckling.

1.2.3 Koiter reduction methods

The Koiter reduction methods are based on a specific perturbation technique, Koiter's perturbation technique, to reduce the number of degrees of freedom in the finite element model. The main advantage of Koiter's theory [43] is that it can provide a quick and accurate enough description of the buckling capability and also the initial postbuckling behavior of a structure. The postbuckling coefficients obtained by Koiter perturbation expansion are used to describe the buckling characteristics of the structure. In addition, when the buckling loads are very close, the interactions of these closely spaced buckling modes can be easily taken into account using Koiter perturbation method. Based on the closely spaced buckling modes and using the postbuckling coefficients, a reduced nonlinear system of equations is constructed at the bifurcation point to approximate the initial postbuckling path of the structure. For the imperfection analysis, the effect of geometrical imperfections can easily be introduced and results in a force term that can be added to the already constructed reduced order model of the perfect structure.

For many yeas, Koiter's theory has been regarded to be only suitable in analytical and semi-analytical contexts, and many relevant work [54, 55, 56, 57, 58, 59, 60] has been done to obtain the stability behavior of a structure only for academic interest. Recently, considerable research efforts have been put into finding a proper implementation of Koiter's work in an FE context [7, 8]. In the beginning, Gallagher [61] outlined some difficulties involved in the finite element implementation of Koiter's perturbation approach. Obtaining the b coefficient with a good accuracy and convergence is a key issue in the FE implementation. Many researchers [62, 63, 64, 65, 66, 67] have tried to find a suitable kinematic model that can be used to obtain good accuracy and convergence for the b coefficient. Antman [62] has proposed a consistent kinematical model which shows an extremely fast convergence in the determination of the initial postbuckling coefficients. Later, a geometrically exact beam based on Antman's [62] kinematical model was proposed by Pacoste [64] to obtain an accurate b coefficient. In addition, a bad convergence of the b coefficient will cause a locking phenomena in the implementation of the perturbation approach into the finite element context. This locking phenomena is due to the fact that the components of the in-plane displacement are interpolated to a lower degree than the components of the out-of-plane [7]. This causes inaccurate calculation of postbuckling response and consequently it gives rise to an extremely slow convergence of the post-buckling curvature b. Olesen and Byskov [68, 69], and Poulsen and Damkilde [70] respectively used Lagrange multipliers and a local stress contribution to tackle this problem. Research done by Garcea [67] has shown that the elements based on the co-rotational (CR) formulation can settle these problems very well, and some numerical examples of beam and shell models have been used to verify this

viewpoint.

The Koiter reduction methods are based on Koiter's perturbation technique and Koiter's asymptotic expansion is used only once at the bifurcation point. Hence, the perturbation approach used in this research is valid asymptotically in the neighborhood of the starting point of the perturbation expansion. In most of the research work, the expansion of the displacement field is up to the second order which is often enough to capture the initial postbuckling response of structures. Damil and Potier-Ferry [48] have tried to adopt higher order terms to increase the range of validity of the perturbation expansion further. Increasing the order terms of the displacement should obtain a wider range of validity. Yet, the reduced order model obtained by a single perturbation expansion still has a limited range of validity that cannot be determined a priori.

Koiter's theory is often used to handle problems characterized by bifurcation type buckling. The Koiter reduction methods discussed above only consider bifurcation type buckling. Problems with the limit type buckling, such as snap through and snap back, were initially considered by Haftka et al. [71] and later by Carnoy [72] and Salerno et al. [73]. In their work, they assumed there is a bifurcation point in a fictitious perfect structure and an intrinsic imperfection is applied to predict the behavior of the real structure. Using some numerical examples, it demonstrates that this approach worked well with some beam structures but not with the same level of success for the case of shell structures. In Carnoy's [72] paper, some measures have been proposed to improve the application in shells.

The interactions of the closely spaced buckling modes may degrade the load carrying capacity of a structure, and buckling modes being stable in isolation may exhibit an unstable postbuckling behavior and imperfection sensitivity when they are subject to modal interaction, hence a multi mode study is very important in the buckling analysis. Thin-walled structures are the most classical engineering applications that exhibit many close bifurcation points near the lowest critical load, and some research work has found that the number of closely spaced buckling modes is greater if the structure is thinner. In the early time, Koiter [74, 75] considered the modal interaction issue for continua in an analytical frame. Later on, many scholars, such as Byskov and Hutchinso [76], Peek and Kheyrkhahan [77] and Salerno and Casciaro [78] did some more detailed research into applying the closely spaced modes case in the perturbation approach. Lanzo and Garcea [79], Garcea and Casciaro [80], Salerno and Casciaro [78] and Garcea [81] used high continuity finite elements [82, 83] and Salerno's perturbation expansion [78] to study the model interactions and the worst imperfection shape [84, 85] in the buckling analysis. In Bilotta's [86] work, shear deformability and composite plates were considered, and he found that the secondary bifurcation paths obtained using the perturbation approach matched

very well with the results from a full model analysis based on a path-following approach in the neighborhood of the bifurcation point. This conclusion was also drawn by Garcea [87]. Menken et al. [88, 89], Erp and Menken [90, 91] and Schreppers and Menken [92] used the expansion given by Byskov and Hutchinson [76] and used a spline finite-strip type element to explore the phenomenon of the modal interaction in folded plate type structures. Some research work [93, 94] has been done on thin-walled structures, such as the isotropic cylindrical and spherical shells. In addition, Kouhia and Mikkola [95], Huang and Atluri [96], and Magnusson [97] used the perturbation approach carried out at any bifurcation point as a predictor for the path following through any specific bifurcating branch.

In a general path-following analysis, only second order accuracy is needed to recover the elastic response vector and the tangent stiffness matrix [98]. While, the asymptotic approach used in reduction methods needs a fourth order expansion of the strain energy. It is usually complex and perhaps not possible to apply a fourth order accurate strain model into the FE context. The co-rotational approach (CR) [99, 100] which is able to provide a fourth order accurate description of the element motion appears to be suitable to overcome this difficulty. The basic idea of the co-rotational description is to refer each element to a local frame which moves together with the element, thus filtering its rigid motion. Initially, Garcea [67] researched to implement the Koiter's asymptotic approach into nonlinear structural FE models which are based on a co-rotational frame. Later, Eriksson and Pacoste [64] investigated the possibility of using co-rotational formulation. Recently, Zagari [98, 101] has presented a co-rotational formulation, suitable for a nonlinear, fourth order accurate asymptotic postbuckling analysis of shell structures exploiting the three dimensional finite rotations in his PhD thesis.

As discussed in the background and motivation section of this chapter, the buckling and postbuckling behaviors of structures are strongly influenced by the prebuckling nonlinearity of such structures. While, in the literatures listed above, the prebuckling state is often assumed to be linear in the Koiter reduction methods. Actually, this linear assumption for the prebuckling state will often overestimate the buckling load of an important class of engineering problems the prebuckling of which is obvious nonlinear. Therefore, the effect of prebuckling nonlinearity should be taken into account in the buckling analysis. Much of the work on Koiter's theory are based on the alternative procedure proposed by Budiansky and Hutchinson [102], which assumes that the prebuckling is linear. Cohen [56] and Fitch [57], and later Arbocz and Hol [60, 103] derived the modifications necessary to make Budiansky and Hutchinson's work [102] include prebuckling nonlinearity. Recently, Rahman [104, 105, 8], Zagari [67, 98] have made use of the derivations done by Arbocz and Hol [60, 103] within a finite element context to consider the nonlinearity of the prebuckling of a structure. In their work, first, a standard nonlinear analysis is performed to reach, as closely

as possible, the critical point of a structure without encountering any negative diagonal term in the system stiffness matrix to get a basic state, and then they apply Koiter's asymptotic expansion at this basic state to obtain a more accurate initial postbuckling response which considers the effect of the prebuckling nonlinearity of a structure.

In general, Koiter reduction methods, which are based on Koiter's initial postbuckling theory, give very easy handling of buckling/imperfection sensitive cases especially if the structure has closely spaced buckling modes, however, these reduction methods have some disadvantages. They experience difficulties when dealing with limit point type buckling. Using general nonlinear finite elements it is very complicated to compute the fourth order derivatives needed for the asymptotic expansion. These reduction methods are only valid for a small range near the bifurcation point due to Koiter's asymptotic expansion being used only once at the bifurcation point. The effect of the prebuckling nonlinearity of a structure can only be considered using a general nonlinear finite element analysis in a full finite element model.

1.3 Thesis layout

This thesis is organized as follows.

The background and motivation of the present research together with a literature survey for the selected areas of application is presented in chapter 1. Particular attention is paid to the comparison of the current reduction methods.

A new approach termed the Koiter-Newton is presented for the numerical solution of a class of elastic nonlinear structural response problems in chapter 2. It is a combination of a reduction method inspired by Koiter's post-buckling analysis and the Newton arc-length method so that it is accurate over the entire equilibrium path and it is also computationally efficient in the presence of buckling. The Koiter-Newton approach combines Koiter's analysis as a predictor and the Newton arc-length method as a corrector. A detailed introduction of the reduction method in one expansion step for this new approach will be given. Then, the selection of perturbation loads is discussed, especially when the expansion step is applied on the unstable part of the equilibrium path. Next, the effect of the imperfection loads is taken into account to get a load term that can be added to the already formed reduced order model for the perfect structure. After obtaining the reduced order model, with and without the imperfections, a path-following technique called the normal flow method is reviewed and used to simulate the ROM and obtain the

response curve of the structure. Finally, an automated technique is applied to make the proposed approach trace the entire nonlinear equilibrium path automatically, and the corresponding computational cost is counted.

Implementations of the Koiter-Newton approach into the beam and shell elements based on the co-rotational kinematics are presented in chapters 3 and 4. The derivatives of the co-rotational frame with respect to the element degrees of freedom are presented, and the equilibrium equations of a third-order form at the expansion equilibrium point are obtained to construct the reduced order model. For the shell element, three configurations during the deformation are defined to make the description easier, and the nonlinear rotation matrix is used to describe the large/finite rotation accurately. Some numerical examples involving beams and shells are used to evaluate the performance of the Koiter-Newton analysis using co-rotational kinematics. The results are compared with results produced for the same problems using a full nonlinear analysis (ABAQUS), with the same number of nodes and elements.

The Von Kármán kinematical model is adopted in chapter 5 and used to achieve the Koiter-Newton approach. The Von Kármán kinematics do not take into account fully nonlinearities in the element, hence using them it is much faster and easier than using co-rotational kinematics to obtain a fourth order expansion of the strain energy. In the cases where the nonlinear in-plane rotations of the structure can be neglected, but the rotations of the normals to the mid-surface are finitely large, an acceptable accuracy of a nonlinear structural analysis can be obtained using the Von Kármán kinematics. Some previous used numerical examples which have already been tested using co-rotational kinematics are used to evaluate the performance of the Koiter-Newton analysis using Von Kármán kinematics, and some new examples which need a very fine mesh are also analyzed in this chapter.

The conclusions drawn from the research discussed in this thesis are summarized in chapter 6.

Chapter 2

Koiter-Newton approach

2.1 Introduction

The main aim of the research reported here is to find a new analytical approach to nonlinear structural problems with the presence of the buckling. As discussed in the literature review section of the first chapter, current Koiter reduction methods, which are based on Koiter's initial postbuckling theory and can handle the buckling/imperfection case very well, still have some main drawbacks as follows. They are not well suited to dealing with limit point type buckling and it is quite difficult to take into consideration prebuckling nonlinearity using these methods. In the traditional Koiter's theory, Koiter's asymptotic expansion is carried out only once at the bifurcation point, so the range of validity of these Koiter reduction methods is only near the bifurcation point. In order to overcome these disadvantages, a new approach called Koiter-Newton is presented here for the numerical solution of a class of elastic nonlinear structural analysis problems [9, 106]. This method combines ideas from Koiter's initial postbuckling analysis and Newton arc-length methods to obtain an algorithm that is accurate over the entire equilibrium path and efficient in the presence of buckling and/or imperfection sensitivity.

The basic premise behind the method is to use Koiter's asymptotic expansion from the beginning rather than using it only once at the bifurcation point. In every step of the Koiter-Newton approach, a reduced order model (ROM) is constructed based on Koiter's initial post-buckling theory. This ROM is used to make an initial prediction of the response of the structure. At the new predicted point, the exact

unbalanced force residual is calculated using the full finite element model. Then in a corrector step, this residual is driven to zero in a manner similar to that used in the traditional Newton arc-length methods. As the solution proceeds to higher and higher load levels, the quality of the ROM is assessed, based on the norm of force residuals, and if needed the ROM is updated to reflect changes in structural stiffness and load distribution.

The proposed approach will significantly improve the efficiency of nonlinear static finite element analysis by incorporating information from Koiter's analysis while retaining the complete generality usually associated with finite element modeling. The number of linear FEM systems of equations need to be solved is much less than that for the classical arc-length methods. This is due to the better prediction provided by the nonlinear reduced order model compared to linear predictors especially within the nonlinear segments of the original response curve, thus allowing the algorithm to use fairly large step sizes. In addition, perturbation loads corresponding to buckling modes are considered in the reduced order model. The ROM provides a convenient and cheap way to assess imperfection sensitivity of a structure.

First, the construction of the reduced order model in one expansion step of the Koiter-Newton approach is presented using a functional notation. The selection of the perturbation loads, especially when the expansion point is on the unstable part of the equilibrium path, is then discussed. Next, the imperfection loads are also taken into account in the reduced order model to model the geometric imperfections, and the normal flow algorithm is introduced to simulate the reduced order model. Finally, the automated technique and the computational effort associated with the proposed approach are given.

2.2 Construction of the reduced order model

The essence of the reduction methods for nonlinear problems is to use the asymptotic technique to replace the governing equations of the structure by a reduced system of equations with considerably fewer unknowns. Here, the reduced system of equations is just the reduced order model of the original model. Then, instead of solving a large nonlinear finite element model, the nonlinear responses of the structure can be obtained by solving this reduced order model with much fewer degrees of freedom. So, the reduced order model is the most important part in a reduction method, and it determines the characteristics and functions of the method that will be used. In the present Koiter-Newton approach, the constructional way of reduced order model is quite different from other reduction methods, which makes the present approach

synthesizing the best aspects of the others.

This section is ordered as follows. First, the governing equations and their asymptotic expansions are given at an known equilibrium point. The reduced order model is then established at this equilibrium point to approximate the equilibrium equations.

2.2.1 Governing equations and asymptotic expansions

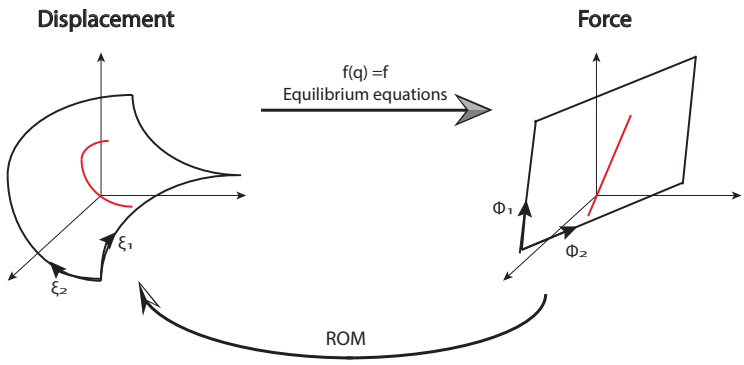

Figure 2.1: Mapping from the displacement space to the force space

The discretized equilibrium equations of a structure can be reduced to a set of nonlinear equations of the form:

$$\mathbf{f}(\mathbf{q}) = \lambda \mathbf{f}_{ex} \tag{2.1}$$

where $\mathbf{f}$ and $\mathbf{f}_{ex}$ are respectively the internal force vector and the external load vector, λ is the load parameter, and $\mathbf{q}$ is the vector of degrees of freedom. The degrees of freedom $\mathbf{q}$ fully describe the current configuration of the structure, usually with respect to a reference configuration.

The discrete equilibrium equations (2.1) define a curve in the $(\mathbf{q}, \lambda)$ space, as shown in Fig. 2.1, that is referred to as the equilibrium path. Using a path-following technique, e.g. [19] and [107], the relationship between the displacement $\mathbf{q}$ and load parameter λ, that is the nonlinear response of structures, can be obtained.

In the proposed Koiter-Newton approach, a reduced order model is established to approximate the equilibrium equations in the neighborhood of a known equilibrium state $(\mathbf{q}_0, \lambda_0)$. The vector $\mathbf{q}_0$ describes the configuration at this equilibrium state, which we will refer to as the nominal configuration. Let $\mathbf{q}$ be the unknown displacement vector near this nominal state, it results in:

$$\mathbf{q} = \mathbf{q}_0 \circ \mathbf{u} \tag{2.2}$$

where $\mathbf{u}$ describes the current configuration with respect to the nominal configuration. The composition of $\mathbf{q}_0$ and $\mathbf{u}$ is not always a simple addition, and for beams and shells where rotational degrees of freedom are used, the composition operation will depend on the parametrization of rotations.

As discussed above, $(\mathbf{q}_0, \lambda_0)$ is the nominal equilibrium state, $(\mathbf{q}, \lambda)$ is the current equilibrium state, and $(\mathbf{u}, \Delta\lambda)$ describes the current equilibrium state with respect to the nominal equilibrium state. So, the load parameters should satisfy the following relation:

$$\Delta\lambda = \lambda - \lambda_0 \tag{2.3}$$

As an equilibrium state, the nominal state $(\mathbf{q}_0, \lambda_0)$ should also satisfy the equilibrium equations (2.1), leading to:

$$\mathbf{f}(\mathbf{q}_0) = \lambda_0 \mathbf{f}_{ex} \tag{2.4}$$

According to Eq. (2.2), the equilibrium equations (2.1) can be rewritten as:

$$\mathbf{f}(\mathbf{q}_0 \circ \mathbf{u}) = \lambda \mathbf{f}_{ex} \tag{2.5}$$

The equilibrium equations (2.1) may be interpreted geometrically as a mapping from the displacement space to the force space, see the straight arrow in Fig. 2.1. Equivalently, we may think of the equilibrium path as the pre-image of the line $\mathbf{f} = \lambda \mathbf{f}_{ex}$ in the displacement space.

The proposed technique aims to be applicable for buckling sensitive structures. In the presence of buckling, multiple secondary equilibrium branches that intersect with the primary path at the buckling, bifurcation, points exist. For the method to

work in such cases, the possibility of some perturbation loads that may excite the secondary branches need to be taken into account. Thus, in the proposed reduction method, a linear subspace of the force space containing the loading line is defined, as shown in Fig. 2.1. The subspace is defined as the span of predefined set of force vectors, and as such it can be parametrised by coordinates ϕ along the predefined force directions. The force subspace can then be represented as:

$$\mathbf{f} = \mathsf{F}\boldsymbol{\phi}, \tag{2.6}$$

where F is a load matrix the α-th column of which is formed by the sub-load vector $\mathbf{f}_\alpha$, and the coordinates ϕ represent the amplitudes of the sub-loads. The first sub-load vector $\mathbf{f}_1 = \mathbf{f}_{ex}$ is the external load, and the sub-loads $\mathbf{f}_\alpha, \alpha = 2, \ldots, m+1$ are the perturbation loads, where m is the number of perturbation loads. The selection of the perturbation loads will be addressed later.

The pre-image of the force subspace in the displacement space is in general a non-linear surface, and this back-mapping procedure is presented by the curve arrow in Fig. 2.1. The surface is parametrised using a set of coordinates $\boldsymbol{\xi}$. The relation between $\boldsymbol{\phi}$ and $\boldsymbol{\xi}$ is the reduced order model. In general, it is not a simple task to construct the pre-image and as such we seek to find an approximation of the surface in terms of a Taylor series expansion.

In order to simplify the complicated nonlinearity of the equilibrium equations, Eq. (2.1) is expanded to a third order expression with respect to $\mathbf{u}$ with the use of Eqs. (2.3) and (2.4), leading to:

$$\mathcal{L}(\mathbf{u}) + \mathcal{Q}(\mathbf{u}, \mathbf{u}) + \mathcal{C}(\mathbf{u}, \mathbf{u}, \mathbf{u}) = \Delta\lambda \mathbf{f}_{ex} \tag{2.7}$$

where $\mathcal{L}$ is a linear form, $\mathcal{Q}$ is quadratic and $\mathcal{C}$ is cubic. These can also be considered as two-dimensional, three-dimensional and four-dimensional tensors, respectively. For example, use $\mathcal{Q}(\mathbf{u}, \mathbf{v}) = Q_{pij} u_i v_j$, where u_i and v_j are respectively the components of the vectors $\mathbf{u}$ and $\mathbf{v}$, Q_{pij} is the component of the tensor Q, and the summation convention is applied.

For conservative systems, the internal loads are derivable from a scalar potential. In this case, the tensors L, Q and C are symmetric with respect to all their subscripts.

Extending the equilibrium equations to consider the force subspace defined in Eq. (2.6), the equations of equilibrium (2.7) take the form:

$$\mathcal{L}(\mathbf{u}) + \mathcal{Q}(\mathbf{u}, \mathbf{u}) + \mathcal{C}(\mathbf{u}, \mathbf{u}, \mathbf{u}) = \mathsf{F}\boldsymbol{\phi} \tag{2.8}$$

2.2.2 Reduced order model

The solution for $\mathbf{u}$ of Eq. (2.8) lies, in general, on an $m+1$ dimensional surface where m is the number of perturbation loads. The numerical construction of such a surface would be computationally prohibitive. To circumvent this, an approximate solution can be obtained using Taylor series expansion, which defines a nonlinear displacement subspace in Fig. 2.1. This equilibrium surface is parametrised in terms of generalised displacements $\boldsymbol{\xi}$, and the equilibrium displacement is expanded to the third order with respect to $\boldsymbol{\xi}$ as follows:

$$\mathbf{u} = \mathbf{u}_\alpha \xi_\alpha + \mathbf{u}_{\alpha\beta}\xi_\alpha\xi_\beta + \mathbf{u}_{\alpha\beta\gamma}\xi_\alpha\xi_\beta\xi_\gamma, \tag{2.9}$$

where the greek subscripts vary over the range $1, 2, \ldots, m+1$, and the summation convention is applied. The first order displacements $\mathbf{u}_\alpha$ define the tangent plane to the equilibrium surface at the approximation point. The second order displacements $\mathbf{u}_{\alpha\beta}$ and third order displacements $\mathbf{u}_{\alpha\beta\gamma}$ describe the interactions among first and second order displacement fields, respectively.

The equilibrium surface may be parametrised with an infinite number of choices for $\boldsymbol{\xi}$. To fix the parameterization, we choose the vector $\boldsymbol{\xi}$ such that it is work conjugate to the load amplitudes $\boldsymbol{\phi}$, leading to:

$$(\mathsf{F}\boldsymbol{\phi})^t \delta\mathbf{u} \equiv \boldsymbol{\phi}^t \delta\boldsymbol{\xi} \tag{2.10}$$

Substituting the expansion of the displacement (2.9) into the left hand side of Eq. (2.10), it results in:

$$\begin{aligned}
(\mathsf{F}\boldsymbol{\phi})^t \delta\mathbf{u} &= \boldsymbol{\phi}^t \mathsf{F}^t (\mathbf{u}_\alpha \delta\xi_\alpha + \mathbf{u}_{\alpha\beta}\delta\xi_\alpha\xi_\beta + \mathbf{u}_{\alpha\beta}\xi_\alpha\delta\xi_\beta + ...) \\
&= \phi_p \mathbf{f}_p^t (\mathbf{u}_\alpha \delta\xi_\alpha + \mathbf{u}_{\alpha\beta}\delta\xi_\alpha\xi_\beta + \mathbf{u}_{\alpha\beta}\xi_\alpha\delta\xi_\beta + ...) \\
&= (\mathbf{f}_p^t \mathbf{u}_\alpha)\phi_p\delta\xi_\alpha + (\mathbf{f}_p^t \mathbf{u}_{\alpha\beta})\phi_p\delta\xi_\alpha\xi_\beta + (\mathbf{f}_p^t \mathbf{u}_{\alpha\beta})\phi_p\xi_\alpha\delta\xi_\beta + ... \\
&\equiv \boldsymbol{\phi}^t \delta\boldsymbol{\xi}
\end{aligned} \tag{2.11}$$

In order to make the identical equation (2.11) tenable forever with respect to any value of $\boldsymbol{\xi}$, the coefficients of the various derivatives of $\boldsymbol{\xi}$ should satisfy the following constraint equations about the sub-loads and displacement fields, given by:

$$\begin{cases} \mathbf{f}_\alpha^t \mathbf{u}_\beta = \delta_{\alpha\beta} \\ \mathbf{f}_\alpha^t \mathbf{u}_{\beta\gamma} = 0 \\ \mathbf{f}_\alpha^t \mathbf{u}_{\beta\gamma\delta} = 0 \end{cases} \tag{2.12}$$

where $\delta_{\alpha\beta}$ is the Kronecker delta. It means that the sub-loads $\mathbf{f}_\alpha$ are orthogonal to all the second and third order displacement fields($\mathbf{u}_{\beta\gamma}$,$\mathbf{u}_{\beta\gamma\delta}$).

Consistent with the displacement expansion (2.9), we assume the expansion for the load amplitudes $\boldsymbol{\phi}$ to be:

$$\boldsymbol{\phi} = \bar{\mathcal{L}}(\boldsymbol{\xi}) + \bar{\mathcal{Q}}(\boldsymbol{\xi}, \boldsymbol{\xi}) + \bar{\mathcal{C}}(\boldsymbol{\xi}, \boldsymbol{\xi}, \boldsymbol{\xi}) \tag{2.13}$$

where the $\bar{\mathcal{L}}$, $\bar{\mathcal{Q}}$ and $\bar{\mathcal{C}}$ are, still to be determined, linear, quadratic, and cubic forms. These three forms have the same characteristics with the forms of the $\mathcal{L}$, $\mathcal{Q}$ and $\mathcal{C}$ in the equilibrium equations (2.7). The tensors $\bar{\mathsf{L}}$, $\bar{\mathsf{Q}}$ and $\bar{\mathsf{C}}$ should be their corresponding matrix forms.

Introducing the displacement expansion (2.9) and the load expansion (2.13) into the equilibrium equations (2.8), and then regrouping it with respect to $\boldsymbol{\xi}$, we obtain:

$$\begin{aligned} &\left\{\mathcal{L}(\mathbf{u}_\alpha) - \mathsf{F}\bar{\mathbf{L}}_\alpha\right\}\xi_\alpha + \left\{\mathcal{L}(\mathbf{u}_{\alpha\beta}) + \mathcal{Q}(\mathbf{u}_\alpha, \mathbf{u}_\beta) - \mathsf{F}\bar{\mathbf{Q}}_{\alpha\beta}\right\}\xi_{\alpha\beta} + \\ &\{\mathcal{L}(\mathbf{u}_{\alpha\beta\gamma}) + (2/3)\left[\mathcal{Q}(\mathbf{u}_{\alpha\beta}, \mathbf{u}_\gamma) + \mathcal{Q}(\mathbf{u}_{\beta\gamma}, \mathbf{u}_\alpha) + \mathcal{Q}(\mathbf{u}_{\gamma\alpha}, \mathbf{u}_\beta)\right] + \\ &\mathcal{C}(\mathbf{u}_\alpha, \mathbf{u}_\beta, \mathbf{u}_\gamma) - \mathsf{F}\bar{\mathbf{C}}_{\alpha\beta\gamma}\} \xi_{\alpha\beta\gamma} \\ &= 0 \end{aligned} \tag{2.14}$$

where the expressions $\bar{\mathbf{L}}_\alpha$, $\bar{\mathbf{Q}}_{\alpha\beta}$ and $\bar{\mathbf{C}}_{\alpha\beta\gamma}$ represent the vector in the multiple dimensional tensors $\bar{\mathsf{L}}$, $\bar{\mathsf{Q}}$ and $\bar{\mathsf{C}}$, respectively.

Equating the coefficients of the various powers of ξ to zero, three sets of linear equations are obtained as:

$$\mathcal{L}(\mathbf{u}_\alpha) = \mathsf{F}\bar{\mathbf{L}}_\alpha \tag{2.15}$$

$$\mathcal{L}(\mathbf{u}_{\alpha\beta}) + \mathcal{Q}(\mathbf{u}_\alpha, \mathbf{u}_\beta) = \mathsf{F}\bar{\mathbf{Q}}_{\alpha\beta} \tag{2.16}$$

$$\mathcal{L}(\mathbf{u}_{\alpha\beta\gamma}) + \frac{2}{3}\left[\mathcal{Q}(\mathbf{u}_{\alpha\beta}, \mathbf{u}_\gamma) + \mathcal{Q}(\mathbf{u}_{\beta\gamma}, \mathbf{u}_\alpha) + \mathcal{Q}(\mathbf{u}_{\gamma\alpha}, \mathbf{u}_\beta)\right] + \mathcal{C}(\mathbf{u}_\alpha, \mathbf{u}_\beta, \mathbf{u}_\gamma) = \mathsf{F}\bar{\mathbf{C}}_{\alpha\beta\gamma} \tag{2.17}$$

Taking the first order term Eq. (2.15), together with the first equation of orthogonality constraints (2.12), we can write them together as:

$$\begin{cases} \mathcal{L}(\mathbf{u}_\alpha) = \mathsf{F}\bar{\mathbf{L}}_\alpha \\ \mathbf{f}_\alpha^t \mathbf{u}_\beta = \delta_{\alpha\beta} \end{cases} \tag{2.18}$$

In order to be convenient for the implementation of the finite element method, the notations in Eq. (2.18) can be replaced by the FE notations:

$$\begin{cases} \mathsf{K}_t \mathbf{u}_\alpha = \mathsf{F}\bar{\mathbf{L}}_\alpha \\ \mathsf{F}^t \mathbf{u}_\alpha = \mathbf{E}_\alpha \end{cases} \tag{2.19}$$

where $\mathsf{K}_t = \mathsf{L}$ is the tangent stiffness matrix at the approximation/nominal configuration. The vectors $\mathbf{E}_\alpha$ are the unit basis vectors and are such that the α-th component is one and all the other components are zero.

Rewriting above equations in a matrix form, we obtain a set of linear systems of equations:

$$\begin{bmatrix} \mathsf{K}_t & -\mathsf{F} \\ -\mathsf{F}^t & \mathsf{0} \end{bmatrix} \begin{Bmatrix} \mathbf{u}_\alpha \\ \bar{\mathbf{L}}_\alpha \end{Bmatrix} = \begin{Bmatrix} \mathbf{0} \\ -\mathbf{E}_\alpha \end{Bmatrix} \tag{2.20}$$

In the same way, we combine the second order term Eq. (2.16) and the second equation of orthogonality constraints (2.12), leading to:

$$\begin{cases} \mathcal{L}(\mathbf{u}_{\alpha\beta}) + \mathcal{Q}(\mathbf{u}_\alpha, \mathbf{u}_\beta) = \mathsf{F}\bar{\mathbf{Q}}_{\alpha\beta} \\ \mathbf{f}_\alpha^t \mathbf{u}_{\beta\gamma} = 0 \end{cases} \tag{2.21}$$

Then, replacing the notations in Eq. (2.21) and rewriting them in a matrix form, we can obtain another set of linear systems of equations:

$$\begin{bmatrix} \mathsf{K}_t & -\mathsf{F} \\ -\mathsf{F}^t & \mathsf{0} \end{bmatrix} \begin{Bmatrix} \mathbf{u}_{\alpha\beta} \\ \bar{\mathbf{Q}}_{\alpha\beta} \end{Bmatrix} = \begin{Bmatrix} -\mathcal{Q}(\mathbf{u}_\alpha, \mathbf{u}_\beta) \\ \mathbf{0} \end{Bmatrix} \tag{2.22}$$

The vector $\bar{\mathbf{L}}_\alpha$ in the tensor $\bar{\mathsf{L}}$ and the vector $\bar{\mathbf{Q}}_{\alpha\beta}$ in the tensor $\bar{\mathsf{Q}}$ can be achieved respectively by Eqs. (2.20) and (2.22).

In order to simplify the algebra in constructing the reduced order model, the components of the tensors $\bar{\mathsf{L}}$ and $\bar{\mathsf{Q}}$ should be obtained from their vectors $\bar{\mathbf{L}}_\alpha$ and $\bar{\mathbf{Q}}_{\alpha\beta}$,respectively.

We work on the components $\bar{L}_{\alpha\beta}$ of the tensor $\bar{\mathsf{L}}$ firstly. Multipling the transpose of the first order displacement vector $\mathbf{u}_\beta$ on both sides of the first order term Eq. (2.15), we obtain:

$$\mathbf{u}_\beta^t \mathcal{L}(\mathbf{u}_\alpha) = \mathbf{u}_\beta^t \mathsf{F} \bar{\mathbf{L}}_\alpha \tag{2.23}$$

where the right hand side can be rewritten as:

$$\mathbf{u}_\beta^t \mathsf{F} \bar{\mathbf{L}}_\alpha = \left(\mathsf{F}^t \mathbf{u}_\beta\right)^t \bar{\mathbf{L}}_\alpha = \mathbf{E}_\beta^t \bar{\mathbf{L}}_\alpha = \bar{L}_{\beta\alpha} \tag{2.24}$$

where the equation $\mathsf{F}^t \mathbf{u}_\beta = \mathbf{E}_\beta$ exist referring to the first equation of the orthogonality constraints (2.12), the unit basis vectors $\mathbf{E}_\beta$ are such that the β-th component is one and all the other components are zero.

Then, Eqs. (2.23) and (2.24) demonstrate that the components of the tensor $\bar{\mathsf{L}}$ can be calculated as follows:

$$\bar{L}_{\beta\alpha} = \mathbf{u}_\beta^t \mathcal{L}(\mathbf{u}_\alpha) \tag{2.25}$$

where for conservative systems the tensors L is symmetric in all indices, hence the tensor $\bar{\mathsf{L}}$ is also symmetric in all indices.

The components $\bar{Q}_{\alpha\beta\gamma}$ of the tensor $\bar{\mathsf{Q}}$ can also be achieved in a similar way. We multiply the transpose of the first order displacement vector $\mathbf{u}_\gamma$ on both sides of the second order term Eq. (2.16), leading to:

$$\mathbf{u}_\gamma^t \mathcal{L}(\mathbf{u}_{\alpha\beta}) + \mathbf{u}_\gamma^t \mathcal{Q}(\mathbf{u}_\alpha, \mathbf{u}_\beta) = \mathbf{u}_\gamma^t \mathsf{F} \bar{\mathbf{Q}}_{\alpha\beta} \tag{2.26}$$

where the left hand side can be rewritten to be a more compact notation:

$$\begin{aligned}\mathbf{u}_\gamma^t \mathcal{L}(\mathbf{u}_{\alpha\beta}) + \mathbf{u}_\gamma^t \mathcal{Q}(\mathbf{u}_\alpha, \mathbf{u}_\beta) &= \mathbf{u}_{\alpha\beta}^t \mathcal{L}(\mathbf{u}_\gamma) + \mathbf{u}_\gamma^t \mathcal{Q}(\mathbf{u}_\alpha, \mathbf{u}_\beta) \\ &= \left(\mathsf{F}^t \mathbf{u}_{\alpha\beta}\right)^t \bar{\mathbf{L}}_\gamma + \mathbf{u}_\gamma^t \mathcal{Q}(\mathbf{u}_\alpha, \mathbf{u}_\beta) \\ &= \mathbf{u}_\gamma^t \mathcal{Q}(\mathbf{u}_\alpha, \mathbf{u}_\beta)\end{aligned} \tag{2.27}$$

where the derivations is based on the assumption of conservative systems, hence $\mathbf{u}_\gamma^t \mathcal{L}(\mathbf{u}_{\alpha\beta}) = \mathbf{u}_{\alpha\beta}^t \mathcal{L}(\mathbf{u}_\gamma)$. We have also used the facts that $\mathcal{L}(\mathbf{u}_\gamma) = \mathsf{F}\bar{\mathbf{L}}_\gamma$ from Eq. (2.15) and $\mathsf{F}^t \mathbf{u}_{\alpha\beta} = \mathbf{0}$ due to the second equation of the orthogonality constraints (2.12).

The right hand side of Eq. (2.26) can be expressed as:

$$\mathbf{u}_\gamma^t \mathsf{F} \bar{\mathbf{Q}}_{\alpha\beta} = \left(\mathsf{F}^t \mathbf{u}_\gamma\right)^t \bar{\mathbf{Q}}_{\alpha\beta} = \mathbf{E}_\gamma^t \bar{\mathbf{Q}}_{\alpha\beta} = \bar{Q}_{\gamma\alpha\beta} \tag{2.28}$$

where $\mathsf{F}^t \mathbf{u}_\gamma = \mathbf{E}_{\boldsymbol{\gamma}}$ due to the first equation of the orthogonality constraints (2.12), and the unit basis vectors $\mathbf{E}_\gamma$ are such that the γ-th component is one and all the other components are zero.

Then, combining Eqs. (2.27) and (2.28), the components of the tensor $\bar{\mathsf{Q}}$ can be calculated as follows:

$$\bar{Q}_{\gamma\alpha\beta} = \mathbf{u}_\gamma^t \mathcal{Q}(\mathbf{u}_\alpha, \mathbf{u}_\beta) \tag{2.29}$$

where tensor $\bar{\mathsf{Q}}$ is also symmetric in all indices due to conservative systems.

In the third order term, the component of $\bar{\mathsf{C}}$ can be obtained by the scalar multiplication of both sides of Eq. (2.17) with $\mathbf{u}_\delta$, leading to:

$$\begin{aligned}&\mathbf{u}_\delta^t \mathcal{L}(\mathbf{u}_{\alpha\beta\gamma}) + \mathbf{u}_\delta^t \frac{2}{3} \left[\mathcal{Q}(\mathbf{u}_{\alpha\beta}, \mathbf{u}_\gamma) + \mathcal{Q}(\mathbf{u}_{\beta\gamma}, \mathbf{u}_\alpha) + \mathcal{Q}(\mathbf{u}_{\gamma\alpha}, \mathbf{u}_\beta)\right] + \\ &\mathbf{u}_\delta^t \mathcal{C}(\mathbf{u}_\alpha, \mathbf{u}_\beta, \mathbf{u}_\gamma) = \left(\mathsf{F}^t \mathbf{u}_\delta\right)^t \bar{\mathbf{C}}_{\alpha\beta\gamma}\end{aligned} \tag{2.30}$$

where the subscript δ also runs from 1 to $m+1$, and the first term $\mathbf{u}_\delta^t \mathcal{L}(\mathbf{u}_{\alpha\beta\gamma})$ is represented as:

$$\mathbf{u}_\delta^t \mathcal{L}(\mathbf{u}_{\alpha\beta\gamma}) = \mathbf{u}_{\alpha\beta\gamma}^t \mathcal{L}(\mathbf{u}_\delta) = \left(\mathsf{F}^t \mathbf{u}_{\alpha\beta\gamma}\right)^t \bar{\mathbf{L}}_\delta = \mathbf{0} \tag{2.31}$$

where $\mathbf{u}_\delta^t \mathcal{L}(\mathbf{u}_{\alpha\beta\gamma}) = \mathbf{u}_{\alpha\beta\gamma}^t \mathcal{L}(\mathbf{u}_\delta)$ is based on conservative systems, and $\mathsf{F}^t \mathbf{u}_{\alpha\beta\gamma} = \mathsf{0}$ comes from the third equation of the orthogonality constraints (2.12).

The right hand side of Eq. (2.30) can be rewritten as the following form:

$$\left(\mathsf{F}^t\mathbf{u}_\delta\right)^t \bar{\mathbf{C}}_{\alpha\beta\gamma} = \mathbf{E}_\delta^t \bar{\mathbf{C}}_{\alpha\beta\gamma} = \bar{C}_{\delta\alpha\beta\gamma} \tag{2.32}$$

where $\mathsf{F}^t\mathbf{u}_\delta = \mathbf{E}_\delta$ due to the using of the first equation in orthogonality constraints (2.12), and the unit basis vectors $\mathbf{E}_\delta$ are such that the δ-th component is one and all the other components are zero.

Then, substituting Eqs. (2.31) and (2.32) into Eq. (2.30), the expression of the components of $\bar{\mathsf{C}}$ can be written as:

$$\mathbf{u}_\delta^t \frac{2}{3}[\mathcal{Q}(\mathbf{u}_{\alpha\beta}, \mathbf{u}_\gamma) + \mathcal{Q}(\mathbf{u}_{\beta\gamma}, \mathbf{u}_\alpha) + \mathcal{Q}(\mathbf{u}_{\gamma\alpha}, \mathbf{u}_\beta)] + \mathbf{u}_\delta^t \mathcal{C}(\mathbf{u}_\alpha, \mathbf{u}_\beta, \mathbf{u}_\gamma) = \bar{C}_{\delta\alpha\beta\gamma} \tag{2.33}$$

A simpler expression for $\bar{C}_{\alpha\beta\gamma\delta}$ may be obtained in the case of conservative systems where, L, Q, and C are symmetric in all indices. In this case, it results in:

$$\bar{C}_{\alpha\beta\gamma\delta} = \mathcal{C}(\mathbf{u}_\alpha, \mathbf{u}_\beta, \mathbf{u}_\gamma, \mathbf{u}_\delta) - \frac{2}{3}[\mathbf{u}_{\alpha\beta}^t \mathcal{L}(\mathbf{u}_{\delta\gamma}) + \mathbf{u}_{\beta\gamma}^t \mathcal{L}(\mathbf{u}_{\delta\alpha}) + \mathbf{u}_{\gamma\alpha}^t \mathcal{L}(\mathbf{u}_{\delta\beta})] \tag{2.34}$$

At this point, the expressions of $\bar{\mathsf{L}}$, $\bar{\mathsf{Q}}$, $\bar{\mathsf{C}}$ in Eq. (2.13) and the displacement vectors $\mathbf{u}_\alpha$, $\mathbf{u}_{\alpha\beta}$ have been obtained. Actually, the expansion of load amplitudes of Eq. (2.13) is just the reduced order model at the approximation/nominal point, that is:

$$\bar{\mathcal{L}}(\boldsymbol{\xi}) + \bar{\mathcal{Q}}(\boldsymbol{\xi}, \boldsymbol{\xi}) + \bar{\mathcal{C}}(\boldsymbol{\xi}, \boldsymbol{\xi}, \boldsymbol{\xi}) = \boldsymbol{\phi} \tag{2.35}$$

We can summarize the equations related to the reduced order model as follows:

The reduced order model (ROM) is:

$$\bar{\mathcal{L}}(\boldsymbol{\xi}) + \bar{\mathcal{Q}}(\boldsymbol{\xi},\boldsymbol{\xi}) + \bar{\mathcal{C}}(\boldsymbol{\xi},\boldsymbol{\xi},\boldsymbol{\xi}) = \boldsymbol{\phi}$$

in which the following two sets of augmented linear FEM systems need to be solved

$$\begin{bmatrix} \mathsf{K}_t & -\mathsf{F} \\ -\mathsf{F}^t & 0 \end{bmatrix} \begin{Bmatrix} \mathbf{u}_\alpha \\ \bar{\mathbf{L}}_\alpha \end{Bmatrix} = \begin{Bmatrix} \mathbf{0} \\ -\mathbf{E}_\alpha \end{Bmatrix}$$

$$\begin{bmatrix} \mathsf{K}_t & -\mathsf{F} \\ -\mathsf{F}^t & 0 \end{bmatrix} \begin{Bmatrix} \mathbf{u}_{\alpha\beta} \\ \bar{\mathbf{Q}}_{\alpha\beta} \end{Bmatrix} = \begin{Bmatrix} -\mathcal{Q}(\mathbf{u}_\alpha, \mathbf{u}_\beta) \\ \mathbf{0} \end{Bmatrix}$$

to obtain the components of $\bar{\mathcal{L}}$, $\bar{\mathcal{Q}}$ and $\bar{\mathcal{C}}$ in the ROM.

$$\bar{L}_{\alpha\beta} = \mathbf{u}_\alpha^t \mathcal{L}(\mathbf{u}_\beta)$$

$$\bar{Q}_{\alpha\beta\gamma} = \mathbf{u}_\alpha^t \mathcal{Q}(\mathbf{u}_\beta, \mathbf{u}_\gamma)$$

$$\bar{C}_{\alpha\beta\gamma\delta} = \mathcal{C}(\mathbf{u}_\alpha, \mathbf{u}_\beta, \mathbf{u}_\gamma, \mathbf{u}_\delta) - \frac{2}{3}[\mathbf{u}_{\alpha\beta}^t \mathcal{L}(\mathbf{u}_{\delta\gamma}) + \mathbf{u}_{\beta\gamma}^t \mathcal{L}(\mathbf{u}_{\delta\alpha}) + \mathbf{u}_{\gamma\alpha}^t \mathcal{L}(\mathbf{u}_{\delta\beta})]$$

Summary of the reduced order model in the Koiter-Newton approach

For conservative systems, the tensors $\bar{\mathsf{L}}$, $\bar{\mathsf{Q}}$ and $\bar{\mathsf{C}}$ in the reduced order model (2.35) are symmetric in all indices. Thus a conservative system is approximated with a conservative reduced order model.

The left hand side of the reduced order model (2.35) are achieved mainly by solving two sets of linear systems of equations (2.20) and (2.22). From the aspect of computational costs, the solution of these systems are needed requiring factoring of one matrix, since they have the same coefficient matrix. The dimension of this coefficient matrix is the summation of the number N of DOFs in the full finite element model and the number $(m+1)$ of DOFs in the reduced order model, that is $(N+(m+1))$. Since $(m+1)$ is generally very small compared with N, these two sets of systems can be regarded as augmented linear FEM equations. The components of $\bar{\mathsf{C}}$ are obtained from Eq. (2.34), which is an algebraic expression and does not need matrix factoring.

The right hand side of the reduced order model, which is the load amplitudes $\boldsymbol{\phi}$, can be expressed by the load parameter $\Delta\lambda$ in the equilibrium equations (2.7), as:

$$\boldsymbol{\phi} = \Delta\lambda \mathbf{E}_1 \tag{2.36}$$

where the unit basis vectors $\mathbf{E}_1$ are such that the 1-th component is one and all the other components are zero. The dimension of the load amplitudes $\boldsymbol{\phi}$ is $m+1$. The first component $\Delta\lambda$ is the load parameter of the external load $\mathbf{f_1}$; The other components are the load parameters of the perturbation loads $\mathbf{f}_\alpha, \alpha = 2, \ldots, m+1$ and all are set equal to zero to simulate the response of the structure to actual loads.

If the buckling does not happen in the analysis, e.g. the stiffness of a structure is increased with the increase of the load, only the external load and its corresponding load parameter $\Delta\lambda$ need to be considered and there will be only one degree of freedom in the reduced order model. Otherwise, the total number of degrees of freedom is related to the number m of closely-spaced buckling modes and will be $m+1$.

If the structure has many closely spaced buckling modes, buckling modes associated with simultaneous or nearly simultaneous buckling loads, these closely spaced modes will interact and influence the buckling characteristics of a structure. So, the selection of perturbation loads should also consider this case. As a simple rule, the buckling modes with buckling loads within 20% of the first buckling load are considered to be closely spaced modes and used to construct the perturbation loads which will be dicussed in the next section.

Having constructed the reduced order model (2.35), a path following technique may be used to solve the reduced order model, and the relationship between the load parameter $\Delta\lambda$ and displacement parameter $\boldsymbol{\xi}$ is obtained. In order to get the nonlinear response (λ - $\mathbf{q}$), the definitions $\lambda = \lambda_0 + \Delta\lambda$ and $\mathbf{q} = \mathbf{q}_0 \circ \mathbf{u}$ are used and the displacement expansion is invoked:

$$\mathbf{u} = \mathbf{u}_0 + \mathbf{u}_\alpha \xi_\alpha + \mathbf{u}_{\alpha\beta} \xi_\alpha \xi_\beta \tag{2.37}$$

2.3 Selection of the perturbation loads

As discussed in the previous section, a linear subspace of the force space parametrized by coordinates ϕ is defined as the span of predefined set of load vectors. In the proposed approach, the first load vector is always the external load $\mathbf{f}_{ex}$, and the other load vectors are perturbation loads. The selection of these perturbation loads is arbitrary within the restriction that the system matrix in Eqs. (2.20) and (2.22) is invertible.

To make the proposed approach suitable for buckling-sensitive structures the Koiter-Newton approach is related to the traditional Koiter perturbation approach. Inspired by Koiter perturbation approach, the perturbation loads should excite the buckling branches near the bifurcation points using knowledge of the buckling modes.

The basic premise behind the method is the use of Koiter's asymptotic expansion from the beginning and at any point along the equilibrium path rather than using it only at the bifurcation point. On the basis of the stability of the equilibrium point at which the asymptotic expansion is applied, two cases need to be distinguished in the selection of the perturbation loads related to the stable and unstable segments of the equilibrium path.

2.3.1 Expansion on the stable path

Case one is when the asymptotic expansion is applied on the stable part of the equilibrium path, which often happens in the prebuckling stage. In this case, the tangent stiffness matrix $\mathsf{K}_t = \mathsf{L}$ is positive definite.

In Koiter's work, the first order displacements are selected along the buckling modes. In the proposed approach, the primary path is also considered in the first order displacements. Our purpose is that when the expansion is applied near the bifurcation point, the first order displacements $\mathbf{u}_\alpha$ would be in the direction of the active buckling modes $\mathbf{v}_\alpha$. To this end, the perturbation loads $\mathbf{f}_\alpha, \alpha = 2, \ldots, m+1$ are proposed as:

$$\mathbf{f}_\alpha = \mathsf{K}_g \mathbf{v}_\varphi \tag{2.38}$$

where $\mathbf{v}_\varphi, \varphi = 1, 2, \ldots, m$ are the closely-spaced linearized buckling modes; K_g is the geometric stiffness matrix which can be calculated as follows:

$$\mathsf{K}_g = -\frac{d\mathsf{K}_t}{d\lambda} = -\frac{d\mathsf{K}_t}{d\mathbf{q}}\frac{d\mathbf{q}}{d\lambda} \tag{2.39}$$

where $d\mathsf{K}_t/d\mathbf{q}$ is the second order derivative of the internal force at the approximation point, that is $2\mathsf{Q}$. We assume $\mathbf{q}_{,\lambda}$ can be determined by deriving the equilibrium equations, Eq. (2.1), with respect to λ to give:

$$\mathsf{K}_t \mathbf{q}_{,\lambda} = \mathbf{f}_{ex} \tag{2.40}$$

Then, using the displacement $\mathbf{q}_{,\lambda}$ obtained by solving Eq. (2.40), the final expression

of the geometric matrix K_g will be:

$$\mathsf{K}_g = -2\mathcal{Q}(\mathbf{q}_{,\lambda}) \tag{2.41}$$

In order to obtain the linearized buckling modes $\mathbf{v}_\varphi$ in Eq. (2.38), one linear buckling eigenvalue problem at the approximation point needs to be solved as:

$$\mathsf{K}_t\mathbf{v} = \mu\mathsf{K}_g\mathbf{v} \tag{2.42}$$

where the scaler μ is the eigenvalue or buckling load parameter, and the vector $\mathbf{v}$ is the buckling mode.

The eigenvalue problem (2.42) is solvable since the tangent stiffness matrix K_t is always positive definite on the stable part of the equilibrium path.

If the expansion point is exactly at the bifurcation point, the condition $\mathbf{f}_{ex}^t\mathbf{v}_\alpha = 0$ is satisfied. Moreover, the properties of eigenvalue problem (2.42) necessitate that $\mathbf{v}_\beta^t\mathsf{K}_g\mathbf{v}_\alpha = 0, \alpha \neq \beta$ which can be written as $\mathbf{f}_\beta^t\mathbf{v}_\alpha = 0, \beta > 1$. These two conditions indicate that $\mathbf{v}_\alpha$ is orthogonal to all forces except to $\mathbf{f}_\alpha$. Hence we deduce that $\mathbf{u}_\alpha = c_\alpha\mathbf{v}_\alpha$, no sum on α. This result guarantees that the present selection of forces guarantees similar results near the bifurcation point to Koiter's initial post-buckling theory.

2.3.2 Expansion on the unstable path

Case two is when the asymptotic expansion/approximation point is on the unstable part of the equilibrium path, such as on the postbuckling path. In such cases, the tangent stiffness matrix is no longer positive definite and the above eigenvalue problem (2.42) is unsolvable. To circumvent this problem a modified eigenvalue problem needs to be constructed to find out the necessary modes.

In this case, two families of modes must be considered in the analysis. Family one includes the modes $\mathbf{w}$ which are already unstable, and the second family contains the buckling prone modes $\mathbf{v}$. Then, the total perturbation loads $\mathbf{f}_\alpha, \alpha = 2, \ldots, m+1$ are composed of two sets of perturbation loads constructed by these two types of modes, respectively. It results in:

$$\{\mathbf{f}_2, ..., \mathbf{f}_\alpha, ..., \mathbf{f}_{m+1}\} = \left\{\hat{\mathbf{f}}_1, ..., \hat{\mathbf{f}}_\beta, ..., \hat{\mathbf{f}}_{m_a}, \tilde{\mathbf{f}}_1, ..., \tilde{\mathbf{f}}_\gamma, ..., \tilde{\mathbf{f}}_{m_b}\right\} \tag{2.43}$$

where $\hat{\mathbf{f}}_\beta, \beta = 1, \ldots, m_a$ are the perturbation loads related to already unstable modes and m_a is the number, $\tilde{\mathbf{f}}_\gamma, \gamma = 1, \ldots, m_b$ are the perturbation loads related to buckling prone modes and m_b is the number. The relationship $m = m_a + m_b$ is satisfied.

Already Unstable Modes

For the modes that are already unstable, we can split the tangent stiffness into two parts, the material stiffness K_m and the stress stiffness K_σ, as follows:

$$\mathsf{K}_t = \mathsf{K}_m + \mathsf{K}_\sigma \tag{2.44}$$

Then, the eigenvalue problem based on these two matrices can be constructed as Eq. (2.45). Because the material matrix is always positive definite at any point, this eigenvalue problem is solvable at all times, given by:

$$\mathsf{K}_\sigma \mathbf{w} = \widehat{\mu} \mathsf{K}_m \mathbf{w} \tag{2.45}$$

where $\widehat{\mu}$ is the eigenvalue and $\mathbf{w}$ is the eigenvector or mode. Among all the modes, $\mathbf{w}_\beta, \beta = 1, 2, \ldots, m_a$ are the already unstable modes. The selection criterion is that the mode $\mathbf{w}$, the eigenvalue $\widehat{\mu}$ of which satisfies the inequation $(1+\widehat{\mu}) \leq 0$, is already unstable. The reason is as follows. Multiply the modes $\mathbf{w}$ and $\mathbf{w}^t$ on both sides of Eq. (2.44), thus after some straightforward algebra it leads to:

$$\mathbf{w}^t \mathsf{K}_t \mathbf{w} = \mathbf{w}^t \mathsf{K}_m \mathbf{w} + \mathbf{w}^t \mathsf{K}_\sigma \mathbf{w} = \mathbf{w}^t \mathsf{K}_m \mathbf{w}(1 + \frac{\mathbf{w}^t \mathsf{K}_\sigma \mathbf{w}}{\mathbf{w}^t \mathsf{K}_m \mathbf{w}}) = \mathbf{w}^t \mathsf{K}_m \mathbf{w}(1 + \widehat{\mu}) \tag{2.46}$$

where $\mathbf{w}^t \mathsf{K}_\sigma \mathbf{w} / \mathbf{w}^t \mathsf{K}_m \mathbf{w} = \widehat{\mu}$ comes from Eq. (2.45).

Eq. (2.46) demonstrates that the tangent matrix will be not positive definite, that is $\mathbf{w}^t \mathsf{K}_t \mathbf{w} \leq 0$, only if $\widehat{\mu}$ satisfies $(1 + \widehat{\mu}) \leq 0$.

The perturbation loads $\hat{\mathbf{f}}_\beta, \beta = 1, 2, \ldots, m_a$ which are related to the already unstable modes are constructed as follows:

$$\hat{\mathbf{f}}_\beta = \mathsf{K}_m \mathbf{w}_\beta \tag{2.47}$$

Buckling Prone Modes

At the unstable equilibrium point of the equilibrium path, excepting the already unstable modes $\mathbf{w}$, the modes $\mathbf{v}$ that might go unstable are also important. The perturbation loads which are constructed by these modes can excite buckling branches which may occur later along the equilibrium path. In order to make Eq. (2.42) solvable at the unstable equilibrium point, the eigenvalue problem based on the tangent stiffness and the geometric stiffness to make it is restricted to stable modes rendering it solvable. Hence, an additional orthogonality constraint about the buckling modes $\mathbf{v}$ and the perturbation loads $\hat{\mathbf{f}}_\beta$ related to the already unstable modes is added into the former eigenvalue problem (2.42). It results in:

$$\begin{cases} \mathsf{K}_t \mathbf{v} = \widetilde{\mu} \mathsf{K}_g \mathbf{v} \\ \hat{\mathbf{f}}_\beta^t \mathbf{v} = 0 \end{cases} \tag{2.48}$$

where $\widetilde{\mu}$ is the eigenvalue and $\mathbf{v}$ is the buckling prone mode. The closely spaced buckling modes $\mathbf{v}_\gamma, \gamma = 1, \ldots, m_b$ are selected using the proposed simple rule.

After obtaining the buckling modes, perturbation loads related to these buckling prone modes $\tilde{\mathbf{f}}_\gamma$ can be constructed as follows:

$$\tilde{\mathbf{f}}_\gamma = \mathsf{K}_g \mathbf{v}_\gamma \tag{2.49}$$

The selection of the perturbation loads is summarized as follows:

- If the asymptotic expansion is applied on the stable part of the equilibrium path, the perturbation loads $\mathbf{f}_\alpha$ are:

$$\mathbf{f}_\alpha = \mathsf{K}_g \mathbf{v}_\varphi$$

  where the buckling modes $\mathbf{v}_\varphi$ is calculated by:

$$\mathsf{K}_t \mathbf{v} = \mu \mathsf{K}_g \mathbf{v}$$

- If the asymptotic expansion is applied on the unstable part of the equilibrium path, the perturbation loads $\mathbf{f}_\alpha$ are composed by two parts, $\hat{\mathbf{f}}_\beta$ and $\tilde{\mathbf{f}}_\gamma$, as follows:

  1. $\hat{\mathbf{f}}_\beta$ is constructed by the already unstable modes $\mathbf{w}_\beta$, as given by:

$$\hat{\mathbf{f}}_\beta = \mathsf{K}_m \mathbf{w}_\beta$$

     where $\mathbf{w}_\beta$ is obtained by:

$$\mathsf{K}_\sigma \mathbf{w} = \widehat{\mu} \mathsf{K}_m \mathbf{w}, \quad (1 + \widehat{\mu}) \leq 0$$

  2. $\tilde{\mathbf{f}}_\gamma$ is constructed by the buckling prone modes $\mathbf{v}$, as given by:

$$\tilde{\mathbf{f}}_\gamma = \mathsf{K}_g \mathbf{v}_\gamma$$

     where $\mathbf{v}_\gamma$ is obtained by:

$$\begin{cases} \mathsf{K}_t \mathbf{v} = \widetilde{\mu} \mathsf{K}_g \mathbf{v} \\ \hat{\mathbf{f}}_\beta^t \mathbf{v} = 0 \end{cases}$$

Summary of the selection of the perturbation loads in the Koiter-Newton approach

2.4 Reduced order model with imperfections

When talking about buckling analysis, perfect structures and imperfect structures are often mentioned by researchers. Actually, there are two types of *perfect* struc-

tures. One type refers to the exactly perfect structures, and another type to the nominal perfect structures. For the exactly perfect structures, e.g. the Eular column and the flat plat under the axial compression, the structure is geometrical symmetrical and the loading is not offset. In these cases, the buckling phenomenon does not happen if there are no imperfection perturbations. In reality, these types of structures always have some small initial imperfections during the manufacture and use. The nominal perfect cases mean that the structures do not exist any imperfections but their geometries and loadings are not symmetrical. This type of structures is very common in engineering, for instance, curved beams and panels under lateral loads or compression belong to this case. For the nominal perfect structures, the loading capability of a postbuckling is very sensitive to imperfections, thus an imperfection analysis is very important in the buckling design of structures.

The reduced order model (2.35) in section 2.2 is only constructed for the perfect structure. Now we will show how the behavior of the imperfect structure can be derived from the properties of the perfect structure [108]. Geometric imperfections are the most common imperfections used in the imperfection analysis. The deformations caused by the initial imperfection loads can be used as the geometric imperfection. In the Koiter-Newton approach, imperfection loads are very convenient for implementing in the model. Here, two different ways of the implementation of imperfection loads are presented. The first way is based on the sub-loads, and the second way is to use the independent imperfection loads.

2.4.1 Imperfection loads based on the sub-loads

We use the vector $\Delta\mathbf{f}$ to indicate the imperfection loads applied on the discrete finite element model. It can be expressed as an approximate linear combination of the sub-loads $\mathbf{f}_\alpha, \alpha = 1, \ldots, m+1$ mentioned in the multiple loading form of the equilibrium equations (2.8), which leads to:

$$\Delta\mathbf{f} \approx \Delta\bar{\lambda}_1\mathbf{f}_1 + \Delta\bar{\lambda}_2\mathbf{f}_2 + ... + \Delta\bar{\lambda}_\alpha\mathbf{f}_\alpha + ... \tag{2.50}$$

where $\Delta\bar{\boldsymbol{\lambda}} = \left\{\Delta\bar{\lambda}_1, \Delta\bar{\lambda}_2, ..., \Delta\bar{\lambda}_\alpha, ...\right\}, \alpha = 1, \ldots, m+1$ is the combination coefficient vector which can also refer to as the imperfection coefficient vector, the sub-load $\mathbf{f}_1$ is the external load $\mathbf{f}_{ex}$, and the sub-loads $\mathbf{f}_\alpha, \alpha = 2, \ldots, m+1$ are the perturbation loads, where m is the number of perturbation loads or closely spaced buckling modes.

Multiplying the first order displacement fields $\mathbf{u}_\alpha^t$ on both sides of Eq. (2.50) and using the orthogonality constraints (2.12), these imperfection coefficients can be

obtained by:

$$\Delta\bar{\lambda}_\alpha \approx \mathbf{u}_\alpha^t \Delta\mathbf{f} \tag{2.51}$$

Eq. (2.51) means that the imperfection coefficient $\Delta\bar{\lambda}_\alpha$ can be calculated by the multiplication of the corresponding displacement field $\mathbf{u}_\alpha^t$ and the imperfection load $\Delta\mathbf{f}$.

The reduced order model (2.35) is constructed only for the perfect structure, thus its right hand side which is the load amplitude vector $\boldsymbol{\phi}$ is defined to be such that only the first component is nonzero, see Eq. (2.36). If considering the imperfections, we can directly superpose the imperfection coefficient vector $\Delta\bar{\boldsymbol{\lambda}}$ on the right hand side of the reduced order model, which results in:

$$\bar{\mathcal{L}}(\boldsymbol{\xi}) + \bar{\mathcal{Q}}(\boldsymbol{\xi},\boldsymbol{\xi}) + \bar{\mathcal{C}}(\boldsymbol{\xi},\boldsymbol{\xi},\boldsymbol{\xi}) = \boldsymbol{\phi} + \Delta\bar{\boldsymbol{\lambda}} \tag{2.52}$$

where the components, excluding the first one, of the right hand side vector are not all zeros, thus the effect of imperfections is considered in the reduced order model.

As the imperfection loads are implemented only in the right hand side of Eq. (2.52), the reduced order model is computed only once for the perfect structure and the effect of various imperfections can be obtained afterwards with very little additional computational cost for each imperfection pattern, which makes the Koiter-Newton approach to be much more efficient for imperfection analyses.

Then, the relation between the load parameter $\Delta\lambda$ and displacement parameter $\boldsymbol{\xi}$ can be obtained by using a path following technique to solve the reduced order model with imperfections. Finally, after introducing it into the equations $\lambda = \lambda_0 + \Delta\lambda, \mathbf{q} = \mathbf{q}_0 \circ \mathbf{u}$ and Eq. (2.37), we get the nonlinear response (λ - $\mathbf{q}$) of the structure with imperfections.

2.4.2 Independent imperfection loads

The implementation of imperfection loads introduced in subsection 2.4.1 will be invalid when the buckling mode is orthogonal to the imperfection load vector $\Delta\mathbf{f}$. In this case, the corresponding first order displacement field may also be almost

orthogonal to the imperfection load vector, which makes the corresponding imperfection coefficients approach to zero according to Eq. (2.51). Another way for the implementation of imperfection loads introduced in this subsection can overcome this drawback and be more convenient for implementation.

Excluding the external loads $\mathbf{f_{ex}}$ applied on the structure, the independent imperfection loads are also applied as some kind of external loads to model the imperfections. Hence, the differences after considering the imperfection loads start from the expansion of the equilibrium equations:

$$\mathcal{L}(\mathbf{u}) + \mathcal{Q}(\mathbf{u},\mathbf{u}) + \mathcal{C}(\mathbf{u},\mathbf{u},\mathbf{u}) = \mathsf{F}^{im}\boldsymbol{\phi} \tag{2.53}$$

where the load matrix F^{im} is different from F in Eq. (2.8). The α-th column of F^{im} is also formed by the sub-load vector $\mathbf{f}_\alpha$, however the sub-loads here are composed of three types of loads. The first sub-load vector $\mathbf{f}_1 = \mathbf{f}_{ex}$ is the external load; The sub-loads $\mathbf{f}_\alpha, \alpha = 2,\ldots,I+1$ are the independent imperfection loads, and I is number of imperfection loads; The sub-loads $\mathbf{f}_\alpha, \alpha = I+2,\ldots,m+I+1$ are the perturbation loads, where m is the number of perturbation loads or closely spaced buckling modes.

Then, following the derivatives written in section 2.2.2, the reduced order model with the imperfection loads is given by:

$$\bar{\mathcal{L}}(\boldsymbol{\xi}) + \bar{\mathcal{Q}}(\boldsymbol{\xi},\boldsymbol{\xi}) + \bar{\mathcal{C}}(\boldsymbol{\xi},\boldsymbol{\xi},\boldsymbol{\xi}) = \boldsymbol{\phi} \tag{2.54}$$

where the reduced order model is a $(m+I+1)$th order nonlinear system of equations, $\boldsymbol{\phi}$ here is the load amplitude vector considering the imperfection loads, which is a $(m+I+1)\times 1$ vector.

The definition of the load amplitude vector $\boldsymbol{\phi}$ is not the same as the definition in Eq. (2.36). Consistent with the sub-loads, the components of $\boldsymbol{\phi}$ also consist of three parts. The first part is $\boldsymbol{\phi}_1 = \Delta\lambda$, which is the load increment parameter of the external load $\mathbf{f}_{ex}$; The second part contains the load parameters $\phi_\alpha, \alpha = 2,\ldots,I+1$ of all the independent imperfection loads $\mathbf{f}_\alpha, \alpha = 2,\ldots,I+1$; The third part encompass the load parameters $\phi_\alpha, \alpha = I+2,\ldots,m+I+1$ of the perturbation loads $\mathbf{f}_\alpha, \alpha = I+2,\ldots,m+I+1$ and are all set equal to zero to simulate the response of the structure under actual loads.

For a given pattern of imperfection loads, the load parameters $\phi_\alpha, \alpha = 2,\ldots,I+1$ of the independent imperfection loads are fixed to be some certain values during the simulation of the reduced order model using a path following technique. For a

different pattern of imperfection loads, only the values of $\phi_\alpha, \alpha = 2, \ldots, I+1$ need to be changed, and the reduced order model is always the one for the corresponding perfect structure. We only need to reanalyze the reduced order model for a different imperfection pattern, and do not need to reconstruct the reduced order model. The advantage of saving computational cost in imperfection analyses also exists.

2.5 Simulation of the reduced order model

As discussed above, the reduced order model is actually a low-order nonlinear system of equations. A path following technique should be used to simulate the reduced oder model to obtain the relationship between the load parameter $\Delta\lambda$ and displacement parameter $\boldsymbol{\xi}$. Then, together with Eqs. (2.2), (2.3) and (2.37), the structural nonlinear response, $\mathbf{q}$ vs. λ, is achieved. The path following technique used for simulating the reduced order model is presented in this section.

There are many kinds of path following techniques for solving the nonlinear system. Newton-Raphson algorithm is the most classical one, and the arc-length method is good at handling the snap-through and snap-back cases. Compared with them, the normal flow algorithm is well known in numerical path-following analysis due to its computational efficiency and numerical stability. Hence, in the present work the normal flow algorithm is chosen to simulate the reduced order model. Ragon, Gürdal [19] and Saffari [12] have given a very detailed introduction to this algorithm. Here, we will simply review the basics of the normal flow algorithm following the original reference [19] in this section.

The discretized nonlinear equilibrium equations of a structure with m degrees of freedom may be presented as a nonlinear function of a load parameter λ and a displacement vector $\mathbf{q}$, which leads to:

$$\mathbf{f}(\lambda, \mathbf{q}) = \mathbf{0} \tag{2.55}$$

where $\mathbf{f}$ is a nonlinear function. In a path-following technique, Eq. (2.55) is solved in a step by step manner, from the undeformed state ($\mathbf{q} = 0$), to trace the equilibrium path. As discussed in Ragon and Gürdal's paper [19], each step is composed of a prediction phase and a Newton-Raphson correction phase.

In the normal flow algorithm, successive Newton-Raphson correction iterations have been conducted along the path perpendicular to the Davidenko flow curves[109]. In the view of the mathematical point, Davidenko flow curves are described by

considering a perturbation parameter η into the nonlinear system of equations, which governs the problem as the following form:

$$\mathbf{f}(\lambda, \mathbf{q}) = \eta \tag{2.56}$$

A family of response curves called Davidenko flow is obtained by changing the perturbation parameter η and solving the nonlinear system of equations (2.56). In Fig. 2.2, the dashed curves represent the Davidenko flow curves for a system with just one degree of freedom. As discussed above, to gain an acceptable convergence rate, the correction iterations for solving the problem are conducted along the path perpendicular to the Davidenko flow curves. As shown in Fig. 2.2, for a given step, we start at a converged equilibrium point A, then a point B can be found using the direction of the tangent vector in an initial prediction phase. Finally, the normal flow algorithm will converge to a new equilibrium point C along the path perpendicular to the Davidenko flow curves in a Newton-Raphson correction phase.

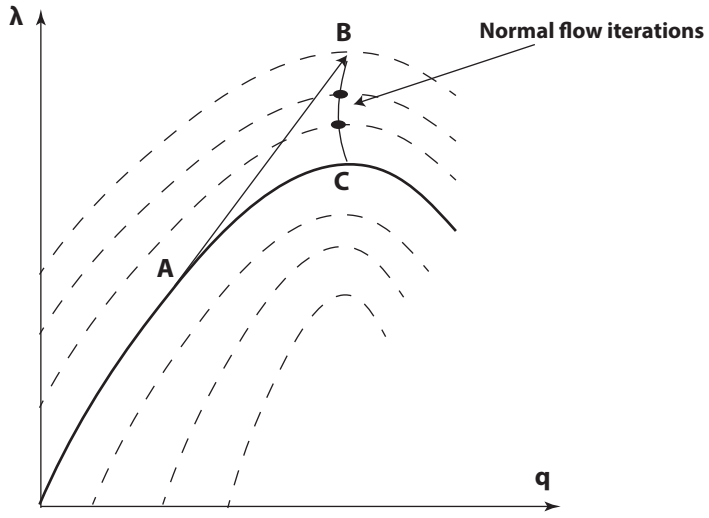

Figure 2.2: Normal flow algorithm

To describe this correction phrase in detail, the ith iteration in the step $(n+1)$ can be presented as:

$$\begin{cases} [D\mathbf{f}(\mathbf{s}_{n+1}^{i-1})]\Delta\mathbf{s} = -\mathbf{f}(\mathbf{s}_{n+1}^{i-1}) \\ \\ \mathbf{c}(\mathbf{s}_{n+1}^{i}) = \mathbf{0} \end{cases} \tag{2.57}$$

$$\mathbf{s}_{n+1}^{i} = \mathbf{s}_{n+1}^{i-1} + \Delta\mathbf{s}, \quad i = 1, 2, \ldots \tag{2.58}$$

and:

$$\Delta\mathbf{s} = \mathbf{v} - \frac{\mathbf{v}^t\mathbf{u}}{\mathbf{u}^t\mathbf{u}}\mathbf{u} \tag{2.59}$$

where $\mathbf{s}_{n+1}^{i} = (\lambda_{n+1}^{i}, \mathbf{q}_{n+1}^{i})^t$ is the solution of the ith iteration in the step $(n+1)$. The second equation in (2.57) is an auxiliary constraint equation which is the core of the normal flow algorithm. For different path-following techniques, this constraint equation is constructed in a different way to present a different correction strategy. $[D\mathbf{f}]$ is a $m \times (m+1)$ Jacobian matrix of the system (2.55). $\Delta\mathbf{s}$ is an solution increment between the $(i-1)$th iteration and the ith iteration. It can be seen that the number of solution increments in the first equation of system (2.57) is infinite, however a minimum solution $\Delta\mathbf{s}$, which is unique, can be obtained in the correction phase of the normal flow algorithm using a particular solution $\mathbf{v}$ and a vector $\mathbf{u}$. A particular solution $\mathbf{v}$ to system (2.57) can be obtained by selecting a constraint equation. A vector $\mathbf{u}$ is any vector in the kernel of $[D\mathbf{f}]$, and it can be chose to be the tangent vector $\bar{\mathbf{s}}_n^*$ which has already been obtained in each step.

In this way, after $*$th iteration, a new equilibrium point $\mathbf{s}_{n+1}^*$ on the equilibrium path is obtained and a new step will begin from this known point.

2.6 Koiter-Newton arclength method

A traditional drawback of reduced order models is that they have a limited range of validity. The reduced order model(ROM) proposed in section 2.2 should have a wider range of validity than for example the use of path derivatives [35] as it accounts for possible branching into quickly softening modes. Yet, it will still have some limited range of validity that cannot be determined *a priori*.

2.6.1 Automated techniques

In order to construct an efficient algorithm, analysis of the range of validity should be automated. While the reduced order model was simulated using a path following technique, the exact unbalanced force was calculated using the full finite element model at the end of each solution step. The norm of the residual force was used to judge whether the ROM was sufficiently accurate. The simulation of the reduced order model was stopped when:

$$\frac{\|\mathbf{R}\|}{\lambda \|\mathbf{f}_{ex}\|} > \varepsilon \tag{2.60}$$

where, ε is a prespecified tolerance, λ is the current load parameter, and $\mathbf{R}$ is the unbalanced (residual) force and can be calculated as follows:

$$\mathbf{R} = \lambda \mathbf{f}_{ex} - \mathbf{f} \tag{2.61}$$

where $\mathbf{f}$ is the current internal force.

A fully general and automatic procedure can be devised at this stage. Starting from a given equilibrium point, usually the undeformed configuration, a Koiter's asymptotic expansion is carried out and a ROM is constructed. Using the constructed ROM, a path following technique is applied, and the solution of the ROM is used to estimate the response of the full model, see Fig. 2.3. The ROM is used until it is no longer valid according to Eq. (2.60). This is considered to be a *predictor* step. A conventional Newton-based arc-length method can then be used to restore the equilibrium of the full model in a corrector step. The new convergent point on the equilibrium path, see Fig. 2.3, is denoted the expansion point for the next step of the algorithm.

The flow chart for the Koiter-Newton approach can be seen in Fig. 2.4.

A few remarks about the advantages of the approach are in order.

- In the present approach, the reduced order model is based on Koiter's initial post-buckling theory, which can easily capture the buckling branches accurately, even for perfect structure. Branch detection can be checked for the ROM easily leading to improved robustness without increased computational cost. Conventional nonlinear FE methods, and many reduction methods that

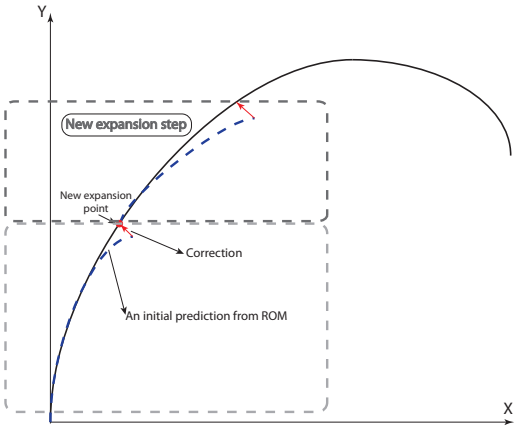

Figure 2.3: Nonlinear response curve of structures

do not incorporate buckling information explicitly, will face difficulties in tracing the response curve of buckling sensitive structures, especially if the structures have many closely spaced buckling modes.

- In contrast to a traditional Koiter reduction, the proposed Koiter-Newton approach uses an asymptotic expansion that can be constructed at any *equilibrium* point, rather than only at the bifurcation point. The present approach can be carried out in a step by step manner automatically by driving the residual force calculated by the full FE model to zero in the corrector step. The corrector step can also be regarded as a link between the full finite element model and the reduced order model. The proposed approach completely retains the generality usually associated with finite element modeling, while also retaining the power of Koiter's reduction to resolve nonlinear interactions amongst modes.

2.6.2 Computational costs

There are in total three basic parts in each expansion step of the Koiter-Newton approach. They are construction of the reduced order model, solution of the reduced order model, and correction of the prediction produced by the reduced order model.

During construction of the reduced order model, two sets of augmented linear FEM

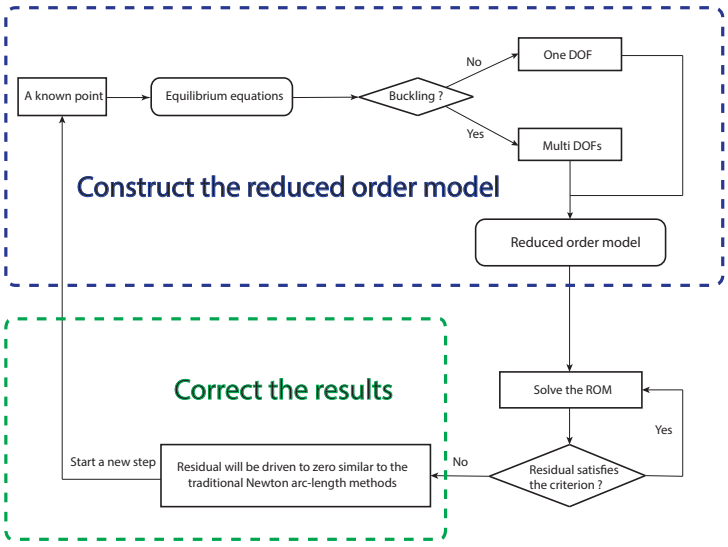

Figure 2.4: Flow chart of the Koiter-Newton approach

equations, which are Eqs. (2.20) and (2.22), are solved. All the systems of equations share the same coefficient matrix. So, only one stiffness matrix factorization is needed. Hence, the computing cost for constructing the reduced order model is almost equivalent to the cost of solving one linear FEM system, assuming that the cost is dominated by the factorization and not by a forward and back substitution.

Because the scale of the reduced order model is very small, the computational cost of simulating the reduced order model is considered to be negligible.

During correction of the prediction produced by the ROM, some general Newton iterations will be needed and the computing cost for each iteration is equal to the cost of solving a linear FEM system. So, the total number $\mathcal{N}$ of the linear FEM systems which need to be solved in the Koiter-Newton approach will be:

$$\mathcal{N} = \sum_{p=1}^{n} (1 + \mathcal{N}_c^p) \tag{2.62}$$

where n is the total number of steps taken by the method, and $\mathcal{N}_c^p$ is the number of linear FEM systems for correction in step p.

The better prediction provided by the reduced order model compared to linear predictors which classical Newton methods usually use, allows the algorithm to use fairly large step sizes during K-N iterations.

Based on the discussion above, the proposed approach will significantly improve the efficiency of nonlinear static finite element analysis, especially for buckling sensitive structures as will be demonstrated in the numerical examples of chapters 4 and 5.

2.7 Conclusions

A new approach denoted the Koiter-Newton is presented for the numerical solution of a class of elastic nonlinear structural response problems. It is a combination of a reduction method inspired by Koiter's post-buckling analysis and the Newton arc-length method which makes the method accurate over the entire nonlinear equilibrium path, and also computationally efficient in the presence of buckling; The Koiter-Newton approach can also consider imperfections in a structure and do the required imperfection analyses in a computationally economic manner; The computational costs of using the Koiter-Newton approach are summarized to show the high efficiency in the nonlinear structural analysis.

Chapter 3

Koiter-Newton analysis using co-rotational beam kinematics

3.1 Introduction

A structure usually undergoes a large motion in the presence of buckling, hence geometrically nonlinear mechanics is usually employed in a buckling analysis [110]. In Felippa's book [111], geometrically nonlinear problems have been discussed in detail, hence we will simply review the basics of geometrically nonlinear mechanics, especially the co-rotational kinematics, following Felippa's book in this section.

Currently, three Lagrangian kinematic descriptions that exist in the literature are used for finite element analysis of geometrically nonlinear structures [111, 112]: (1) total Lagrangian (TL) formulation, (2) updated Lagrangian (UL) formulation, and (3) co-rotational (CR) formulation. Among them, the CR formulation was the last to be developed, and it has received considerable attention recently. In the beginning, the CR formulation was not designed to be implemented in a general finite element for the nonlinear analysis of structures, since the application of this formulation is limited by a priori kinematics assumptions. This assumption demands that the CR formulation can only be used in the case where the displacements and rotations may be arbitrarily large, but the deformations must be small [111]. To make the CR

formulation more widely applicable, the idea of multiple frames [113] was proposed for the CR formulation. Instead of one CR frame for a whole structure, each element of a structure is given one independent frame called a CR element frame. This modification helps to fulfill the above assumption, and it is achieved by making the element deformational displacements and rotations small with respect to the CR element frame. Even if the assumption is violated for a coarse mesh, we can refine the mesh to make the element size small enough. Then, the domain of application for the CR formulation is extended in the geometrically nonlinear structural analysis [114].

Instead of introducing new element formulations, the current popular way is to construct a systematic and efficient procedure to update the existing linear element library to take into consideration the nonlinear kinematics. One good choice for this purpose is to use the element independent co-rotational frame [115, 116, 117, 98]. In this CR frame, the element motion is split into two parts, a rigid part and a deformational part. The rigid part indicates the average motion of the CR frame which moves together with the element from the reference configuration to the current configuration. The deformational part is the local motion within this CR frame. As discussed above, this deformational part can be made small enough by refining the mesh. The element strain energy is only related to the deformational part, hence some simplified kinematics, such as the linear kinematics, can be used in the CR frame. It can be seen that the basic idea of the CR formulation is to extract the deformational part of the total motion by purging the rigid part before the element computations. It can be performed outside the standard element routines and thus is independent of element type [111].

The basic procedure of the Koiter-Newton approach is presented in chapter 2 in detail, and for wide applicability in engineering, this approach should be implemented into the finite element environment. According to the derivations given in chapter 2, the expressions of the $\mathcal{L}$, $\mathcal{Q}$ and $\mathcal{C}$ in the equilibrium equations (2.8) should be obtained to construct the reduced order model, and these expressions are related to the element formulations. In the present thesis, the co-rotational formulation is used for the FE implementation of the Koiter-Newton approach. The reasons are as follows:

- the element independent co-rotational frame are more accurate for the large displacement and large rotation cases in the geometrically nonlinear analysis, by purging the rigid part from the total motion.
- the co-rotational formulation can address the accuracy and convergence problems which often occurs in the implementation of Koiter perturbation approach into the finite element context [67, 8].

- the proposed Koiter-Newton approach presented in Chapter 2 requires derivatives of the element load vectors with respect to degrees of freedom up to the third order. This is two orders more than traditionally needed for Newton's method. Nonlinear elements based on the element independent co-rotational frame can facilitate the differentiations. Automatic differentiation is used to find the derivatives of the co-rotational frame with respect to element degrees of freedom. In this way, full nonlinear kinematics are taken into account when constructing the reduced order model.

- due to the element independent characteristic of the co-rotational frame, any type of the linear elements in the current element library can be used for the Koiter-Newton approach, and the geometric nonlinearity is taken into account by the derivatives of the local co-rotational frame with respect to the global frame.

The Koiter-Newton approach using co-rotational beam kinematics is presented in this chapter, and the focus of chapter 4 is the co-rotational shell kinematics. The rest of this chapter is organized as follows. The finite element implementation of the co-rotational beam kinematics is presented, then, the performance of the Koiter-Newton analysis is evaluated using some numerical examples of the beam model.

3.2 Co-rotational beam kinematics

In this section, we introduce the descriptions of the beam element in a co-rotational frame, then based on it, the local and global degrees of freedom of the beam element are given.

A simple co-rotational beam element using Kirchhoff theory is presented in Crisfield's book [112]. Deformation of a 2-D beam element from the initial undeformed configuration, that is the initial reference configuration, to the current deformed configuration under the loading is shown in Fig. 3.1. The two nodes of the beam element are denoted as a and b, and there are three degrees of freedom of each node which are two translations u, v and one rotation θ. In Fig. 3.1, the coordinate system $x - y$ is the global system, and the coordinate system $e_x - e_y$ located on the node a is the co-rotational system of element which moves together with the element. The e_x axis of the co-rotational system is always along the direction from node a to node b, and the e_y axis is perpendicular to the e_x axis in the 2D beam plane.

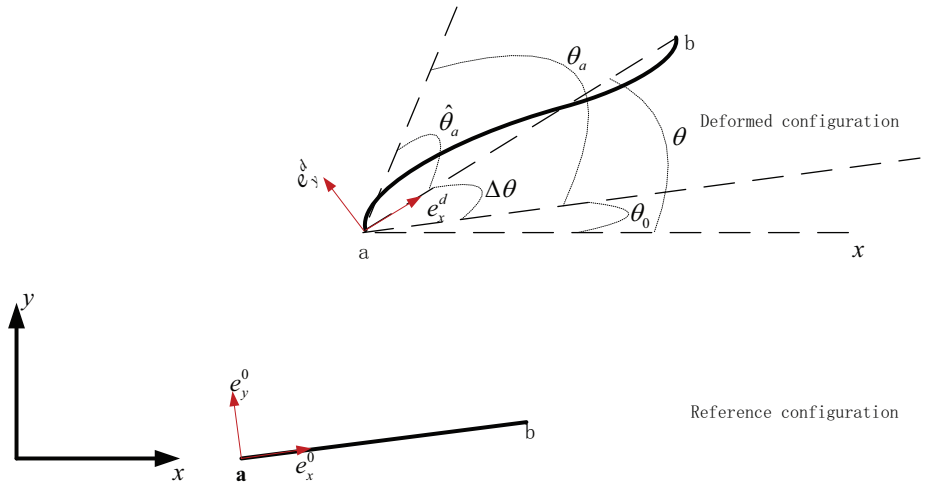

Figure 3.1: Sketch of the beam element in a co-rotational frame

Then, the global degrees of freedom of the beam element in the global coordinate system $x - y$ are given as:

$$\mathbf{q} = \{u_a, v_a, \theta_a, u_b, v_b, \theta_b\}^t \tag{3.1}$$

where the subscripts a and b are the node numbers.

When a large displacement or large rotation happens, most of the global degrees of freedom are caused by the rigid motion. Since the strain energy depends only on the deformational part, the local degrees of freedom which cause the deformation can be selected in the co-rotational frame, which results in:

$$\widehat{\mathbf{q}} = \left\{0, 0, \widehat{\theta}_a, \widehat{u}_b, 0, \widehat{\theta}_b\right\}^t \tag{3.2}$$

where, based on the definition of the local co-rotational coordinate system, the two local translations $\widehat{u}_a$, $\widehat{v}_a$ of node a and the local vertical translation $\widehat{v}_b$ of node b are zeros at all times during the deformation of the element. The local rotations $\widehat{\theta}_a$

and $\widehat{\theta}_b$ can also be called local co-rotational slopes [112]. Hence, the local degrees of freedom $\widehat{\mathbf{q}}$ of the beam element can be reduced to:

$$\widehat{\mathbf{q}} = \left\{\widehat{u}_b, \widehat{\theta}_a, \widehat{\theta}_b\right\}^t \tag{3.3}$$

It can be seen from Fig. 3.1 that the global and local degrees of freedom of the beam element should satisfy the following geometrical relations, given by:

$$\begin{cases} \widehat{u}_b = l_n - l \\ \widehat{\theta}_a = \theta_a - \Delta\theta = \theta_a - (\theta - \theta_0) = \theta_a - \theta + \theta_0 \\ \widehat{\theta}_b = \theta_b - \Delta\theta = \theta_b - (\theta - \theta_0) = \theta_b - \theta + \theta_0 \end{cases} \tag{3.4}$$

where the l and l_n are the initial and current length of the beam element, respectively, θ is the angle between the current configuration of the beam and the x axis of the global coordinate system, θ_0 is the angle between the initial configuration of the beam and the x axis of the global coordinate system, and $\Delta\theta$ is the angle between the initial and current configuration of the beam.

We assume that the position vectors of the nodes a and b in the initial configuration are $\mathbf{r}_a$ and $\mathbf{r}_b$,respectively, and the position vectors of the nodes a and b in the current configuration are $\mathbf{d}_a$ and $\mathbf{d}_b$, respectively, see Fig. 3.2. Then, the current length l_n of the beam element after the deformation can be expressed as:

$$l_n^2 = l^2 + 2(\mathbf{r}_b - \mathbf{r}_a)^t(\mathbf{d}_b - \mathbf{d}_a) + (\mathbf{d}_b - \mathbf{d}_a)^t(\mathbf{d}_b - \mathbf{d}_a) \tag{3.5}$$

Next, the strain of the beam element can be written as:

$$\varepsilon = \frac{\widehat{u}_b}{l} = \frac{l_n - l}{l} = \frac{l_n^2 - l^2}{l(l_n + l)} = \frac{2(\mathbf{r}_b - \mathbf{r}_a)^t(\mathbf{d}_b - \mathbf{d}_a) + (\mathbf{d}_b - \mathbf{d}_a)^t(\mathbf{d}_b - \mathbf{d}_a)}{l(l_n + l)} \tag{3.6}$$

The curvature of the beam element can be expressed as:

$$\kappa = \frac{\widehat{\theta}_b - \widehat{\theta}_a}{l} \tag{3.7}$$

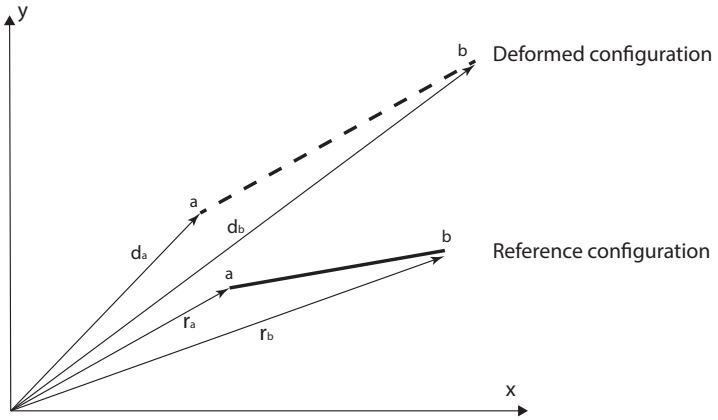

Figure 3.2: Position vectors of the two nodes in a beam element

3.3 Equilibrium equations in a third order form

The strain energy of the beam element is given based on the descriptions in section 3.2, then the $\mathcal{L}$, $\mathcal{Q}$ and $\mathcal{C}$ in the equilibrium equations of a third order form can be obtained by differentiating the strain energy with respect to the global degrees of freedom. To achieve these differentiations, the derivatives of the strain energy with respect to the local degrees of freedom and the derivatives of the local degrees of freedom with respect to the global degrees of freedoms are respectively presented.

3.3.1 Strain energy of the co-rotational beam element

The strain energy of the beam element can be obtained by introducing the strain (3.6) and the curvature (3.7) into the expression of the strain energy and integrating along the length of the beam, which results in:

$$\begin{aligned}\overline{U} &= \overline{U}\left(\widehat{u}_b, \widehat{\theta}_a, \widehat{\theta}_b\right) \\ &= \frac{1}{2}\int_0^l \left(\kappa^t EI\kappa + \varepsilon^t EA\varepsilon\right) dl \\ &= \frac{1}{2}EAl\varepsilon^2 + \frac{2EI}{l}\left(\widehat{\theta}_a^2 + \widehat{\theta}_a\widehat{\theta}_b + \widehat{\theta}_b^2\right) \\ &= \frac{1}{2}EA\frac{\widehat{u}_b^2}{l^2} + \frac{2EI}{l}\left(\widehat{\theta}_a^2 + \widehat{\theta}_a\widehat{\theta}_b + \widehat{\theta}_b^2\right)\end{aligned} \tag{3.8}$$

where E is the Young's modulus of the beam, and A is the area of the cross section. In Eq. (3.8), the strain energy $\overline{U}$ is expressed as a function of the local degrees of freedom $\left(\widehat{u}_b, \widehat{\theta}_a, \widehat{\theta}_b\right)$, which will facilitate the differentiations in the following subsection.

After obtaining the expression of the strain energy $\overline{U}$, the internal load vector $\mathbf{f}$, tangent stiffness matrix L, three-dimensional matrix Q and four-dimensional matrix C can be achieved by the first to fourth order derivatives of the strain energy with respect to the global degrees of freedom $\mathbf{q}$. Since the strain energy is an explicit function of the local degrees of freedom $\widehat{\mathbf{q}}$, we should differentiate the strain energy with respect to the local degrees of freedom firstly, and then multiply the derivatives of the local degrees of freedom with respect to the global degrees of freedom. The components of $\mathbf{f}$, L, Q and C can be calculated as follows:

$$f_p = \frac{\partial \overline{U}}{\partial q_p} = \frac{\partial \overline{U}}{\partial \widehat{q}_m}\frac{\partial \widehat{q}_m}{\partial q_p} \tag{3.9}$$

$$L_{pi} = \frac{\partial^2 \overline{U}}{\partial \widehat{q}_m \partial \widehat{q}_n}\frac{\partial \widehat{q}_n}{\partial q_i}\frac{\partial \widehat{q}_m}{\partial q_p} + \frac{\partial \overline{U}}{\partial \widehat{q}_m}\frac{\partial^2 \widehat{q}_m}{\partial q_p \partial q_i} \tag{3.10}$$

$$\begin{aligned}2Q_{pij} =& \frac{\partial^2 \overline{U}}{\partial \widehat{q}_m \partial \widehat{q}_n}\frac{\partial^2 \widehat{q}_n}{\partial q_i \partial q_j}\frac{\partial \widehat{q}_m}{\partial q_p} + \frac{\partial^2 \overline{U}}{\partial \widehat{q}_m \partial \widehat{q}_n}\frac{\partial \widehat{q}_n}{\partial q_i}\frac{\partial^2 \widehat{q}_m}{\partial q_p \partial q_j} \\ &+ \frac{\partial^2 \overline{U}}{\partial \widehat{q}_m \partial \widehat{q}_n}\frac{\partial \widehat{q}_n}{\partial q_j}\frac{\partial^2 \widehat{q}_m}{\partial q_p \partial q_i} + \frac{\partial \overline{U}}{\partial \widehat{q}_m}\frac{\partial^3 \widehat{q}_m}{\partial q_p \partial q_i \partial q_j}\end{aligned} \tag{3.11}$$

$$
\begin{aligned}
6C_{pijk} =& \frac{\partial^2 \overline{U}}{\partial \widehat{q}_m \partial \widehat{q}_n} \frac{\partial^3 \widehat{q}_n}{\partial q_i \partial q_j \partial q_k} \frac{\partial \widehat{q}_m}{\partial q_p} + \frac{\partial^2 \overline{U}}{\partial \widehat{q}_m \partial \widehat{q}_n} \frac{\partial^2 \widehat{q}_n}{\partial q_i \partial q_j} \frac{\partial^2 \widehat{q}_m}{\partial q_p \partial q_k} \\
&+ \frac{\partial^2 \overline{U}}{\partial \widehat{q}_m \partial \widehat{q}_n} \frac{\partial^2 \widehat{q}_n}{\partial q_i \partial q_k} \frac{\partial^2 \widehat{q}_m}{\partial q_p \partial q_j} + \frac{\partial^2 \overline{U}}{\partial \widehat{q}_m \partial \widehat{q}_n} \frac{\partial \widehat{q}_n}{\partial q_i} \frac{\partial^3 \widehat{q}_m}{\partial q_p \partial q_j \partial q_k} \\
&+ \frac{\partial^2 \overline{U}}{\partial \widehat{q}_m \partial \widehat{q}_n} \frac{\partial^2 \widehat{q}_n}{\partial q_j \partial q_k} \frac{\partial^2 \widehat{q}_m}{\partial q_p \partial q_i} + \frac{\partial^2 \overline{U}}{\partial \widehat{q}_m \partial \widehat{q}_n} \frac{\partial \widehat{q}_n}{\partial q_j} \frac{\partial^3 \widehat{q}_m}{\partial q_p \partial q_i \partial q_k} \\
&+ \frac{\partial^2 \overline{U}}{\partial \widehat{q}_m \partial \widehat{q}_n} \frac{\partial \widehat{q}_n}{\partial q_k} \frac{\partial^3 \widehat{q}_m}{\partial q_p \partial q_i \partial q_j} + \frac{\partial \overline{U}}{\partial \widehat{q}_m} \frac{\partial^4 \widehat{q}_m}{\partial q_p \partial q_i \partial q_j \partial q_k}
\end{aligned}
\tag{3.12}
$$

where the subscripts p, i, j, k, m and n run from 1 to 6, and 6 is the number of the total degrees of freedom in the beam element. The summation convention is only applied on m and n.

Since the strain energy (3.8) is a quadratic function of the local degrees of freedom, the derivatives of the strain energy are only to second order. The first order derivative of the strain energy is the local internal load, and the second order derivative is the linear stiffness matrix of the beam element. So, Eqs. (3.9) $\sim$ (3.12) demonstrate that any linear beam element can be adopted in the Koiter-Newton approach, and the geometric nonlinearity is taken into account only by the derivatives of the local co-rotational frame with respect to the global degrees of freedom.

After obtaining the expressions of the $\mathcal{L}$, $\mathcal{Q}$ and $\mathcal{C}$ from Eqs. (3.9) $\sim$ (3.12) and substituting them into Eq. (2.8), the equilibrium equations in a third order form for the beam element are achieved.

There are two unknown parts in Eqs. (3.9) $\sim$ (3.12), which are the derivatives of the strain energy $\overline{U}$ with respect to the local degrees of freedom $\widehat{\mathbf{q}}$ and the derivatives of the local degrees of freedom $\widehat{\mathbf{q}}$ with respect to the global degrees of freedom $\mathbf{q}$. The calculations of these two parts will be presented in the following two subsections.

3.3.2 Derivatives of the strain energy with respect to the local degrees of freedom

In Eq. (3.8), it can be seen that the strain energy $\overline{U}$, which is a scalar, is a function of the local degrees of freedom $\widehat{\mathbf{q}}$. The first order derivative of the strain energy with respect to the local degrees of freedom should be the local internal load, results in:

$$\frac{\partial \overline{U}}{\partial \widehat{\mathbf{q}}} = \left\{ EA\frac{\widehat{u}_b}{l}, \frac{2EI}{l}\left(2\widehat{\theta}_a + \widehat{\theta}_b\right), \frac{2EI}{l}\left(\widehat{\theta}_a + 2\widehat{\theta}_b\right) \right\}^t \tag{3.13}$$

Next, the second order derivative of the strain energy with respect to the local degrees of freedom will be a constant matrix which is just the linear stiffness matrix, given by:

$$\frac{\partial^2 \overline{U}}{\partial \widehat{\mathbf{q}}^2} = \begin{bmatrix} \frac{EA}{l} & 0 & 0 \\ 0 & \frac{4EA}{l} & \frac{2EA}{l} \\ 0 & \frac{2EA}{l} & \frac{4EA}{l} \end{bmatrix} \tag{3.14}$$

The strain energy is a quadratical function of the local degrees of freedom $\widehat{\mathbf{q}}$, hence the derivative of the strain energy with respect to the local degrees of freedom is only up to second order.

3.3.3 Derivatives of the local degrees of freedom with respect to the global degrees of freedom

The first order derivative of the local degrees of freedom $\widehat{\mathbf{q}}$ with respect to the global degrees of freedom $\mathbf{q}$ is a two-dimensional matrix of 3 by 6:

$$\frac{\partial \widehat{\mathbf{q}}}{\partial \mathbf{q}} = \begin{bmatrix} \frac{\partial \widehat{u}_b}{\partial q_1} & \cdots & \frac{\partial \widehat{u}_b}{\partial q_6} \\ \frac{\partial \widehat{\theta}_a}{\partial q_1} & \cdots & \frac{\partial \widehat{\theta}_a}{\partial q_6} \\ \frac{\partial \widehat{\theta}_b}{\partial q_1} & \cdots & \frac{\partial \widehat{\theta}_b}{\partial q_6} \end{bmatrix} \tag{3.15}$$

where a and b are the node numbers.

In the same way, we can know that the second to fourth order derivatives of the local degrees of freedom with respect to the global degrees of freedom will be the three-dimensional matrix of 3 by 6 by 6, the four-dimensional matrix of 3 by 6 by 6 by 6 and the five-dimensional matrix of 3 by 6 by 6 by 6 by 6, the forms of which are very complicated and are not listed here. Actually, these matrices are formed by three groups of derivatives, which are listed only to the second order as follows:

$$\frac{\partial \widehat{u}_b}{\partial q_i} = \frac{\partial l_n}{\partial q_i}; \quad \frac{\partial^2 \widehat{u}_b}{\partial q_i \partial q_j} = \frac{\partial^2 l_n}{\partial q_i \partial q_j}; \cdots \tag{3.16}$$

$$\frac{\partial \widehat{\theta}_a}{\partial q_i} = \begin{cases} 1, & if \quad i = 3 \\ 0, & if \quad i = 6 \\ \dfrac{\partial \theta}{\partial q_i}, & if \quad i = others \end{cases} ; \quad \frac{\partial^2 \widehat{\theta}_a}{\partial q_i \partial q_j} = \begin{cases} 0, & if \quad i,j = 3,6 \\ \dfrac{\partial^2 \theta}{\partial q_i \partial q_j}, & if \quad i,j = others \end{cases} \tag{3.17}$$

$$\frac{\partial \widehat{\theta}_b}{\partial q_i} = \begin{cases} 1, & if \quad i = 3 \\ 0, & if \quad i = 6 \\ \dfrac{\partial \theta}{\partial q_i}, & if \quad i = others \end{cases} ; \quad \frac{\partial^2 \widehat{\theta}_b}{\partial q_i \partial q_j} = \begin{cases} 0, & if \quad i,j = 3,6 \\ \dfrac{\partial^2 \theta}{\partial q_i \partial q_j}, & if \quad i,j = others \end{cases} \tag{3.18}$$

where the subscripts i and j run from 1 to 6, and the fact of the geometrical relations (3.4) are used.

From Eqs. (3.16) to (3.18) it can be seen that the unknown terms are the derivatives of the current length l_n and the rigid rotation θ with respect to the global degrees of freedom. The detailed calculations of these two unknown groups of derivatives will be presented in the rest of this subsection.

Referring to Fig. 3.1, the following geometrical relation can be easily found in a triangle formed by the current configuration and the x axis, which results in:

$$\{l_n \cos\theta, l_n \sin\theta\} = \{\mathbf{d}_b - \mathbf{d}_a\} = \Delta\mathbf{r}(\mathbf{q}) \tag{3.19}$$

where the vector $\Delta\mathbf{r}(\mathbf{q})$ is related to the global degrees of freedom $\{u_a, v_a, u_b, v_b\}$, and can be calculated by:

$$\Delta\mathbf{r}(\mathbf{q}) = \{(x_{0b} - x_{0a}) + (u_b - u_a), (y_{0b} - y_{0a}) + (v_b - v_a)\} \tag{3.20}$$

where (x_{0a}, y_{0a}) and (x_{0b}, y_{0b}) are respectively the coordinates of nodes a and b of the initial undeformed beam.

Differentiating Eq. (3.19) with respect to the global degrees of freedom, the following equation can be obtained:

$$\frac{\partial l_n}{\partial q_i}(\cos\theta, \sin\theta) + l_n(-\sin\theta, \cos\theta)\frac{\partial\theta}{\partial q_i} = \frac{\Delta\mathbf{r}(\mathbf{q})}{\partial q_i} \tag{3.21}$$

where the subscript i runs from 1 to 6, and the right hand side of Eq. (3.21) can be obtained by differentiating Eq. (3.20), which leads to:

$$\frac{\Delta\mathbf{r}(\mathbf{q})}{\partial q_i} = \begin{cases} (-1,0) & if \quad i = 1 \\ (0,-1) & if \quad i = 2 \\ (1,0) & if \quad i = 4 \\ (0,1) & if \quad i = 5 \\ (0,0) & if \quad i = 3,6 \end{cases} \tag{3.22}$$

Then, if both sides of Eq. (3.21) is multiplied by the vector $(\cos\theta, \sin\theta)^t$, the first order derivative of the current length l_n of the beam element with respect to the global degrees of freedom can be obtained by:

$$\frac{\partial l_n}{\partial q_i} = \frac{\Delta\mathbf{r}(\mathbf{q})}{\partial q_i}(\cos\theta, \sin\theta)^t \tag{3.23}$$

Next, if both sides of Eq. (3.21) is multiplied by the vector $(-\sin\theta, \cos\theta)^t$, the first order derivative of the rigid rotation θ with respect to the global degrees of freedom can be obtained by:

$$l_n \frac{\partial \theta}{\partial q_i} = \frac{\Delta \mathbf{r}(\mathbf{q})}{\partial q_i} \left(-\sin\theta, \cos\theta\right)^t \tag{3.24}$$

In the same way, the other derivatives of the current length l_n of the beam element and the rigid rotation θ with respect to the global degrees of freedom can be achieved as follows (up to the fourth order):

$$\begin{cases} \dfrac{\partial^2 l_n}{\partial q_i \partial q_j} = l_n \dfrac{\partial \theta}{\partial q_i} \dfrac{\partial \theta}{\partial q_j} \\ l_n \dfrac{\partial^2 \theta}{\partial q_i \partial q_j} = -\left(\dfrac{\partial l_n}{\partial q_i} \dfrac{\partial \theta}{\partial q_j} + \dfrac{\partial l_n}{\partial q_j} \dfrac{\partial \theta}{\partial q_i} \right) \end{cases} \tag{3.25}$$

$$\begin{cases} \dfrac{\partial^3 l_n}{\partial q_i \partial q_j \partial q_k} = & l_n \dfrac{\partial^2 \theta}{\partial q_i \partial q_j} \dfrac{\partial \theta}{\partial q_k} + l_n \dfrac{\partial^2 \theta}{\partial q_j \partial q_k} \dfrac{\partial \theta}{\partial q_i} + l_n \dfrac{\partial^2 \theta}{\partial q_k \partial q_i} \dfrac{\partial \theta}{\partial q_j} \\ & + \dfrac{\partial l_n}{\partial q_i} \dfrac{\partial \theta}{\partial q_j} \dfrac{\partial \theta}{\partial q_k} + \dfrac{\partial l_n}{\partial q_j} \dfrac{\partial \theta}{\partial q_k} \dfrac{\partial \theta}{\partial q_i} + \dfrac{\partial l_n}{\partial q_k} \dfrac{\partial \theta}{\partial q_i} \dfrac{\partial \theta}{\partial q_j} \\ l_n \dfrac{\partial^3 \theta}{\partial p_i \partial p_j \partial p_k} = & - \dfrac{\partial^2 l_n}{\partial q_i \partial q_j} \dfrac{\partial \theta}{\partial q_k} - \dfrac{\partial^2 l_n}{\partial q_j \partial q_k} \dfrac{\partial \theta}{\partial q_i} - \dfrac{\partial^2 l_n}{\partial q_k \partial q_i} \dfrac{\partial \theta}{\partial q_j} \\ & - \dfrac{\partial l_n}{\partial q_i} \dfrac{\partial^2 \theta}{\partial q_j \partial q_k} - \dfrac{\partial l_n}{\partial q_j} \dfrac{\partial^2 \theta}{\partial q_k \partial q_i} - \dfrac{\partial l_n}{\partial q_k} \dfrac{\partial^2 \theta}{\partial q_i \partial q_j} \\ & + l_n \dfrac{\partial \theta}{\partial q_i} \dfrac{\partial \theta}{\partial q_j} \dfrac{\partial \theta}{\partial q_k} \end{cases} \tag{3.26}$$

$$
\begin{aligned}
\frac{\partial^4 l_n}{\partial q_i \partial q_j \partial q_k \partial q_l} =& \frac{\partial^2 l_n}{\partial q_i \partial q_j}\frac{\partial \theta}{\partial q_k}\frac{\partial \theta}{\partial q_l} + \frac{\partial^2 l_n}{\partial q_j \partial q_k}\frac{\partial \theta}{\partial q_l}\frac{\partial \theta}{\partial q_i} + \frac{\partial^2 l_n}{\partial q_k \partial q_l}\frac{\partial \theta}{\partial q_i}\frac{\partial \theta}{\partial q_j} \\
&+ \frac{\partial^2 l_n}{\partial q_l \partial q_i}\frac{\partial \theta}{\partial q_j}\frac{\partial \theta}{\partial q_k} + \frac{\partial^2 l_n}{\partial q_i \partial q_k}\frac{\partial \theta}{\partial q_j}\frac{\partial \theta}{\partial q_l} + \frac{\partial^2 l_n}{\partial q_j \partial q_l}\frac{\partial \theta}{\partial q_i}\frac{\partial \theta}{\partial q_k} \\
&+ \frac{\partial l_n}{\partial q_i}\frac{\partial^2 \theta}{\partial q_j \partial q_k}\frac{\partial \theta}{\partial q_l} + \frac{\partial l_n}{\partial q_i}\frac{\partial^2 \theta}{\partial q_j \partial q_l}\frac{\partial \theta}{\partial q_k} + \frac{\partial l_n}{\partial q_i}\frac{\partial^2 \theta}{\partial q_k \partial q_l}\frac{\partial \theta}{\partial q_j} \\
&+ \frac{\partial l_n}{\partial q_j}\frac{\partial^2 \theta}{\partial q_i \partial q_l}\frac{\partial \theta}{\partial q_k} + \frac{\partial l_n}{\partial q_j}\frac{\partial^2 \theta}{\partial q_k \partial q_l}\frac{\partial \theta}{\partial q_i} + \frac{\partial l_n}{\partial q_j}\frac{\partial^2 \theta}{\partial q_i \partial q_k}\frac{\partial \theta}{\partial q_l} \\
&+ \frac{\partial l_n}{\partial q_k}\frac{\partial^2 \theta}{\partial q_i \partial q_l}\frac{\partial \theta}{\partial q_j} + \frac{\partial l_n}{\partial q_k}\frac{\partial^2 \theta}{\partial q_j \partial q_l}\frac{\partial \theta}{\partial q_i} + \frac{\partial l_n}{\partial q_k}\frac{\partial^2 \theta}{\partial q_i \partial q_j}\frac{\partial \theta}{\partial q_l} \\
&+ \frac{\partial l_n}{\partial q_l}\frac{\partial^2 \theta}{\partial q_i \partial q_k}\frac{\partial \theta}{\partial q_j} + \frac{\partial l_n}{\partial q_l}\frac{\partial^2 \theta}{\partial q_j \partial q_k}\frac{\partial \theta}{\partial q_i} + \frac{\partial l_n}{\partial q_l}\frac{\partial^2 \theta}{\partial q_i \partial q_j}\frac{\partial \theta}{\partial q_k} \\
&+ l_n \frac{\partial^3 \theta}{\partial q_i \partial q_j \partial q_k}\frac{\partial \theta}{\partial q_l} + l_n \frac{\partial^3 \theta}{\partial q_i \partial q_j \partial q_l}\frac{\partial \theta}{\partial q_k} + l_n \frac{\partial^3 \theta}{\partial q_j \partial q_k \partial q_l}\frac{\partial \theta}{\partial q_i} \\
&+ l_n \frac{\partial^3 \theta}{\partial q_i \partial q_k \partial q_l}\frac{\partial \theta}{\partial q_j} + l_n \frac{\partial^2 \theta}{\partial q_i \partial q_j}\frac{\partial^2 \theta}{\partial q_k \partial q_l} + l_n \frac{\partial^2 \theta}{\partial q_i \partial q_l}\frac{\partial^2 \theta}{\partial q_j \partial q_k} \\
&+ l_n \frac{\partial^2 \theta}{\partial q_i \partial q_k}\frac{\partial^2 \theta}{\partial q_j \partial q_l} - l_n \frac{\partial \theta}{\partial q_i}\frac{\partial \theta}{\partial q_j}\frac{\partial \theta}{\partial q_k}\frac{\partial \theta}{\partial q_l}
\end{aligned}
\tag{3.27}
$$

$$
\begin{aligned}
l_n \frac{\partial^4\theta}{\partial q_i \partial q_j \partial q_k \partial q_l} = &- \frac{\partial^3 l_n}{\partial q_i \partial q_j \partial q_k}\frac{\partial \theta}{\partial q_l} - \frac{\partial^3 l_n}{\partial q_i \partial q_j \partial q_l}\frac{\partial \theta}{\partial q_k} - \frac{\partial^3 l_n}{\partial q_i \partial q_k \partial q_l}\frac{\partial \theta}{\partial q_j} \\
&- \frac{\partial^3 l_n}{\partial q_j \partial q_k \partial q_l}\frac{\partial \theta}{\partial q_i} - \frac{\partial^2 l_n}{\partial q_i \partial q_j}\frac{\partial^2 \theta}{\partial q_k \partial q_l} - \frac{\partial^2 l_n}{\partial q_k \partial q_l}\frac{\partial^2 \theta}{\partial q_i \partial q_j} \\
&- \frac{\partial^2 l_n}{\partial q_i \partial q_k}\frac{\partial^2 \theta}{\partial q_j \partial q_l} - \frac{\partial^2 l_n}{\partial q_i \partial q_l}\frac{\partial^2 \theta}{\partial q_j \partial q_k} - \frac{\partial^2 l_n}{\partial q_j \partial q_k}\frac{\partial^2 \theta}{\partial q_i \partial q_l} \\
&- \frac{\partial^2 l_n}{\partial q_j \partial q_l}\frac{\partial^2 \theta}{\partial q_i \partial q_k} - \frac{\partial l_n}{\partial q_k}\frac{\partial^3 \theta}{\partial q_i \partial q_j \partial q_l} - \frac{\partial l_n}{\partial q_l}\frac{\partial^3 \theta}{\partial q_i \partial q_j \partial q_k} \\
&- \frac{\partial l_n}{\partial q_i}\frac{\partial^3 \theta}{\partial q_j \partial q_k \partial q_l} - \frac{\partial l_n}{\partial q_j}\frac{\partial^3 \theta}{\partial q_i \partial q_k \partial q_l} + \frac{\partial l_n}{\partial q_l}\frac{\partial \theta}{\partial q_i}\frac{\partial \theta}{\partial q_j}\frac{\partial \theta}{\partial q_k} \\
&+ \frac{\partial l_n}{\partial q_k}\frac{\partial \theta}{\partial q_i}\frac{\partial \theta}{\partial q_j}\frac{\partial \theta}{\partial q_l} + \frac{\partial l_n}{\partial q_i}\frac{\partial \theta}{\partial q_j}\frac{\partial \theta}{\partial q_k}\frac{\partial \theta}{\partial q_l} + \frac{\partial l_n}{\partial q_j}\frac{\partial \theta}{\partial q_i}\frac{\partial \theta}{\partial q_k}\frac{\partial \theta}{\partial q_l} \\
&+ l_n \frac{\partial^2 \theta}{\partial q_i \partial q_l}\frac{\partial \theta}{\partial q_j}\frac{\partial \theta}{\partial q_k} + l_n \frac{\partial^2 \theta}{\partial q_k \partial q_l}\frac{\partial \theta}{\partial q_i}\frac{\partial \theta}{\partial q_j} + l_n \frac{\partial^2 \theta}{\partial q_j \partial q_l}\frac{\partial \theta}{\partial q_i}\frac{\partial \theta}{\partial q_k} \\
&+ l_n \frac{\partial^2 \theta}{\partial q_i \partial q_k}\frac{\partial \theta}{\partial q_j}\frac{\partial \theta}{\partial q_l} + l_n \frac{\partial^2 \theta}{\partial q_j \partial q_k}\frac{\partial \theta}{\partial q_i}\frac{\partial \theta}{\partial q_l} + l_n \frac{\partial^2 \theta}{\partial q_i \partial q_j}\frac{\partial \theta}{\partial q_k}\frac{\partial \theta}{\partial p_l}
\end{aligned}
\tag{3.28}
$$

Up to this point, all of the essential derivatives are obtained. Introducing them into Eqs. (3.9) $\sim$ (3.12) gives the equilibrium equations of a third order form for the co-rotational beam element. Then, the reduced order model of the CR beam element can be constructed using the $\mathcal{L}$, $\mathcal{Q}$ and $\mathcal{C}$ in the equilibrium equations (2.8).

3.4 Numerical results

Some numerical examples of various beam models are presented here to show the effectiveness of the proposed Koiter-Newton approach and the feasibility of the FE implementation for the nonlinear beam element based on the co-rotational frame. The finite element implementation of the Koiter-Newton approach as well as a path-following technique based on the normal flow algorithm as in [19] has been carried out in MATLAB.

The ability to trace the entire nonlinear equilibrium path of the Koiter-Newton approach is assessed by comparing the results with results obtained for the same problem using ABAQUS, with the same number of elements and nodes. ABAQUS adopts a full nonlinear finite element analysis based on the Newton-Raphson method.

3.4.1 Three beam frame

The following example is characterized by closely spaced buckling loads. The structure consists of three straight beams connected in a reversed Y fashion. The cross section of the members is circular, with diameters of $d_1 = 3$mm and d_2=9mm for the top beam and the lower beams, respectively. The lower tips of the lower beams are pinned, while the upper extremity of the top vertical member is constrained in the horizontal direction. A unit vertical load is applied at the top to compress the structure. A sketch of the frame with the geometrical properties, applied load and boundary conditions is shown in Fig. 3.3 where length $L = 30$mm and Young's modulus $E = 210000\text{N/mm}^2$.

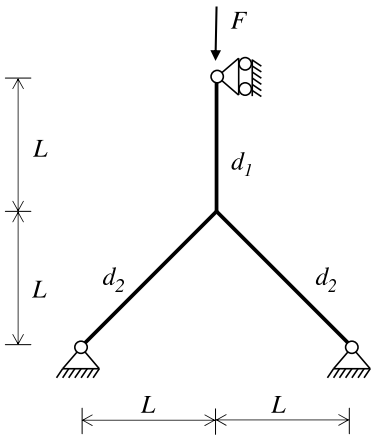

Figure 3.3: The three beam frame [7]

The first two buckling loads, which are 106.4N and 107.3N respectively, are very close. In order to consider the interactions among the closely spaced modes, the first two buckling modes are used to construct the perturbation loads (2.38). There are, in total, three degrees of freedom in the reduced order model. The first DOF is corresponding to the primary path, and the other two DOFs are corresponding

to the first two closely spaced buckling modes. The frame is meshed with 60 beam elements, which means that there are 181 degrees of freedom in the original FE model.

The first two buckling modes are shown in Fig. 3.4, and the first order displacement fields are presented in Fig. 3.5. The first order displacement field $\mathbf{u}_1$ shows a pure compression deformation under the external load, which indicates the deformation on the primary path. It can be seen that the other two first order displacement fields, $\mathbf{u}_2$ and $\mathbf{u}_3$, are very similar to the first two buckling modes. The second order displacement fields which present the interactions among the first order displacement fields are given in Fig. 3.6.

(a) Buckling mode 1 (b) Buckling mode 2

Figure 3.4: The first two buckling modes of the three beam frame

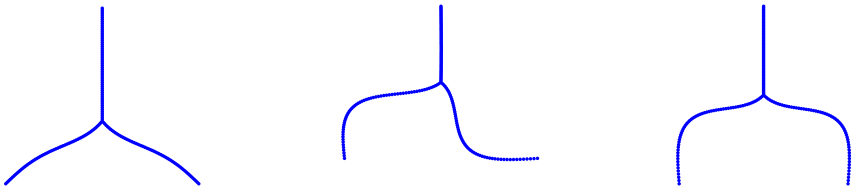

(a) $\mathbf{u}_1$ (b) $\mathbf{u}_2$ (c) $\mathbf{u}_3$

Figure 3.5: The first order displacement fields of the three beam frame

A very small imperfection load is applied horizontally on the cross point of three beams for the nonlinear buckling analysis, and here the imperfection load based on

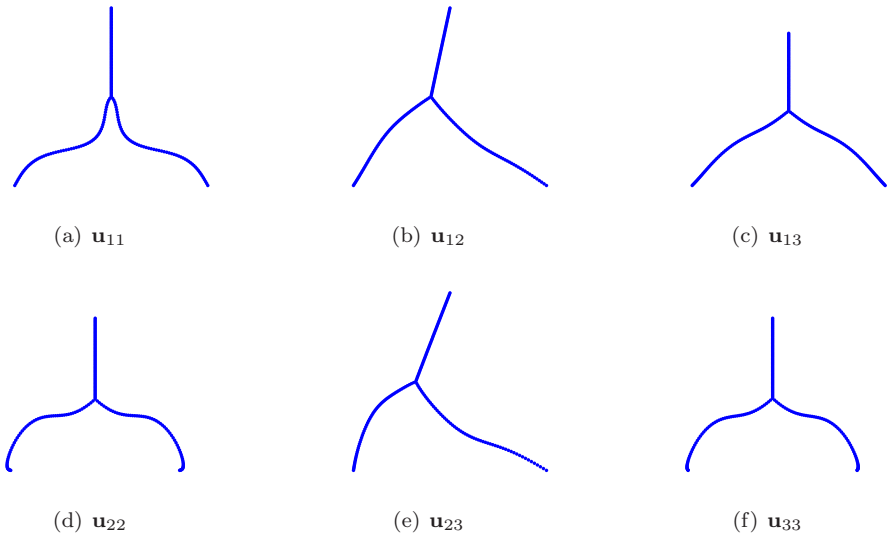

(a) $\mathbf{u}_{11}$ (b) $\mathbf{u}_{12}$ (c) $\mathbf{u}_{13}$

(d) $\mathbf{u}_{22}$ (e) $\mathbf{u}_{23}$ (f) $\mathbf{u}_{33}$

Figure 3.6: The second order displacement fields of the three beam frame

the sub-loads is used. One expansion step is carried out on the undeformed state without any corrections. The vertical displacement of the top point is shown in Fig. 3.7, which shows that the Koiter-Newton approach is able to find the buckling point and follow the initial postbuckling branch accurately in the buckling sensitive case. Since only one expansion step is applied, the range of validity of the reduced order model is not very well in the post-buckling regime. It means that when a structure has an almost linear prebuckling stage, a single step is enough to obtain the complete response of the structure satisfactorily up to the buckling load.

If only the first buckling mode is used to construct the ROM in the analysis, the path-following of the algorithm will fail, see the dotted dashed curve in Fig. 3.7, from which it can be seen that consideration of the interactions of the closely spaced buckling modes is essential in a buckling analysis.

3.4.2 Nonlinear beam examples

In this example, six individual beam configurations following those described in reference [118] and shown in Fig. 3.8 are reanalyzed using the Koiter-Newton approach.

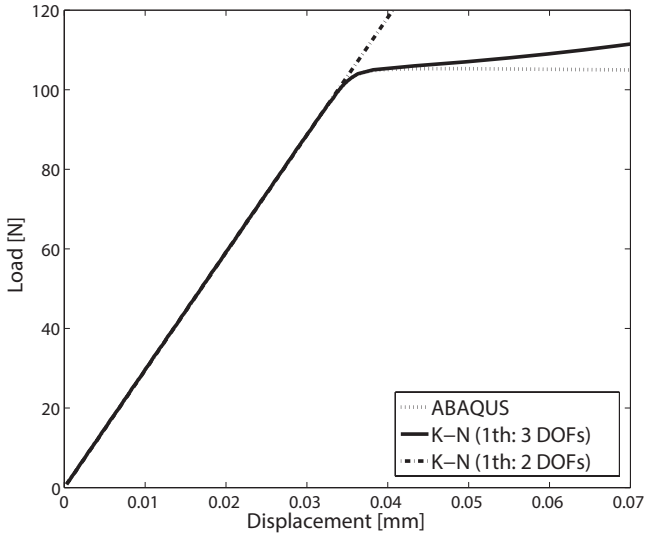

Figure 3.7: Buckling response curves of the three beam frame

Here, the major difference from the three beam frame of the previous example is that the six beams show obvious prebuckling deformation and nonlinearity. The differences in shapes, depths, constraint conditions, and loading positions are detailed in Fig. 3.8. An isotropic material is used, with a Young modulus E of 2000MPa. The area A and moment of inertia I of the cross section are 391mm^2 and 2000mm^4, respectively.

The following steps are taken in the present example:

1. Applying expansion steps on the stable part of the equilibrium path to obtain the complete response of the structure satisfactorily up to the maximum load carrying capability, that is the buckling point.

2. Applying expansion steps on the unstable part of the equilibrium path.

3. Checking the bifurcation point on the equilibrium path before the limit point.

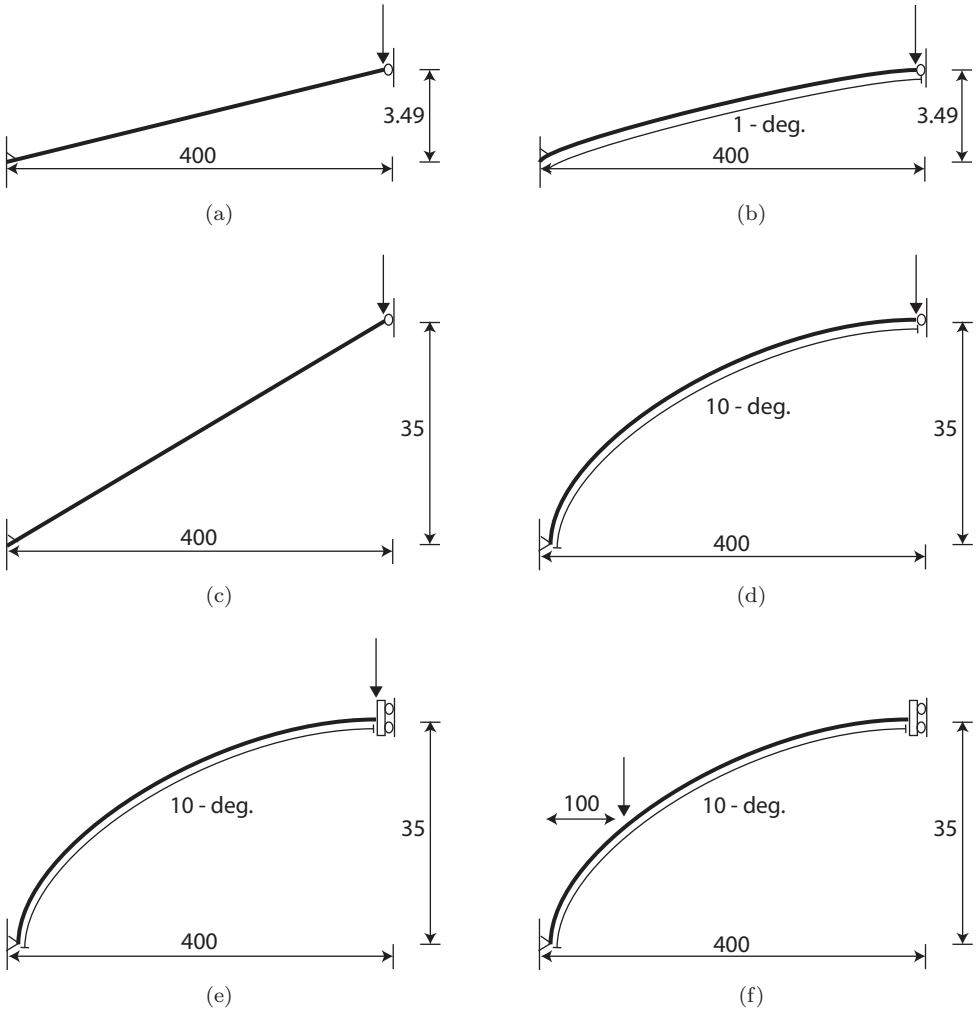

Figure 3.8: Six nonlinear beams

Expansions on the stable equilibrium path

When the asymptotic expansion is applied on the stable part of the equilibrium path, the first buckling load of these six beams is separated from the others, hence only the first buckling mode is chosen and the number of degrees of freedom in the reduced order model is two. While, there are 63 degrees of freedom in the original FE model. The nonlinear response curves, vertical displacement at the loading position vs. load, are shown in Fig. 3.9.

Due to the mild nonlinearity or load distribution in the prebuckling deformation, only one expansion step at the undeformed configuration is enough to obtain an accurate buckling response, including the nonlinear prebuckling stage, limit load and initial postbuckling stage for beams (a), (b), (c).

The prebuckling nonlinearity and the load distribution are very significant for beams (d), (e), (f), hence one single step from the beginning is not enough to capture the accurate nonlinear response. In this case, the automated technique discussed in sec. 2.6 for the path-following is adopted to correct the result and start a new expansion step. In the end, 3, 3 and 4 steps are adopted for beams (d), (e), (f), respectively, to obtain an accurate nonlinear response and maximum load carrying capability for each beam. The curves obtained for the different steps are plotted in Figs. 3.9(d) $\sim$ 3.9(f).

The six beams all show limit point type buckling. From Table 3.4.2 it can be seen that the limit loads of the beams are quite different from the linear buckling loads obtained using the eigenvalue problem (2.42). This indicates that the nonlinearity of the prebuckling stage will greatly affect the structural buckling characteristics of a beam.

Finally, the computational costs for the Koiter-Newton approach are compared to those for using ABAQUS in Table 3.4.2. Tracing to the same equilibrium point on the postbuckling path, a number of linear FEM systems need to be solved and a number of solution steps are shown in Table 3.4.2. Due to the need for one single step without a need for corrections for the first three beams, only one linear FEM system for constructing the reduced order model need to be solved. While, for the other three beams it is necessary to solve some additional systems for corrections. As can be seen from Table 3.4.2, in addition to the total linear FEM system, the number of solution steps taken using the Koiter-Newton approach is also fewer than the number of load steps used for the classical Newton method(ABAQUS), which indicated that a fairly larger step size can be adopted in the proposed Koiter-Newton approach due to the better prediction obtained using the ROM. In general, it is obvious that the

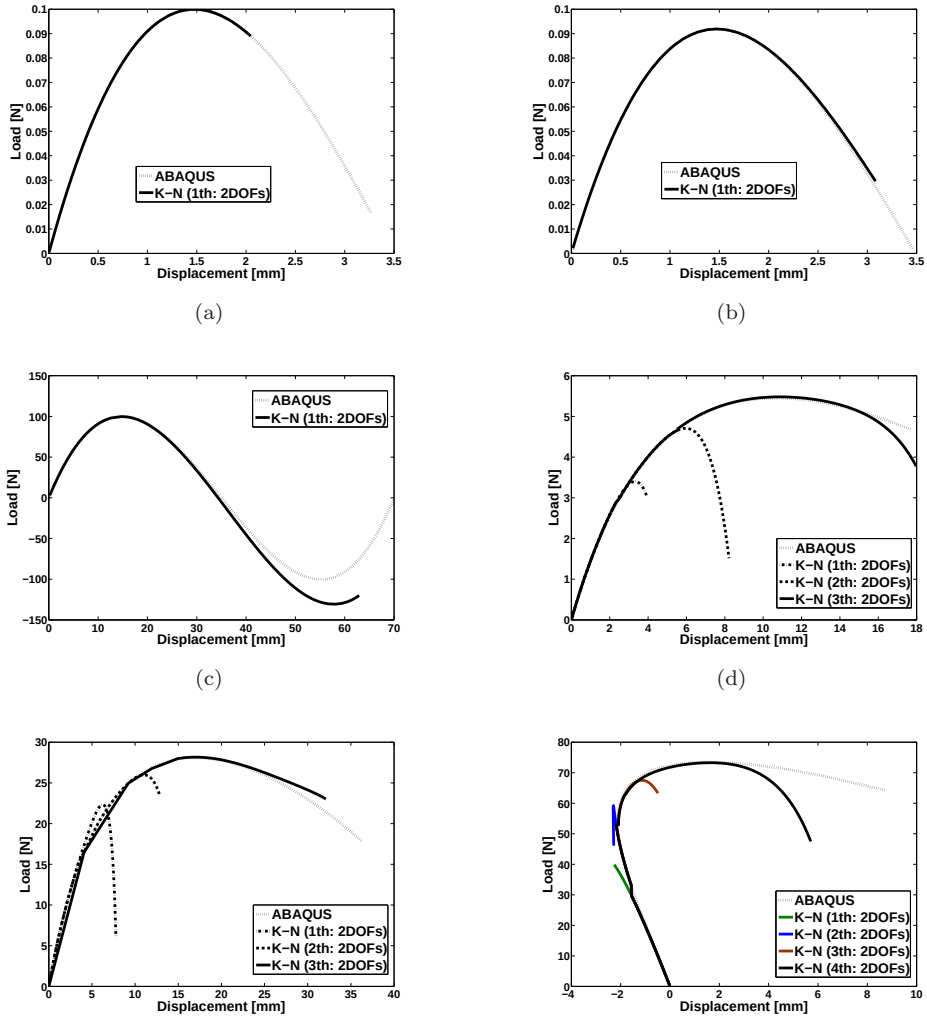

Figure 3.9: Response curves of six nonlinear beams

Koiter-Newton approach is much more efficient than ABAQUS.

Table 3.1: Comparison between the linear buckling load and the limit load

Beam examples	(a)	(b)	(c)	(d)	(e)	(f)
Linear buckling load	0.17	0.16	20.58	3.43	22.3	40.2
limit load	0.1	0.093	100.24	5.75	27	74.3

Table 3.2: Comparison of the computational cost in terms of number of liner FEM solutions

Beam examples	(a)	(b)	(c)	(d)	(e)	(f)
ABAQUS	98	104	112	142	167	174
(number of steps)	(26)	(34)	(40)	(46)	(53)	(64)
Koiter-Newton approach	1	1	1	9	12	12
(number of steps)	(1)	(1)	(1)	(3)	(3)	(4)

Expansions on the unstable equilibrium path

We take the beams (b), (c) and (d) to evaluate the performance of the Koiter-Newton approach on the unstable part of the equilibrium path. When the asymptotic expansion has applied at the unstable equilibrium point, all of the already unstable buckling modes and buckling prone modes are used to construct the reduced order model. The response curves of these three beams are shown in Figs. 3.10 $\sim$ 3.12. Two expansion steps are respectively adopted on the undeformed configuration and descending range for beam (b). For beam (c), we use four expansion steps at the undeformed configuration, limit point, descending range and the re-stiffened range, respectively, to assess the performance of the expansion at the points with different characteristics. For beam (d), one more buckling mode, that is the second buckling mode, is taken into account to construct the reduced order model, hence the step size of the first expansion step which is carried out on the undeformed configuration becomes larger, compared with the size of the first expansion step shown in Fig. 3.9(d). Later, the second step and the third step are respectively applied near the limit point and on the descending range. When our results are compared with the results obtained using ABAQUS, it can be seen that the response curves obtained by the Koiter-Newton approach is accurate along the entire equilibrium path, and the Koiter-Newton approach can use a fairly large step size.

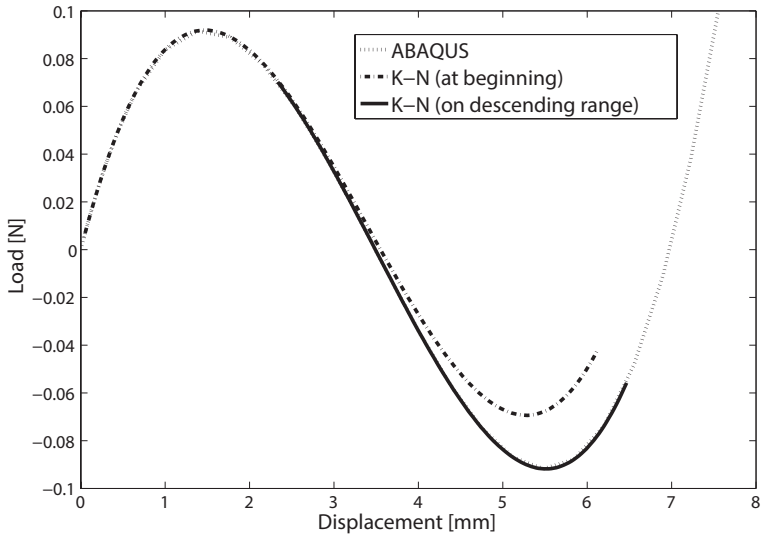

Figure 3.10: Response curves of the beam (b), multiple expansions

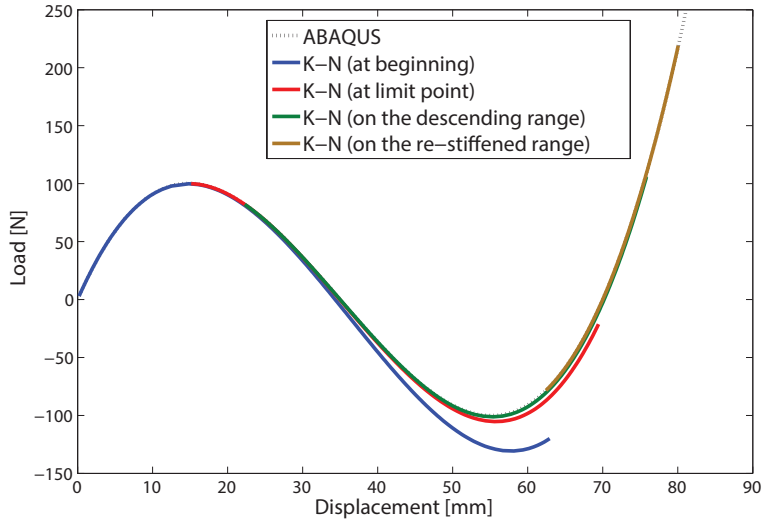

Figure 3.11: Response curves of the beam (c), multiple expansions

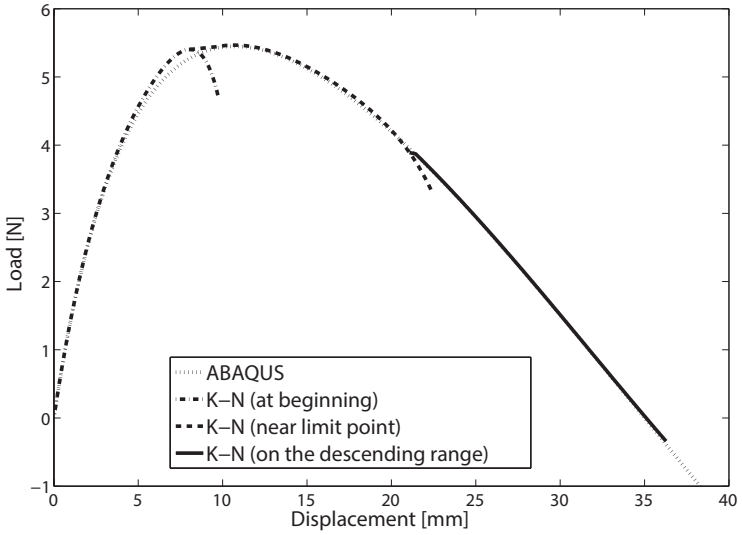

Figure 3.12: Response curves of the beam (d), multiple expansions

Checking the bifurcation points

An axially compressed perfect structure often shows a bifurcation-type buckling. If we apply an asymptotic analysis, the bifurcation point can easily be found. While we may get a limit point instead of the bifurcation point which lies before that limit point by using the nonlinear path-following analysis. Actually, once the bifurcation point has been reached, the initial failure of the perfect structure will be characterized by this bifurcation branch [119]. Hence, the load carrying capability of a structure will be largely overestimated if the bifurcation point is missed during a nonlinear analysis. This case can be avoided by checking the sign of the eigenvalues of the tangent stiffness matrix. Appearance of a negative eigenvalue indicates a bifurcation branch. However, this eigenvalue check is computational expensive due to the typically large tangent stiffness matrix generated from the full finite element model of the structure. One of the advantages of the Koiter-Newton approach is that it can reduce the full nonlinear finite element model with a number of DOFs in the order of 1000 to a reduced order model with a number of DOFs in the order of 10. Then, instead of applying an eigenvalue check on the tangent stiffness generated from the full FE model, we can check the eigenvalues of the tangent stiffness generated from the ROM with a little computational cost.

The above case has applied on beam (c). Fig. 3.9(c) demonstrates that the limit load for beam (c) is roughly 100.24N, however, two bifurcation points exist before that limit point, and both ABAQUS and the Koiter-Newton approach missed these two bifurcation branches. Then, by applying the eigenvalue check for the reduced tangent stiffness matrix generated from the reduced order model, we can find that the first negative eigenvalue appears when the load reaches roughly 20N. The first bifurcation branch is obtained as shown in Fig. 3.13 by applying a small numerical perturbation near this bifurcation point during solving the ROM. ABAQUS can also find this branch by taking into consideration a small perturbation load on the beam.

Although it is not very meaningful in engineering, if we ignore the first branch the second bifurcation branch can also be detected by applying a small numerical perturbation when the second negative eigenvalue appears at load $\approx 70N$, as shown in Fig. 3.13. It demonstrates that the Koiter-Newton approach provides a computational cheap way to detect potential bifurcation points before the limit point, which is unachievable using a general nonlinear finite element analysis.

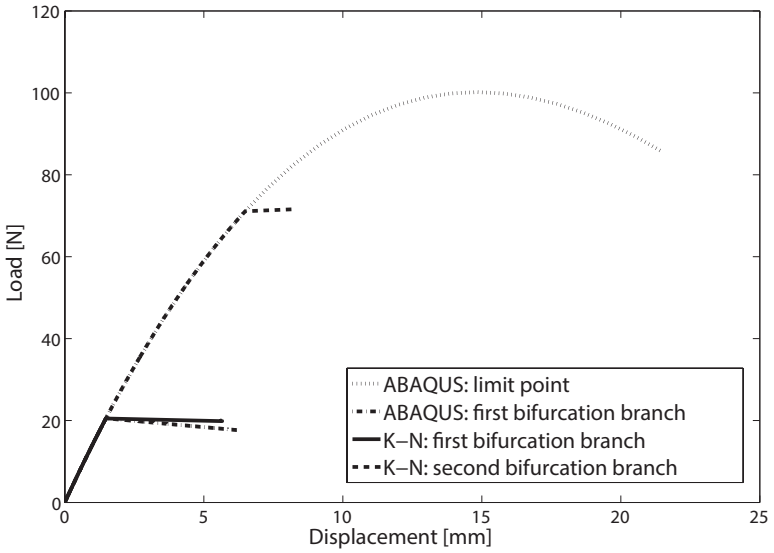

Figure 3.13: Bifurcation branches of the beam c

3.5 Conclusions

In this chapter, the Koiter-Newton approach has been implemented in the beam element based on the co-rotational frame. After differentiating the strain energy to the fourth order with respect to the global degrees of freedom, the equilibrium equations of a third order form is achieved. Then, the reduced order model of the co-rotational beam element is obtained according to the equilibrium equations.

Some numerical examples involving beams are used to evaluate the performance of the Koiter-Newton approach. If prebuckling nonlinearity is mild, a single step is enough to obtain the complete response of the structure satisfactorily up to the maximum load carrying capability, either by buckling or a limit point instability. More steps are needed for structures that show significant prebuckling deformation. A comparison of the results obtained using the Koiter-Newton approach with results obtained using ABAQUS, indicates that the Koiter-Newton approach is automatic, accurate, more efficient and less expensive to use.

Chapter 4

Koiter-Newton analysis using co-rotational shell kinematics

4.1 Introduction

An FE implementation of the Koiter-Newton approach into a co-rotational beam kinematics was presented in chapter 3. In this chapter a more general application of the Koiter-Newton approach will be demonstrated by analyzing shell element based on an element independent co-rotational frame. Compared to a two-dimensional beam element, a shell element is more complicated to describe due to its $3D$ large rotations. As discussed in Argyris's paper [120], infinitesimal rotations in 2D space may be assigned a vectorial identity, however this can not be done for finite rotations. Argyris said that "commutativity, which is one of the three essential properties of a vector, is not satisfied for two or more finite rotations about arbitrary axes in space since the sequential order of their imposition determines in each case a different result and this non-commutativity of finite rotations is, however, not only characteristic of truly large rotations but it holds even when second order effects have to be considered". A large body of work on 3D and finite rotation algebra for the nonlinear analysis of shell structures can be found in the literature [121, 122, 123, 124, 125].

The rest of this chapter is organized as follows. Some basic descriptions about the shell element are introduced. Then, co-rotational shell kinematics are presented.

Next, the equilibrium equations of a third order form for the co-rotational shell element are given, and the technique of automatic differentiations is introduced. Finally, some numerical examples of shell structures are used to assess the performance of the Koiter-Newton approach.

4.2 Some basic descriptions

In the case of the finite rotation, many rules are quite different from those in the case of the infinitesimal rotation, hence a description of finite rotation is given in this section. Three configurations of the shell element are introduced to make the description of the deformation concise, and the basic definition of the deformation gradient tensor is presented.

4.2.1 Finite rotation

In the Cartesian coordinate system, an arbitrary rotation $\boldsymbol{\vartheta} = \{\varphi, \chi, \psi\}$ can be represented by a corresponding rotation matrix R. Then, after rotating a vector $\mathbf{p}$ by $\boldsymbol{\vartheta}$, a new vector $\mathbf{p}'$ can be obtained as [120]:

$$\mathbf{p}' = \mathsf{R}\mathbf{p} \tag{4.1}$$

where the rotation matrix R is an orthogonal matrix, and it is actually a nonlinear function of the rotation $\boldsymbol{\vartheta}$ for the 3D finite rotation.

If a sequence of n successive rotations $\{\boldsymbol{\vartheta}_1, \boldsymbol{\vartheta}_2, ..., \boldsymbol{\vartheta}_n\}$ is applied on the vector $\mathbf{p}$, and the corresponding rotation matrices of them are $\{\mathsf{R}_1, \mathsf{R}_2, ..., \mathsf{R}_n\}$, the final total rotation matrix R of this sequence of rotations can be written as:

$$\mathsf{R} = \mathsf{R}_n \mathsf{R}_{n-1} ... \mathsf{R}_1 \tag{4.2}$$

As mentioned above, the rotation matrix is a nonlinear function of the rotation $\boldsymbol{\vartheta}$ when the rotation is not infinitesimal, which leads to:

$$\mathsf{R} = \exp\left(\widetilde{\boldsymbol{\vartheta}}\right) = \mathsf{I} + \widetilde{\boldsymbol{\vartheta}} + \frac{1}{2!}\widetilde{\boldsymbol{\vartheta}}^2 + \frac{1}{3!}\widetilde{\boldsymbol{\vartheta}}^3 + \dots \tag{4.3}$$

where the matrix I is a 3×3 identity matrix, the operator $\exp(\quad)$ means applying an exponent operation on the matrix in the bracket, and the matrix $\widetilde{\boldsymbol{\vartheta}}$ is an antisymmetric matrix formed by the three components of the rotation vector $\boldsymbol{\vartheta}$, which results in:

$$\widetilde{\boldsymbol{\vartheta}} = \begin{bmatrix} 0 & -\psi & \chi \\ \psi & 0 & -\varphi \\ -\chi & \varphi & 0 \end{bmatrix} \tag{4.4}$$

Eq. (4.3) demonstrates that the rotation matrix can degenerate to the familiar infinitesimal rotation matrix, given by:

$$\mathsf{R} = \mathsf{I} + \widetilde{\boldsymbol{\vartheta}} \tag{4.5}$$

In the case of finite rotations, the derivatives of the rotation matrix R with respect to the three components of the rotation $\boldsymbol{\vartheta}$ can be obtained by differentiating Eq. (4.3). In this procedure, the derivatives of the antisymmetric matrix $\widetilde{\boldsymbol{\vartheta}}$ with respect to these three components are calculated from Eq. (4.4), as follows:

$$\frac{\partial \widetilde{\boldsymbol{\vartheta}}}{\partial \varphi} = \begin{bmatrix} 0 & 0 & 0 \\ 0 & 0 & -1 \\ 0 & 1 & 0 \end{bmatrix}; \quad \frac{\partial \widetilde{\boldsymbol{\vartheta}}}{\partial \chi} = \begin{bmatrix} 0 & 0 & 1 \\ 0 & 0 & 0 \\ -1 & 0 & 0 \end{bmatrix}; \quad \frac{\partial \widetilde{\boldsymbol{\vartheta}}}{\partial \psi} = \begin{bmatrix} 0 & -1 & 0 \\ 1 & 0 & 0 \\ 0 & 0 & 0 \end{bmatrix} \tag{4.6}$$

4.2.2 Three configurations

To make the description of the co-rotational shell concise in later derivations, three configurations during the deformation of the shell element are defined in this thesis, as shown in Fig. 4.1

These three configurations are called the reference configuration, nominal configuration and current configuration, respectively, and defined as follows:

- reference configuration: the initial undeformed configuration of the shell element is the reference configuration.
- nominal configuration: the last known configuration during the deformation of the shell element is the nominal configuration. In the beginning, the nominal

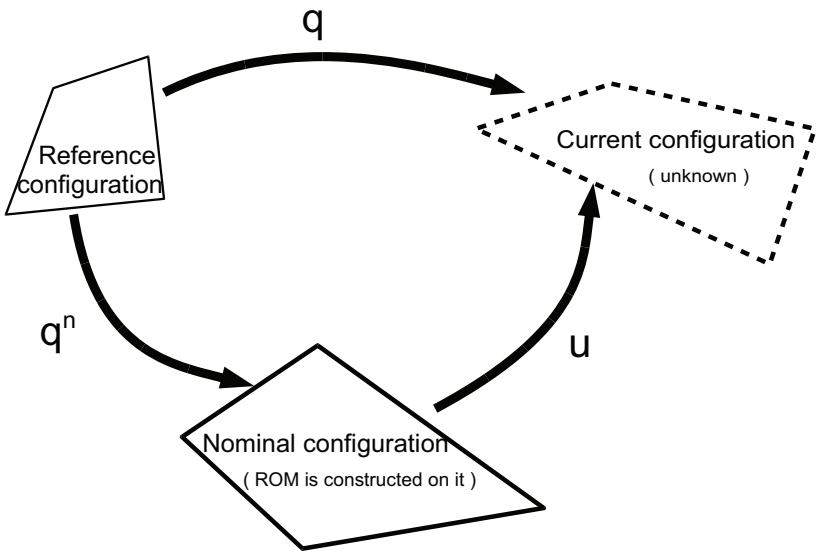

Figure 4.1: Three configurations of the co-rotational shell element

configuration is just the reference configuration. The reduced order model is always constructed on the nominal configuration.

- current configuration: the unknown configuration next to the nominal configuration is the current configuration.

The changes of displacements among these configurations need to be defined: $\mathbf{q}$ is the total displacement from the reference configuration to the current configuration, $\mathbf{q}^n$ is the relative displacement from the reference configuration to the nominal configuration, and $\mathbf{u}$ is the relative displacement from the nominal configuration to the current configuration.

4.2.3 Deformation gradient

A change in the configuration of a continuum body results in a displacement. The displacement of a body has two components: a rigid-body displacement and a deformation, see Fig. 4.2. A rigid-body displacement consists of a simultaneous translation and rotation of the body without changing its shape or size. Deformation

implies a change in shape and/or size of the body from an initial or un-deformed configuration to a current or deformed configuration.

The matrix polar decomposition presents that a square complex matrix, or second-order tensor, is a matrix decomposition of a unitary matrix and a positive semi-definite Hermitian matrix. In the mechanics, the deformation gradient F represents the gradient of the mapping function or functional relation related to both the reference and current configuration, hence like any second-order tensor, the deformation gradient can be decomposed, using the polar decomposition theorem, into a product of two second-order tensors: an orthogonal rotation tensor and a positive definite symmetric deformation tensor, shown in Fig. 4.2, and given by:

$$\mathsf{F} = \mathsf{RU} \tag{4.7}$$

where the orthogonal matrix R which can be called the rotation matrix presents the pure rotation part of the total motion, and the symmetric matrix U named the tension matrix indicates the pure deformation part of the total motion.

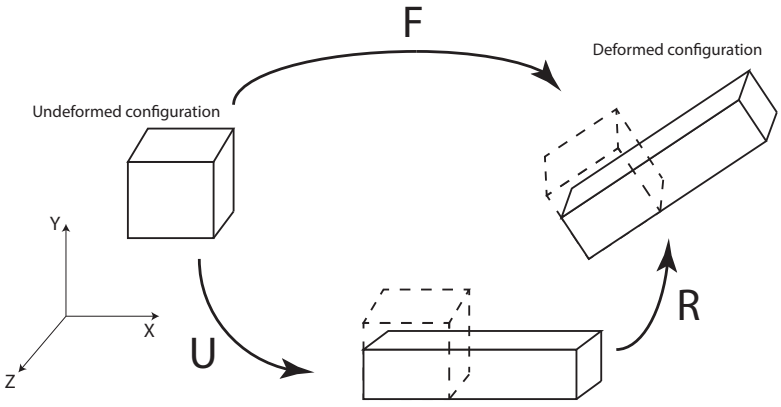

Figure 4.2: Sketch of the polar decomposition of the deformation gradient

4.3 Co-rotational shell kinematics

In this section, we define the deformation gradient and the material coordinate system for a co-rotational shell element, then based on them, the local and global degrees of freedom of the shell element are given.

4.3.1 Decomposition of the deformation gradient for a shell element

A quadrilateral four-node flat shell element with six degrees of freedom per node is used in this chapter. As shown in Fig. 4.3, two configurations of this quadrilateral element during the deformation are defined. The deformation gradient of the element can be obtained from the reference configuration and the nominal configuration of the element. The CR element frames are used to denote the different element configurations. There are many choices of ways to define the element frame, we use the straight lines which connect the middle points of two opposite sides as the coordinate axes 1 and 2, the third axis is naturally orthogonal to the plane formed by the axes 1 and 2. As shown in Fig. 4.3, we assume $\mathsf{T}_0 = \left(\mathbf{d}_1^0, \mathbf{d}_2^0, \mathbf{d}_3^0\right)$ and $\mathsf{T} = (\mathbf{d}_1, \mathbf{d}_2, \mathbf{d}_3)$ as the element frames in the reference configuration and the nominal configuration respectively, then the following relations should be satisfied:

$$\begin{cases} \mathbf{d}_3^0 = \mathbf{d}_1^0 \times \mathbf{d}_2^0 \\ \\ \mathbf{d}_3 = \mathbf{d}_1 \times \mathbf{d}_2 \end{cases} \tag{4.8}$$

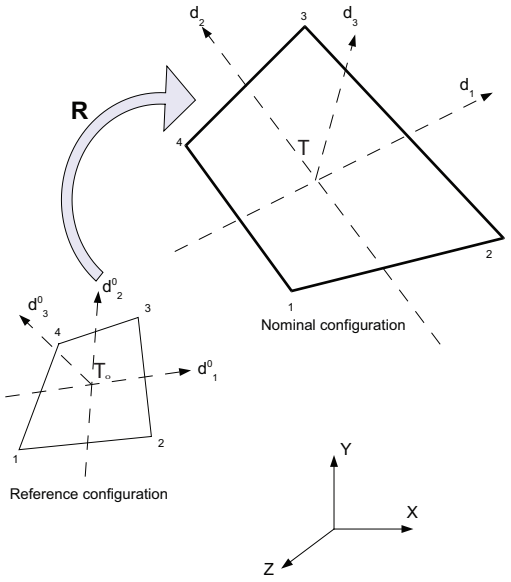

Figure 4.3: Sketch of the element coordinate systems

In order to find the deformation gradient, we assume that two arbitrary vectors, $\mathbf{a}^0$ and $\mathbf{a}$, are located in the reference and nominal configurations respectively, and that they are in the same position relative to the element coordinate systems. Then, the deformation gradient is just the mapping function related to these two vectors. The two vectors, $\mathbf{a}^0$ and $\mathbf{a}$, can be expressed as:

$$\begin{cases} \mathbf{a}^0 = a_1\mathbf{d}_1^0 + a_2\mathbf{d}_2^0 + a_3\mathbf{d}_3^0 \\ \mathbf{a} = a_1\mathbf{d}_1 + a_2\mathbf{d}_2 + a_3\mathbf{d}_3 \end{cases} \tag{4.9}$$

where the a_1, a_2, a_3 are the components of the coordinates.

Based on Eq. (4.9), the vector $\mathbf{a}$ can be expressed by the vector $\mathbf{a}^0$:

$$\mathbf{a} = \{\mathbf{d}_1, \mathbf{d}_2, \mathbf{d}_3\} \left\{\mathbf{d}_1^0, \mathbf{d}_2^0, \mathbf{d}_3^0\right\}^{-1} \mathbf{a}^0 \tag{4.10}$$

According to the definition of the deformation gradient, the deformation gradient in this case can be presented as:

$$\mathsf{F} = \{\mathbf{d}_1, \mathbf{d}_2, \mathbf{d}_3\} \left\{\mathbf{d}_1^0, \mathbf{d}_2^0, \mathbf{d}_3^0\right\}^{-1} \tag{4.11}$$

To obtain the symmetric matrix U which indicates the pure deformation part of the element motion, we can multiply F^t on both sides of Eq. (4.7), which leads to:

$$\mathsf{F}^t\mathsf{F} = \mathsf{F}^t\mathsf{R}\mathsf{U} = \mathsf{U}\mathsf{R}^t\mathsf{R}\mathsf{U} = \mathsf{U}\mathsf{U} \tag{4.12}$$

where the fact that $\mathsf{R}^t\mathsf{R} = \mathsf{I}$ is used.

After obtaining the matrix U, introducing it into Eq. (4.7) the rotation matrix R can be achieved by:

$$\mathsf{R} = \mathsf{F}\mathsf{U}^{-1} \tag{4.13}$$

4.3.2 Material coordinate system

The definition of the material coordinate system for an isotropic material does not affect the final results, however, the material coordinate system of an element is very important for an anisotropic material which is often used in the composites. Since we choose to use the Total-Lagrange formula to describe the large deformation, the material coordinate system can be defined only once on the reference configuration. The primary direction of the material is defined by the user to be $\mathbf{e}_m^0$. According to the element frame T_0 established on the reference configuration, the normal direction of the element is $\mathbf{n}_0$, which given by:

$$\mathbf{n}^0 = \frac{\mathbf{d}_1^0 \times \mathbf{d}_2^0}{\|\mathbf{d}_1^0 \times \mathbf{d}_2^0\|} \tag{4.14}$$

where the normal direction $\mathbf{n}^0$ is just the third axis of the material coordinate system.

The second axis can be obtained by the cross product of the normal direction and the primary direction, leading to:

$$\mathbf{e}_2^0 = \frac{\mathbf{n}^0 \times \mathbf{e}_m^0}{\|\mathbf{n}^0 \times \mathbf{e}_m^0\|} \tag{4.15}$$

Then, the first axis of the material coordinate system can also be achieved by:

$$\mathbf{e}_1^0 = \mathbf{e}_2^0 \times \mathbf{n}^0 \tag{4.16}$$

Finally, the material coordinate system of the element can be written as a matrix:

$$\mathsf{T}_0 = \begin{bmatrix} \mathbf{e}_1^0 & \mathbf{e}_2^0 & \mathbf{n}^0 \end{bmatrix} \tag{4.17}$$

where the element frame T_0 in the reference configuration can be chose to be the material coordinate system of the element, which can make the element also available for the anisotropic material.

4.3.3 Local degrees of freedom

The global and local degrees of freedom of this shell element are expressed by two 24 by 1 vectors, $\mathbf{q}$ and $\widehat{\mathbf{q}}$, respectively. The global degrees of freedom are the degrees of freedom under the global coordinate system $\mathsf{T}_g = (\mathbf{X}, \mathbf{Y}, \mathbf{Z})$ in Fig. 4.3, and the local degrees of freedom are generated from the global degrees of freedom in a co-rotational shell frame.

For a convenient description, the global and local degrees of freedom are divided into two parts, the translation part and the rotation part. For each node a ($a = 1, 2, 3, 4$), the 3 by 1 vectors $\overline{\mathbf{u}}_a$ and $\boldsymbol{\theta}_a$ denote the translation and rotation part of the global degrees of freedom, respectively, and $\widehat{\overline{\mathbf{u}}}_a$ and $\widehat{\boldsymbol{\theta}}_a$ are the corresponding translation and rotation part of the local degrees of freedom, respectively. The local translations $\widehat{\overline{\mathbf{u}}}_a$ and the local rotations $\widehat{\boldsymbol{\theta}}_a$ in the local DOFs are respectively presented in the following two parts.

Local translations

We can assume a vector $\mathbf{r}_a^0$ under the global frame T_g to be the position vector of the node a on the reference configuration in Fig. 4.3, and $\overline{\mathbf{u}}_a$ is a global translation of this vector from the reference configuration to the nominal configuration, hence the position of the new vector on the nominal configuration is $\mathbf{r}_a^0 + \overline{\mathbf{u}}_a$. Then, $\mathsf{T}^t(\mathbf{r}_a^0 + \overline{\mathbf{u}}_a)$ is the local position of this new vector under the nominal frame T, which should be equal to:

$$\mathsf{T}^t(\mathbf{r}_a^0 + \overline{\mathbf{u}}_a) = \mathsf{T}_0^t \mathbf{r}_a^0 + \widehat{\overline{\mathbf{u}}}_a \tag{4.18}$$

where $\mathsf{T}_0^t \mathbf{r}_a^0$ is the local position of the initial vector $\mathbf{r}_a^0$ under the reference configuration, and $\widehat{\overline{\mathbf{u}}}_a$ is the local translation.

The reference frame T_0 and the nominal frame T satisfy the following relationship:

$$\mathsf{T} = \mathsf{R}\mathsf{T}_0 \tag{4.19}$$

Substituting Eq. (4.19) into Eq. (4.18), the expression of the local translation $\widehat{\overline{\mathbf{u}}}_a$ is obtained:

$$\widehat{\overline{\mathbf{u}}}_a = \mathsf{T}_0^t \mathsf{R}^t \overline{\mathbf{u}}_a + \mathsf{T}_0^t (\mathsf{R}^t - \mathsf{I}) \mathsf{T}_0 \mathsf{T}_0^t \mathbf{r}_a^0 \tag{4.20}$$

where R is the rotation matrix, and $\mathbf{r}_a^0, a = 1, 2, 3, 4$ is the position vector of each node in the initial undeformed configuration. We can choose T_0 to be the material coordinate system defined in Eq. (4.17).

The local translations of each node are picked up from the local degrees of freedom, and are given by:

$$\{\widehat{q}_1, \widehat{q}_2, \widehat{q}_3, \cdots, \widehat{q}_7, \widehat{q}_8, \widehat{q}_9, \cdots, \widehat{q}_{13}, \widehat{q}_{14}, \widehat{q}_{15}, \cdots, \widehat{q}_{19}, \widehat{q}_{20}, \widehat{q}_{21}, \cdots\}^t \tag{4.21}$$

According to Eq. (4.20), the three local translations of each node can be expressed as:

$$\left\{ \begin{array}{c} \widehat{q}_i \\ \widehat{q}_{i+1} \\ \widehat{q}_{i+2} \end{array} \right\} = \mathsf{T}_0^t \mathsf{R}^t \left\{ \begin{array}{c} q_i \\ q_{i+1} \\ q_{i+2} \end{array} \right\} + \mathsf{T}_0^t \left(\mathsf{R}^t - \mathsf{I} \right) \mathsf{T}_0 \mathsf{T}_0^t \mathbf{r}_{(i+5)/6}^0 \tag{4.22}$$

where $i = 1, 7, 13, 19$, and q_i, q_{i+1}, q_{i+2} are the global translations for each node.

Local rotations

The local rotations in the local degrees of freedom are discussed as follows. To make the description for the rotation part easier, three configurations were introduced in subsection 4.2.2. Based on these three configurations, the global degrees of freedom $\mathbf{q}$ can be divided into two parts, which are the relative displacement $\mathbf{q}^n$ from the reference configuration to the nominal configuration and the relative displacement $\mathbf{u}$ from the nominal configuration to the current configuration, as given by:

$$\mathbf{q} = \mathbf{q}^n \circ \mathbf{u} \tag{4.23}$$

where as mentioned in Eq. (2.2) the composition $\circ$ is not a simple addition in the case of finite rotations, and will depend on the parametrisation of rotations.

In Fig. 4.4, R is the average global rotation matrix for the shell element, and the four nodes also possess their own global rotation matrix R_a, $a = 1, 2, 3, 4$. $\boldsymbol{\theta}_a$ and

$\widehat{\boldsymbol{\theta}}_a$ are used to denote the global and local rotation vector of node a, respectively. Then, the local rotation matrix $\widehat{\mathsf{R}}_a^0$ related to the local rotation $\widehat{\boldsymbol{\theta}}_a$ of node a under the reference configuration can be expressed as:

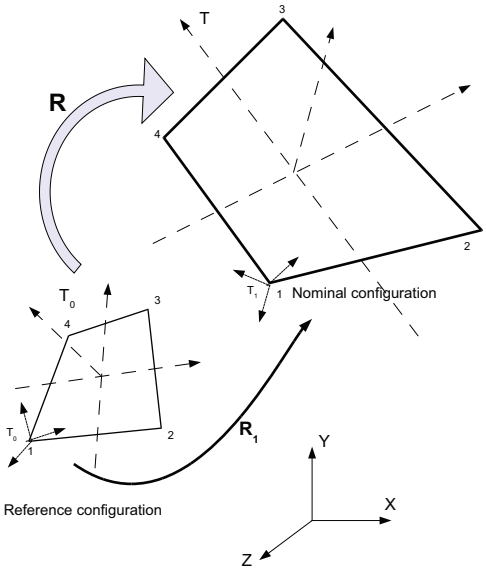

Figure 4.4: Sketch of the element rotations

$$\widehat{\mathsf{R}}_a^0 = \mathsf{T}_0^t \mathsf{R}^t \mathsf{R}_a \mathsf{T}_0 = \exp\left(\widetilde{\widehat{\boldsymbol{\theta}}}_a\right) \tag{4.24}$$

where the operator exp( ) means applying an exponent operation on the matrix in the bracket, and the fact of Eq. (4.3) is used.

In Eq. (4.24), the anti-symmetric matrix $\widetilde{\widehat{\boldsymbol{\theta}}}_a$ is formed by the three components in the local rotation vector $\widehat{\boldsymbol{\theta}}_a$, as shown in Eq. (4.4).

The global rotation $\boldsymbol{\theta}_a$ from the reference to the current configuration may be a finite rotation, while the corresponding local rotation after removing the rigid motion can seem to be infinitesimal small. Thus, the local rotation matrix $\widehat{\mathsf{R}}_a^0$ is rewritten as the following form according to Eq. (4.5):

$$\widehat{\mathsf{R}}_a^0 = \mathsf{T}_0^t \mathsf{R}^t \mathsf{R}_a \mathsf{T}_0 = \exp\left(\widetilde{\widehat{\boldsymbol{\theta}}}_a\right) \approx \mathsf{I} + \widetilde{\widehat{\boldsymbol{\theta}}}_a \tag{4.25}$$

where I is a 3 by 3 identity matrix.

Since any matrix can be written as the summation of a symmetric matrix and anti-symmetric matrix, the anti-symmetric part of the local rotation matrix $\widehat{\mathsf{R}}_a^0$ should be equal to the anti-symmetric matrix $\widetilde{\widehat{\boldsymbol{\theta}}}_a$ in Eq. (4.25), which leads to:

$$\widetilde{\widehat{\boldsymbol{\theta}}}_a = \left[\widehat{\mathsf{R}}_a^0\right] = \left[\mathsf{T}_0^t \mathsf{R}^t \mathsf{R}_a \mathsf{T}_0\right] \tag{4.26}$$

where the operator [ ] means picking up the anti-symmetric part of the matrix in the bracket.

In Eq. (4.26), the global rotation matrix R_a is related to the global rotation $\boldsymbol{\theta}_a$ of each node and is composed of two rotations which are the rotation $\boldsymbol{\theta}_a^n$ between the reference and nominal configurations and the rotation $\boldsymbol{\vartheta}_a$ between the nominal and current configurations. Since these rotations may be finite rotations, the composition here is not a simple addition and it results in:

$$\mathsf{R}_a = \exp\left(\widetilde{\boldsymbol{\vartheta}}_a\right) \exp\left(\widetilde{\boldsymbol{\theta}}_a^n\right) \tag{4.27}$$

Introducing Eq. (4.27) into Eq. (4.26), the anti-symmetric matrix $\widetilde{\widehat{\boldsymbol{\theta}}}_a$ formed by the three components of the local rotation vector $\widehat{\boldsymbol{\theta}}_a$ of the node a can be rewritten as:

$$\widetilde{\widehat{\boldsymbol{\theta}}}_a = \left[\mathsf{T}_0^t \mathsf{R}^t \exp\left(\widetilde{\boldsymbol{\vartheta}}_a\right) \exp\left(\widetilde{\boldsymbol{\theta}}_a^n\right) \mathsf{T}_0\right] \tag{4.28}$$

Then according to Eq. (4.4), the local rotation vector $\widehat{\boldsymbol{\theta}}_a$ can be obtained by its corresponding anti-symmetric matrix $\widetilde{\widehat{\boldsymbol{\theta}}}_a$, given by:

$$\widehat{\boldsymbol{\theta}}_a = \left[\mathsf{T}_0^t \mathsf{R}^t \exp\left(\widetilde{\boldsymbol{\vartheta}}_a\right) \exp\left(\widetilde{\boldsymbol{\theta}}_a^n\right) \mathsf{T}_0\right]^X \tag{4.29}$$

where the operator $[\ ]^X$ means picking up the anti-symmetric part of the matrix in the bracket and then generating a vector using the three independent components

of this anti-symmetric matrix.

4.4 Equilibrium equations in a third order form

The strain energy of the shell element in a co-rotational frame is obtained, then the $\mathcal{L}$, $\mathcal{Q}$ and $\mathcal{C}$ in the equilibrium equations of a third order form can be obtained by differentiating the strain energy with respect to the global degrees of freedom. To achieve these differentiations, the derivatives of the local degrees of freedom with respect to the global degrees of freedoms are presented in detail.

4.4.1 Strain energy of the co-rotational shell element

In a co-rotational frame, the element strain energy only depends on the local degrees of freedom $\widehat{\mathbf{q}}$ which cause the deformational part of the total motion, given by:

$$\overline{U} = \frac{1}{2}\widehat{\boldsymbol{\varepsilon}}^t \mathsf{C} \widehat{\boldsymbol{\varepsilon}} = \frac{1}{2}\widehat{\mathbf{q}}^t \mathsf{K}_L \widehat{\mathbf{q}} \tag{4.30}$$

where the vector $\widehat{\boldsymbol{\varepsilon}}$ is the local strain of the element, the matrix C is the material matrix, and K_L is the linear stiffness matrix of a quadrilateral element. In the present work, this quadrilateral element is formed by assembling four triangular flat elements and merging the middle node. The triangular flat element and the assembly technique are introduced in appendix A.

From Eq. (4.30), it can be seen that the element strain energy $\overline{U}$ is a quadratic function of the local degrees of freedom $\widehat{\mathbf{q}}$, hence we can differentiate $\overline{U}$ up to the second order form, as follows:

$$\frac{\partial \overline{U}}{\partial \widehat{\mathbf{q}}} = \mathsf{K}_L \widehat{\mathbf{q}} = \widehat{\mathbf{f}} \tag{4.31}$$

$$\frac{\partial^2 \overline{U}}{\partial \widehat{\mathbf{q}}^2} = \mathsf{K}_L \tag{4.32}$$

where the first and second order derivatives of the strain energy are the local internal load $\widehat{\mathbf{f}}$ and linear stiffness matrix K_L, respectively.

Substituting Eqs. (4.31) and (4.32) into Eqs. (3.9) $\sim$ (3.12), we can obtain the components of the internal load vector $\mathbf{f}$, tangent stiffness matrix L, three-dimensional matrix Q and four-dimensional matrix C in the equilibrium equations (2.8) for the shell element, as follows:

$$f_p = \frac{\partial \overline{U}}{\partial q_p} = \widehat{\mathbf{f}} \frac{\partial \widehat{q}_m}{\partial q_p} \tag{4.33}$$

$$L_{pi} = \mathsf{K}_L \frac{\partial \widehat{q}_n}{\partial q_i} \frac{\partial \widehat{q}_m}{\partial q_p} + \widehat{\mathbf{f}} \frac{\partial^2 \widehat{q}_m}{\partial q_p \partial q_i} \tag{4.34}$$

$$\begin{aligned} 2Q_{pij} =& \mathsf{K}_L \frac{\partial^2 \widehat{q}_n}{\partial q_i \partial q_j} \frac{\partial \widehat{q}_m}{\partial q_p} + \mathsf{K}_L \frac{\partial \widehat{q}_n}{\partial q_i} \frac{\partial^2 \widehat{q}_m}{\partial q_p \partial q_j} \\ &+ \mathsf{K}_L \frac{\partial \widehat{q}_n}{\partial q_j} \frac{\partial^2 \widehat{q}_m}{\partial q_p \partial q_i} + \widehat{\mathbf{f}} \frac{\partial^3 \widehat{q}_m}{\partial q_p \partial q_i \partial q_j} \end{aligned} \tag{4.35}$$

$$\begin{aligned} 6C_{pijk} =& \mathsf{K}_L \frac{\partial^3 \widehat{q}_n}{\partial q_i \partial q_j \partial q_k} \frac{\partial \widehat{q}_m}{\partial q_p} + \mathsf{K}_L \frac{\partial^2 \widehat{q}_n}{\partial q_i \partial q_j} \frac{\partial^2 \widehat{q}_m}{\partial q_p \partial q_k} \\ &+ \mathsf{K}_L \frac{\partial^2 \widehat{q}_n}{\partial q_i \partial q_k} \frac{\partial^2 \widehat{q}_m}{\partial q_p \partial q_j} + \mathsf{K}_L \frac{\partial \widehat{q}_n}{\partial q_i} \frac{\partial^3 \widehat{q}_m}{\partial q_p \partial q_j \partial q_k} \\ &+ \mathsf{K}_L \frac{\partial^2 \widehat{q}_n}{\partial q_j \partial q_k} \frac{\partial^2 \widehat{q}_m}{\partial q_p \partial q_i} + \mathsf{K}_L \frac{\partial \widehat{q}_n}{\partial q_j} \frac{\partial^3 \widehat{q}_m}{\partial q_p \partial q_i \partial q_k} \\ &+ \mathsf{K}_L \frac{\partial \widehat{q}_n}{\partial q_k} \frac{\partial^3 \widehat{q}_m}{\partial q_p \partial q_i \partial q_j} + \widehat{\mathbf{f}} \frac{\partial^4 \widehat{q}_m}{\partial q_p \partial q_i \partial q_j \partial q_k} \end{aligned} \tag{4.36}$$

where the subscripts p, i, j, k, m and n run from 1 to 24, and the summation convention is applied on m and n.

In Eqs. (4.33) $\sim$ (4.36) the unknowns are the derivatives of the local degrees of freedoms $\widehat{\mathbf{q}}$ with respect to the global degrees of freedom $\mathbf{q}$. Since the description of the shell element is more complicated, we can split the local degrees of freedom $\widehat{\mathbf{q}}$ into two parts, translations and rotations, and then calculate the derivatives of these two parts respectively.

4.4.2 Derivatives of the local translations with respect to the global degrees of freedom

The derivatives of the local translations (4.22) with respect to the global degrees of freedom are presented in this subsection. The first order derivative of the local translations with respect to the global degrees of freedom will be introduced below, and the second to forth order derivatives can be easily achieved in the same way.

The first order derivative of the local degrees of freedom $\widehat{\mathbf{q}}$ with respect to the global degrees of freedom $\mathbf{q}$ is a 24×24 matrix, the components of which are $\dfrac{\partial \widehat{q}_i}{\partial q_j}$. In this subsection, we only list the components that are related to the local translations, which results in:

$$\begin{Bmatrix} \dfrac{\partial \widehat{q}_i}{\partial q_j} \\ \dfrac{\partial \widehat{q}_{i+1}}{\partial q_j} \\ \dfrac{\partial \widehat{q}_{i+2}}{\partial q_j} \end{Bmatrix} = \mathsf{T}_0^t \frac{\partial \mathsf{R}^t}{\partial q_j} \begin{Bmatrix} q_i \\ q_{i+1} \\ q_{i+2} \end{Bmatrix} + \mathsf{T}_0^t \mathsf{R}_0^t \frac{\partial \begin{Bmatrix} q_i \\ q_{i+1} \\ q_{i+2} \end{Bmatrix}}{\partial q_j} + \mathsf{T}_0^t \frac{\partial \mathsf{R}^t}{\partial q_j} \mathsf{T}_0 \mathsf{T}_0^t \mathbf{r}^0_{(i+5)/6} \quad (4.37)$$

where i equals 1, 7, 13 and 19 respectively and j runs from 1 to 24 automatically for each of i.

The term $\mathsf{R}_0^t \dfrac{\partial \begin{Bmatrix} q_i \\ q_{i+1} \\ q_{i+2} \end{Bmatrix}}{\partial q_j}$ in Eq. (4.37) can be obtained as follows:

$$\mathsf{R}_0^t \frac{\partial \begin{Bmatrix} q_i \\ q_{i+1} \\ q_{i+2} \end{Bmatrix}}{\partial q_j} = \begin{cases} \{1,0,0\}^t, & if \quad j = i \\ \{0,1,0\}^t, & if \quad j = i+1 \\ \{0,0,1\}^t, & if \quad j = i+2 \\ \{0,0,0\}^t, & if \quad j = others \end{cases} \quad (4.38)$$

The component of the first derivative of the rotation matrix R with respect to the

global degrees of freedom $\mathbf{q}$, that is the $\dfrac{\partial \mathsf{R}^t}{\partial q_j}$, is calculated as follows.

First, we differentiate both sides of Eq. (4.7) with respect to the global degrees of freedom, and then multiply the transpose of the rotation matrix R^t on both sides, which results in:

$$\mathsf{R}^t \frac{\partial \mathsf{F}}{\partial q_j} = \mathsf{R}^t \frac{\partial \mathsf{R}}{\partial q_j}\mathsf{U} + \frac{\partial \mathsf{U}}{\partial q_i} \tag{4.39}$$

where the fact of $\mathsf{R}^t\mathsf{R} = \mathsf{I}$ is used, since the rotation matrix R is an orthogonal matrix.

Any matrix can be written as a summation of a symmetric matrix and an anti-symmetric matrix. The derivatives of the symmetric matrix U is still a symmetric matrix, which indicates that the anti-symmetric part of Eq. (4.39) is given by:

$$\left[\mathsf{R}^t \frac{\partial \mathsf{R}}{\partial q_j}\mathsf{U}\right] = \left[\mathsf{R}^t \frac{\partial \mathsf{F}}{\partial q_j}\right] \tag{4.40}$$

where the operator [ ] is used to pick up the anti-symmetric part of the matrix in the bracket.

we use P to indicate the matrix $\mathsf{R}^t \dfrac{\partial \mathsf{F}}{\partial q_j}$ in the right hand side of Eq. (4.40), that is:

$$\mathsf{P} = \mathsf{R}^t \frac{\partial \mathsf{F}}{\partial q_j} \tag{4.41}$$

where the term $\dfrac{\partial \mathsf{F}}{\partial q_j}$ is achieved by differentiating Eq. (4.11), as given by:

$$\frac{\partial \mathsf{F}}{\partial q_j} = \left\{\frac{\partial \mathbf{d}_1}{\partial q_j}, \frac{\partial \mathbf{d}_2}{\partial q_j}, \frac{\partial \mathbf{d}_3}{\partial q_j}\right\} \left\{\mathbf{d}_1^0, \mathbf{d}_2^0, \mathbf{d}_3^0\right\}^{-1} \tag{4.42}$$

where the term $\left\{\dfrac{\partial \mathbf{d}_1}{\partial q_j}, \dfrac{\partial \mathbf{d}_2}{\partial q_j}, \dfrac{\partial \mathbf{d}_3}{\partial q_j}\right\}$ can be easily obtained by the geometry and deformation relations.

The matrix $\mathsf{R}^t\dfrac{\partial \mathsf{R}}{\partial q_j}$ in the left hand side of Eq. (4.40) is an anti-symmetric matrix, and this conclusion is obtained by differentiating the equation $\mathsf{R}^t\mathsf{R} = \mathsf{I}$ on both sides, which is given as:

$$\frac{\partial \mathsf{R}^t}{\partial q_j}\mathsf{R} + \mathsf{R}^t\frac{\partial \mathsf{R}}{\partial q_j} = 0 \Rightarrow \mathsf{R}^t\frac{\partial \mathsf{R}}{\partial q_j} = -\left(\mathsf{R}^t\frac{\partial \mathsf{R}}{\partial q_j}\right)^t \tag{4.43}$$

Hence, The matrix $\mathsf{R}^t\dfrac{\partial \mathsf{R}}{\partial q_j}$ can be represented by a anti-symmetric matrix S_j, as:

$$\mathsf{S}_j = \mathsf{R}^t\frac{\partial \mathsf{R}}{\partial q_j} = \begin{bmatrix} 0 & s_{1j} & s_{2j} \\ -s_{1j} & 0 & s_{3j} \\ -s_{2j} & -s_{3j} & 0 \end{bmatrix} \tag{4.44}$$

where s_{1j}, s_{2j} and s_{3j} are the three independent components in this anti-symmetric matrix S_j.

Any anti-symmetric matrix can be expressed by the three independent components, hence the independent components of the two anti-symmetric matrices in Eq. (4.40) should be equal, which leads to a linear system of equations:

$$\begin{bmatrix} U_{11}+U_{22} & U_{23} & -U_{13} \\ U_{23} & U_{11}+U_{33} & U_{12} \\ -U_{13} & U_{12} & U_{22}+U_{33} \end{bmatrix} \begin{Bmatrix} s_{1j} \\ s_{2j} \\ s_{3j} \end{Bmatrix} = \begin{Bmatrix} P_{12}-P_{21} \\ P_{13}-P_{31} \\ P_{23}-P_{32} \end{Bmatrix} \tag{4.45}$$

where the U_{11}, U_{22}, U_{33}, U_{12}, U_{13} and U_{23} are the components of the symmetric matrix U, and P_{12}, P_{21}, P_{13}, P_{31}, P_{23} and P_{32} are the components of the matrix P defined in Eq. (4.41).

After solving this linear system of equations (4.45) and introducing the solution vector $\{s_{1j}, s_{2j}, s_{3j}\}$ into Eq. (4.44), we can obtain the anti-symmetric matrix S_j. Then, according to Eq. (4.44), the component of the first derivative of the rotation matrix with respect to the global degrees of freedom, $\dfrac{\partial \mathsf{R}^t}{\partial q_j}$, is achieved by:

$$\frac{\partial \mathsf{R}^t}{\partial q_j} = \mathsf{R}\mathsf{S}_j \tag{4.46}$$

Finally, introducing Eqs. (4.38) and (4.46) into Eq. (4.37), the first order derivative of the local translations with respect to the global degrees of freedom $\mathbf{q}$ is obtained.

4.4.3 Derivatives of the local rotations with respect to the global degrees of freedom

Based on the expression of the local rotation, the derivatives of the local rotation with respect to the global degrees of freedom can be achieved. From Eq. (4.29), it can be seen that the local rotation vector $\widehat{\boldsymbol{\theta}}_a$ is related to both the rotations and the translations involved in the global rotation matrix R. Since the reduced order model is constructed on the known nominal configuration, the relative displacement $\mathbf{u}$ between the nominal and current configurations should be set to be zero in the derivatives. Here, the first and second order derivatives of the local rotation with respect to the global degrees of freedom are listed below, and the other high order derivatives can be obtained in the same way.

The first order derivative of the local degrees of freedom $\widehat{\mathbf{q}}$ with respect to the global degrees of freedom $\mathbf{q}$ is a 24×24 matrix, the components of which are $\dfrac{\partial \widehat{q}_i}{\partial q_j}$. The components related to the local translations have already been obtained using Eq. (4.37). Here, we only list the components that are related to the local rotations, which results in:

$$\left\{ \begin{array}{c} \dfrac{\partial \widehat{q}_i}{\partial q_j} \\ \\ \dfrac{\partial \widehat{q}_{i+1}}{\partial q_j} \\ \\ \dfrac{\partial \widehat{q}_{i+2}}{\partial q_j} \end{array} \right\} = \left[\mathsf{T}_0^t \left\{ \mathsf{R}_{,j}^t \exp\left(\widetilde{\boldsymbol{\vartheta}}_{(i+2)/6}\right) + \mathsf{R}^t \exp\left(\widetilde{\boldsymbol{\vartheta}}_{(i+2)/6}\right)_{,j} \right\} \exp\left(\widetilde{\boldsymbol{\theta}}^n_{(i+2)/6}\right) \mathsf{T}_0 \right]^X \tag{4.47}$$

where the subscript i equals 4, 10, 16, 12 respectively to denote only the rotation component, while j runs from 1 to 24.

In Eq. (4.47), the derivatives $\mathsf{R}_{,j}$ of the element average rotation matrix with respect to the global degrees of freedom can be obtained by Eq. (4.46). The matrix operator

$\exp(\quad)$ and its derivatives were introduced in subsection 4.2.1. When j runs from 1 to 24 the two terms in the brace of the right hand side of Eq. (4.47) will not always be nonzeros. The following three cases should be considered.

1. If the value of j is related to the translations, only the first term $\mathsf{R}^t_{,j} \exp\left(\widetilde{\boldsymbol{\vartheta}}_{(i+2)/6}\right)$ is nonzero due to the value of $\exp\left(\widetilde{\boldsymbol{\vartheta}}_{(i+2)/6}\right)_{,j}$ in the second term is equal to zero.

2. If the value of j is related to the rotations and also equal to the current rotation $i, i+1, i+2$, only the second term $\mathsf{R}^t \exp\left(\widetilde{\boldsymbol{\vartheta}}_{(i+2)/6}\right)_{,j}$ is nonzero due to the value of $\mathsf{R}^t_{,j}$ in the first term is equal to zero.

3. If the value of j is equal to other values, both of the terms are zero.

The second order derivative of the local degrees of freedom $\widehat{\mathbf{q}}$ with respect to the global degrees of freedom $\mathbf{q}$ is a three dimensional $24 \times 24 \times 24$ matrix, and we can use $\dfrac{\partial^2 \widehat{q}_i}{\partial q_j \partial q_k}$ to express its components. The components that are related to the local rotations are:

$$\left\{ \begin{array}{c} \dfrac{\partial^2 \widehat{q}_i}{\partial q_j \partial q_k} \\ \dfrac{\partial^2 \widehat{q}_{i+1}}{\partial q_j \partial q_k} \\ \dfrac{\partial^2 \widehat{q}_{i+2}}{\partial q_j \partial q_k} \end{array} \right\} = \left[\mathsf{T}^t_0 \left\{ \begin{array}{l} \mathsf{R}^t_{,jk} \exp\left(\widetilde{\boldsymbol{\vartheta}}_{(i+2)/6}\right) \\ + \mathsf{R}^t_{,j} \exp\left(\widetilde{\boldsymbol{\vartheta}}_{(i+2)/6}\right)_{,k} \\ + \mathsf{R}^t_{,k} \exp\left(\widetilde{\boldsymbol{\vartheta}}_{(i+2)/6}\right)_{,j} \\ + \mathsf{R}^t \exp\left(\widetilde{\boldsymbol{\vartheta}}_{(i+2)/6}\right)_{,jk} \end{array} \right\} \exp\left(\widetilde{\boldsymbol{\theta}}^n_{(i+2)/6}\right) \mathsf{T}_0 \right]^X \tag{4.48}$$

where the subscript i equals 4, 10, 16, 12 respectively to denote only the rotation component, while j, k runs from 1 to 24. The second derivatives $\mathsf{R}_{,jk}$ of the element average rotation matrix with respect to the global degrees of freedom can be achieved in the same way as that used in Eq. (4.46).

In Eq. (4.48), five cases should be taken into account to check whether the four terms in the brace of the right hand side of Eq. (4.48) are all zeros or not.

1. If the values of j and k are related to the translations, only the first term $\mathsf{R}^t_{,jk} \exp\left(\widetilde{\boldsymbol{\vartheta}}_{(i+2)/6}\right)$ is nonzero.

2. If the value of j is related to the translations and k is equal to the current rotation $i, i+1, i+2$, only the second term $\mathsf{R}^t_{,j} \exp\left(\widetilde{\boldsymbol{\vartheta}}_{(i+2)/6}\right)_{,k}$ is nonzero.

3. If the value of k is related to the translations and j is equal to the current rotation $i, i+1, i+2$, only the third term $\mathsf{R}^t_{,k} \exp\left(\widetilde{\boldsymbol{\vartheta}}_{(i+2)/6}\right)_{,j}$ is nonzero.

4. If the values of j and k are all equal to the current rotation $i, i+1, i+2$, only the fourth term $\mathsf{R}^t \exp\left(\widetilde{\boldsymbol{\vartheta}}_{(i+2)/6}\right)_{,jk}$ is nonzero.

5. If the values of j and k are equal to other values, all of the four terms in the brace are zero.

Up to this point, the derivatives of the local degrees of freedom with respect to the global degrees of freedom are obtained by combining both the translation part and the rotation part. Introducing them into the Eqs. (4.33) $\sim$ (4.36), the equilibrium equations (2.8) of the shell element in a co-rotational frame are achieved. Then, the reduced order model of the CR shell element can be constructed using the $\mathcal{L}$, $\mathcal{Q}$ and $\mathcal{C}$ in the equilibrium equations (2.8).

4.5 Automatic differentiation

From section 4.4, it can be seen that we need to obtain many high order, to fourth order, differentiations for some variables. In order to make the codes more concise and faster an automatic differentiation technology [126] is adopted in the Matlab codes. In Tsukanov's paper [126] the data structure and algorithms are developed for the direct application of generalized Leibnitz rules to the numerical computation of partial derivatives in forward mode. The proposed data structure provides constant time access to the partial derivatives, which accelerates the automatic differentiation computations. This automatic differentiation technique based on the generalized Leibnitz rules can differentiate a composite function in a forward mode.

Firstly, we will simply review the basics of this technique following Tsukanov's paper. A partial derivative of a product of two functions $f(x) = u(x)v(x)$ is a linear combination of products of partial derivatives of u and v with binomial coefficients. The functions which need high order differentiations and appear in the current research work are products of multiple functions, which can also seem to be a combination of some single products of two functions. Hence, in this section, a standard partial derivative of a product of two functions is given to show how the automatic differentiation technique works. Differentiating the equation $f(x) = u(x)v(x)$ with respect to the variable x, it results in [126]:

$$\frac{\partial^{|\mu|} f}{\partial x_1^{\mu_1} \partial x_2^{\mu_2} \cdots \partial x_n^{\mu_n}} = \sum_{\alpha_1=0}^{\mu_1} \sum_{\alpha_2=0}^{\mu_2} \cdots \sum_{\alpha_n=0}^{\mu_n} \begin{pmatrix} \mu_1 \\ \alpha_1 \end{pmatrix} \begin{pmatrix} \mu_2 \\ \alpha_2 \end{pmatrix} \cdots \begin{pmatrix} \mu_n \\ \alpha_n \end{pmatrix} * \frac{\partial^{|\alpha|} u}{\partial x_1^{\alpha_1} \partial x_2^{\alpha_2} \cdots \partial x_n^{\alpha_n}} * \frac{\partial^{|\mu-\alpha|} v}{\partial x_1^{\mu_1-\alpha_1} \partial x_2^{\mu_2-\alpha_2} \cdots \partial x_n^{\mu_n-\alpha_n}} \tag{4.49}$$

where $|\mu| = \sum_{i=1}^{n} \mu_i$, $0 < |\mu| \leq m$(m is the order of the highest derivative), and $|\alpha| = \sum_{i=1}^{n} \alpha_i$. An additional multi-index α the elements of which serve as counters of summation loops is used. In addition, each term in Eq. (4.49) is multiplied by n binomial coefficient $\begin{pmatrix} \mu_i \\ \alpha_i \end{pmatrix}$, $i = 1, \ldots, n$. In this case, both the computation of positions of partial derivatives given by multi-indices α and $\mu - \alpha$, and the computation of the products of binomial coefficients $\prod_{i=1}^{n} \begin{pmatrix} \mu_i \\ \alpha_i \end{pmatrix}$ are considered in the differentiation of the product includes.

Next, some examples are presented to show the application of the automatic differentiation technique used for the present research. As discussed in section 4.4, there are at least four places where the automatic differentiation technique can be used, and we take these four main applications as examples.

- The first application is for the derivatives of the rotation matrix R with respect to the global degrees of freedom. These derivatives are achieved by differentiating both sides of Eq. (4.7), that is $\mathsf{F} = \mathsf{RU}$. According to Eq. (4.49) these differentiations can be rewritten as:

$$\mathcal{T}^{\alpha}(\mathsf{F}) = \mathsf{R}\mathcal{T}^{\alpha}(\mathsf{U}) + \sum_{0<\beta<\alpha} \left\{\mathcal{T}^{\beta}(\mathsf{R})\mathcal{T}^{\alpha-\beta}(\mathsf{U})\right\} + \mathcal{T}^{\alpha}(\mathsf{R})\mathsf{U} \tag{4.50}$$

where the operator $\mathcal{T}^{\alpha}(\quad)$ expresses the α order differentiation of the matrix in the parentheses with respect to the global degrees of freedom. The derivatives $\mathcal{T}^{\alpha}(\mathsf{F})$ of the deformation gradient can be obtained easily by differentiating Eq. (4.11). Then, each order derivative $\mathcal{T}^{\alpha}(\mathsf{R})$ can be automatically achieved by its lower order derivatives in a forward mode.

- In the expressions (4.33) $\sim$ (4.36) of the internal load $\mathbf{f}$, tangent matrix $\mathcal{L}$, quadratic form $\mathcal{Q}$ and cubic form $\mathcal{C}$, the derivatives, Eqs. (4.31) and (4.32), of the strain energy with respect to the local degrees of freedom need to be obtained. Differentiating the strain energy in Eq. (4.30), the following form based on the automatic differentiation is given:

$$\mathcal{T}^{\alpha}(\overline{U}) = \frac{1}{2}\left\{\mathcal{T}^{\alpha}(\widehat{\mathbf{q}}^{t})\mathsf{K}_{L}\widehat{\mathbf{q}} + \sum_{0<\beta<\alpha} \mathcal{T}^{\beta}(\widehat{\mathbf{q}}^{t})\mathsf{K}_{L}\mathcal{T}^{\alpha-\beta}(\widehat{\mathbf{q}}) + \widehat{\mathbf{q}}^{t}\mathsf{K}_{L}\mathcal{T}^{\alpha}(\widehat{\mathbf{q}})\right\} \tag{4.51}$$

where the linear stiffness matrix K_{L} is a constant.

- The derivatives of the local translations with respect to the global degrees of freedom can also take advantage of the automatic differentiation technique. We can differentiate both sides of Eq. (4.22) with respect to the global degrees of freedom, and obtain the following form:

$$\begin{aligned}\mathcal{T}^{\alpha}\left(\left\{\begin{array}{c}\widehat{q}_i\\ \widehat{q}_{i+1}\\ \widehat{q}_{i+2}\end{array}\right\}\right) =& \mathsf{T}_0^t\mathcal{T}^{\alpha}(\mathsf{R}^t)\left\{\begin{array}{c}q_i\\ q_{i+1}\\ q_{i+2}\end{array}\right\} + \mathsf{T}_0^t\mathsf{R}^t\mathcal{T}^{\alpha}\left(\left\{\begin{array}{c}q_i\\ q_{i+1}\\ q_{i+2}\end{array}\right\}\right)\\ &+ \mathsf{T}_0^t\sum_{0<\beta<\alpha}\mathcal{T}^{\beta}(\mathsf{R}^t)\mathcal{T}^{\alpha-\beta}\left(\left\{\begin{array}{c}q_i\\ q_{i+1}\\ q_{i+2}\end{array}\right\}\right)\\ &+ \mathsf{T}_0^t\mathcal{T}^{\alpha}\left(\mathsf{R}^t\right)\mathsf{T}_0\mathsf{T}_0^t\mathbf{r}^0_{(i+5)/6}\end{aligned} \tag{4.52}$$

where the subscript $i = 1, 7, 13, 19$ denotes the translation degrees of freedom.

- In the same way, by differentiating both sides of Eq. (4.29) with respect to the global degrees of freedom, the derivatives of the local rotation vector $\widehat{\boldsymbol{\theta}}_a$ (where

a is equal to $1, 2, 3, 4$ to denote the node number) with respect to the global degrees of freedom using the automatic differentiation technique are given by:

$$\mathcal{T}^{\alpha}(\widehat{\boldsymbol{\theta}}_a) = \left[\mathsf{T}_0^t \left\{ \begin{array}{l} \mathcal{T}^{\alpha}(\mathsf{R}^t) \exp\left(\widetilde{\boldsymbol{\vartheta}}_a\right) + \mathsf{R}^t \mathcal{T}^{\alpha}(\exp\left(\widetilde{\boldsymbol{\vartheta}}_a\right)) \\ + \sum\limits_{0<\beta<\alpha} \mathcal{T}^{\beta}(\mathsf{R}^t) \mathcal{T}^{\alpha-\beta}(\exp\left(\widetilde{\boldsymbol{\vartheta}}_a\right)) \end{array} \right\} \exp\left(\widetilde{\boldsymbol{\theta}}_a^n\right) \mathsf{T}_0 \right]^X \tag{4.53}$$

where the term $\exp\left(\widetilde{\boldsymbol{\theta}}_a^n\right)$ is related to the rotation vector $\widetilde{\boldsymbol{\theta}}_a^n$ in the known nominal configuration and is a constant for a given value of a.

4.6 Numerical results

In this section several reference problems of the shell models are considered using the Koiter-Newton approach. The imperfection analyses of the structures are also presented. The results are compared with results obtained using ABAQUS based on a full nonlinear analysis, with the same number of elements and nodes.

4.6.1 Flat plate

The Koiter-Newton approach's ability to handle a closely-spaced buckling modes case is well illustrated by the following shell example. This is a flat plate uniformly compressed in the longitudinal direction. The constraint conditions are shown in Fig. 4.5. The sides are $a = 140$mm and $b = 100$mm long, respectively, and the thickness is 0.5mm. The elastic material properties are $E = 70000\text{N/mm}^2$ and $\nu = 0.3$. The plate is meshed with 140 square shell elements.

The following steps are taken in the present example:

1. Some preparation work is done to construct the reduced order model: a linear buckling analysis and the first and second order displacement fields.

2. A nonlinear analysis is applied for the perfect plate using the Koiter-Newton approach.

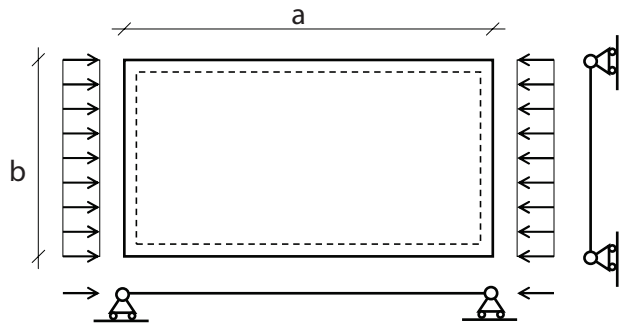

Figure 4.5: The flat plate

3. An imperfection analysis is applied for the plate with a lateral imperfection load.

Preparation work

The aspect ratio of the plate is chosen such that the plate exhibits two almost coincident buckling modes with buckling loads of 343N and 368N respectively, as shown in Fig. 4.6. To consider the interactions of the first two closely-spaced buckling modes, these two degrees of freedom needs to be implemented into the reduced order model. For the later imperfection analysis, a lateral imperfection load (1N) applied in the center of the plate should be considered in advance during construction of the reduced order model. Hence, in total there are four degrees of freedom in the reduced order model. One DOF presents the primary path, another DOF presents the lateral imperfection load, and the others indicate the first two closely-spaced buckling modes. After the reduced order model is constructed on the undeformed configuration, the first and second order displacement fields are also obtained. The first order displacement fields are shown in Fig. 4.7. $\mathbf{u}_1$ is a pure compression on the primary path, and $\mathbf{u}_2$ is caused by the lateral imperfection load. The deformations of $\mathbf{u}_3$ and $\mathbf{u}_4$ are similar to the first two buckling modes, but they are influenced by the lateral imperfection load.

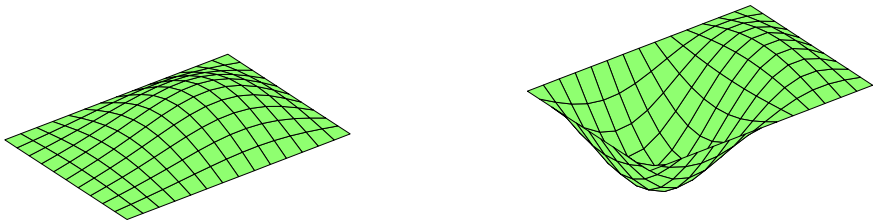

(a) Buckling mode 1 (b) Buckling mode 2

Figure 4.6: The first two buckling modes of the plate

Nonlinear analysis of the perfect plate

The Koiter-Newton approach is adopted to analyze the perfect plate. For the perfect structure, the general nonlinear FE method fails to obtain the response curve with the bifurcation branch. It can only obtain the limit point after introducing the imperfection. Due to the perturbation loads related to the two closely-spaced buckling modes and considered in the reduced order model, the Koiter-Newton approach can trace the response curve of prefect structures to find out the exact bifurcation point. In the right hand side of the reduced order model, the load parameter ϕ_2 of the imperfection load is set to be zero to simulate the perfect case. The response curve, out-of-plane displacement in the center of the plate vs. load, begins to follow the bifurcation branch when the load is roughly equal to the first linear buckling load 343N, as shown in Fig. 4.8.

Imperfection analysis of the plate

The imperfection load parameter ϕ_2 is set to be 0.005 to simulate an 0.005N imperfection load. The nonlinear response curves obtained by one expansion step at the undeformed equilibrium point are compared with those obtained using ABAQUS, see Fig. 4.9. The figures shown in Fig. 4.9 demonstrate that both the out-of-plane displacement and the in-plane shortening results for the Koiter-Newton analysis match the results obtained using ABAQUS very well in the prebuckling stage, at the buckling point and also in the initial postbuckling stage, with the indication that

(a) $\mathbf{u}_1$

(b) $\mathbf{u}_2$

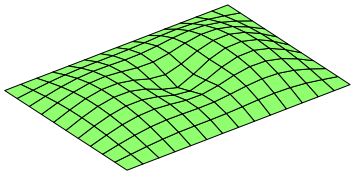

(c) $\mathbf{u}_3$

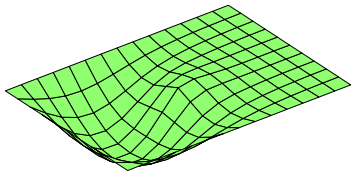

(d) $\mathbf{u}_4$

Figure 4.7: The first order displacement fields of the plate

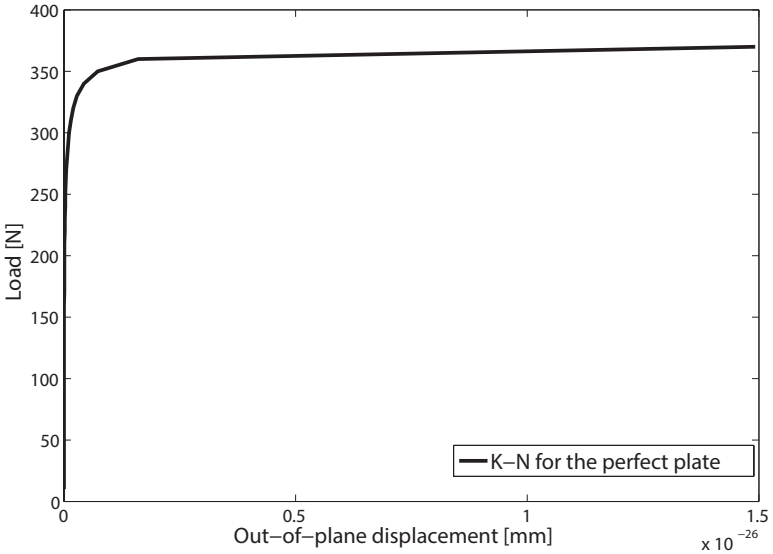

Figure 4.8: The buckling response of the perfect plate

the Koiter-Newton approach works very well in the buckling sensitive case and for the structure, the prebuckling of which is almost linear, just one expansion step is enough to obtain the essential buckling response.

The computational costs of the flat plate for the analyses in Fig. 4.9 are assessed. Tracing to the same equilibrium point on the post-buckling path, the Koiter-Newton approach needs one expansion step to solve one linear FEM system, while ABAQUS needs 37 load steps to solve 62 linear FEM systems.

Then, different amplitudes of the imperfection loads can easily be considered by changing the value of the imperfection load parameter ϕ_2 in the right hand side of the ROM, see the response curves for six different amplitudes of the imperfection loads plotted in Fig. 4.10. It can be seen that the value of the buckling load becomes lower with an increasing imperfection load.

Finally, the computing costs of the imperfection analyses are assessed. For six different imperfection loads, the Koiter-Newton approach just modifies the load term of the reduced order model and does not need to reconstruct the ROM. While, ABAQUS needs to recalculated the full nonlinear FE model six times to obtain these six response curves. Hence, the Koiter-Newton approach only need to solve

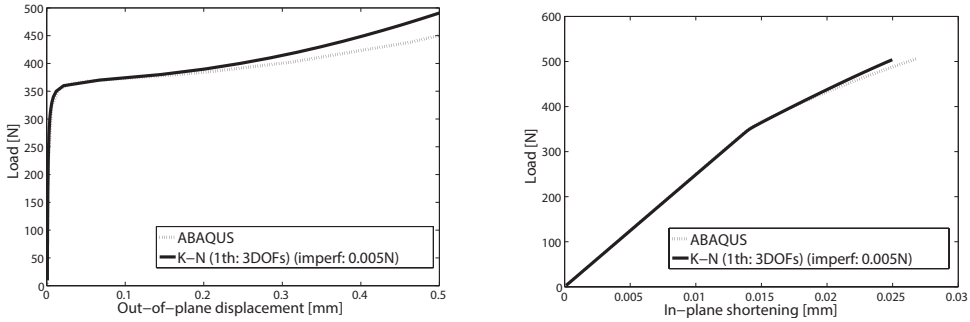

(a) Out-of-plane displacement (b) In-plane shortening

Figure 4.9: Response curves of the plat plate with imperfections

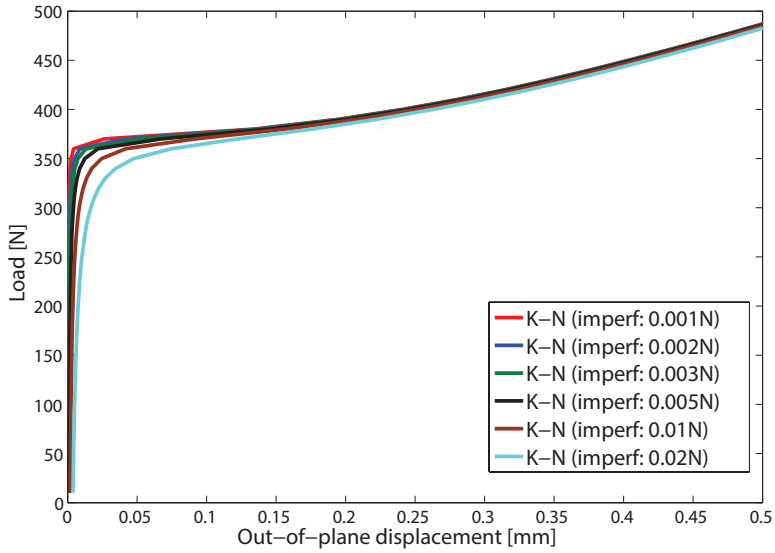

Figure 4.10: Response curves of the plate for six different imperfection loads

one linear FEM system to construct the reduced order model once, and the costs for solving these six low-order ROMs can be neglected. While ABAQUS needs to solve approximate 62 linear FEM systems for each imperfection case, that will be 372 systems for all the six imperfection cases, thus it shows that the advantage of the Koiter-Newton approach in computational costs is more obvious in the imperfection analysis.

4.6.2 Cylindrical shell

A cylindrical shell under a centralized transverse load is presented in this example, see Fig. 4.11, where radius R is 2540, length L is 508, angle θ is 0.1 rad. The shell is made of an isotropic material, with a Young modulus E of 3102.75 MPa and a Poisson ratio ν of 0.3. The two straight edges of the shell are simply supported and another two curved edges are free. There is a centralized lateral load applied vertically to the center of the shell surface, and 100 co-rotational shell elements are used in this example.

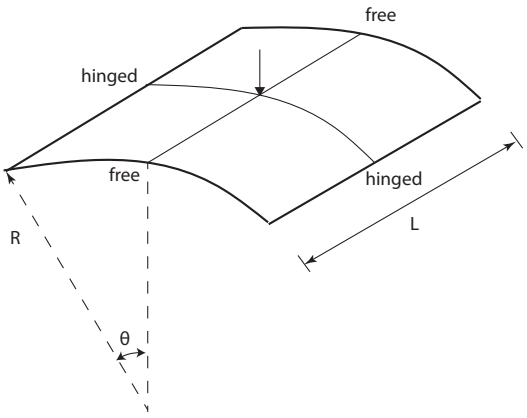

Figure 4.11: The cylindrical shell

Only the first buckling mode needs to be considered and the reduced order model is a nonlinear system with two degrees of freedom. Three expansion steps are adopted at the unloaded configuration, near the limit point, and on the descending range, respectively. The response curves about the lateral displacement at the center of the shell surface are shown in Fig. 4.12. The Koiter-Newton approach uses three steps to solve 9 linear FEM systems to trace to the same equilibrium point on the post-buckling path, in each step, one system is used for constructing the ROM and two systems are used for corrections, while ABAQUS requires 148 steps to solve 232 linear FEM systems. The deformation near the limit point is compared with that produced using ABAQUS in Fig. 4.13 where it can be seen that these two deformations match very well.

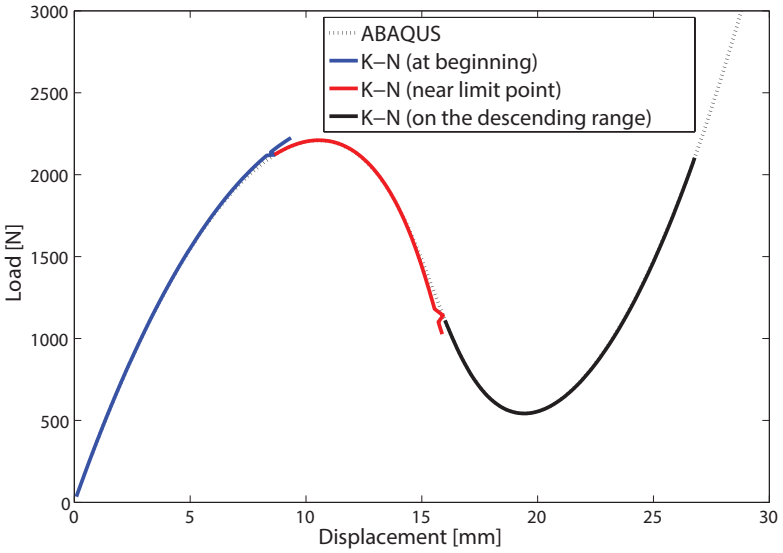

Figure 4.12: Response curves of the cylindrical shell

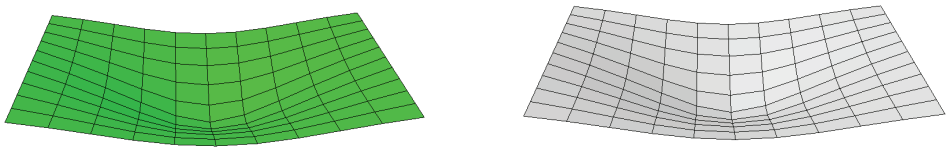

(a) ABAQUS

(b) Koiter-Newton approach

Figure 4.13: Deformations of the cylindrical shell near the limit point

4.6.3 Shallow arch

The sketch of the shallow arch is shown in Fig. 4.14. It is composed of two flat plate, and a uniform press is applied on the cross line of these two plates. The following properties are considered: $E = 1.0 \times 10^6, \nu = 0.3$. This shallow arch is meshed by 160 shell elements.

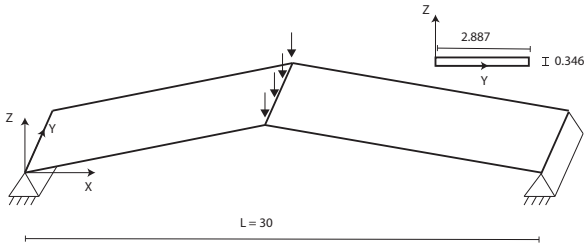

Figure 4.14: The shallow arch

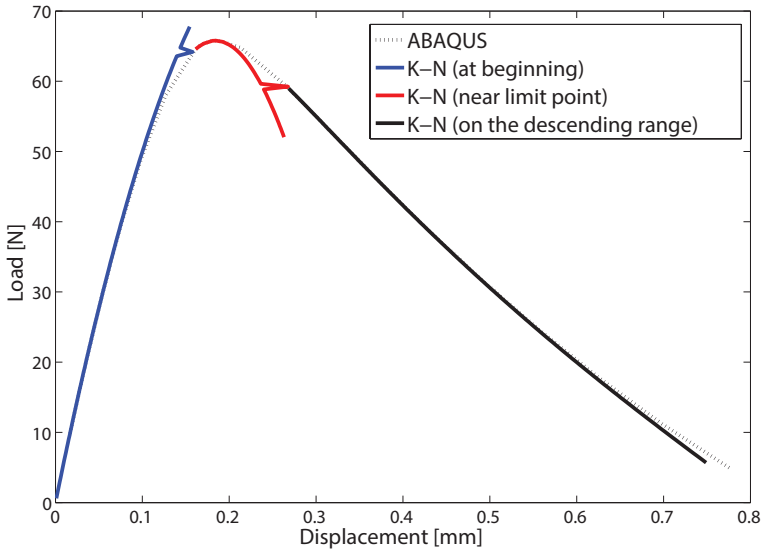

Figure 4.15: Response curves of the shallow arch

In this example, there are only two DOFs in the reduced order model since the first buckling mode is separate from the others. Three expansion steps are adopted

at the unloaded configuration, near the limit point, and on the descending range, respectively. The response curves about the vertical displacement on the loading position are shown in Fig. 4.15. When the Koiter-Newton results are compared with results obtained using ABAQUS, it can be seen that an accurate nonlinear equilibrium path, including the unstable path after the limit point, can be obtained using only three steps for the Koiter-Newton approach, while ABAQUS requires 107 steps to trace to the same equilibrium point. The deformations of the arch near the limit point are also compared for the two methods in Fig. 4.16.

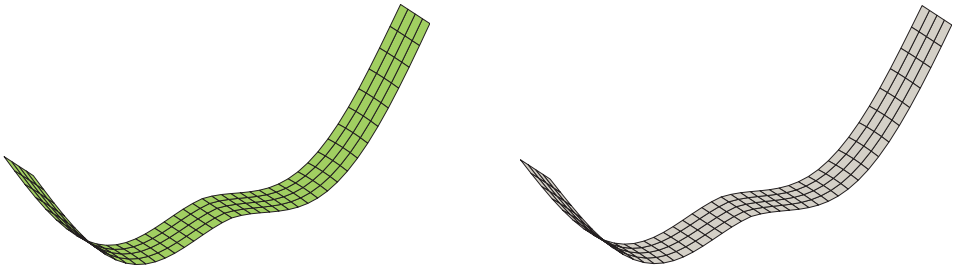

(a) ABAQUS (b) Koiter-Newton approach

Figure 4.16: Deformations of the shallow arch near the limit point

4.6.4 Cylindrical Panel

In this example, the cylindrical panel, given in Fig. 4.17, is a 30^0 curved surface fetched from a whole cylinder. The radius and length of the cylinder are 10.16 and 1.27, respectively, and the shell thickness is 0.01179. The panel is made of an isotropic material, with a Young modulus E of 10.48×10^6 N/mm^2, a Poisson ratio ν of 0.3. A uniform axial compression is applied to both of the curved edges, and the constraint conditions are as follows. At the loaded ends the displacements in the plane of the edge are restrained but the axial displacements are set free. The displacements, excepting the axial direction, of the two straight edges are constrained. Only a single point in the middle of one straight edge is constrained along the axial direction. 720 shell elements are used to capture the accurate deformation.

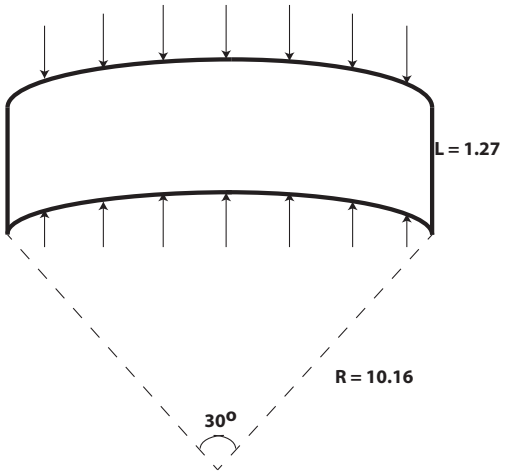

Figure 4.17: The cylindrical panel

Linear buckling analysis of the panel

A linear buckling analysis is done using the Koiter-Newton code. The first four buckling loads are very close, difference is within 20%, and these four closely-spaced buckling modes are shown in Fig. 4.18. In the Koiter-Newton approach, the reduced order model with 6 degrees of freedom is constructed on the undeformed configuration, which is based on the deformation on the primary path, one lateral imperfection load (1N) applied in the center of the panel and these four closely-spaced buckling modes.

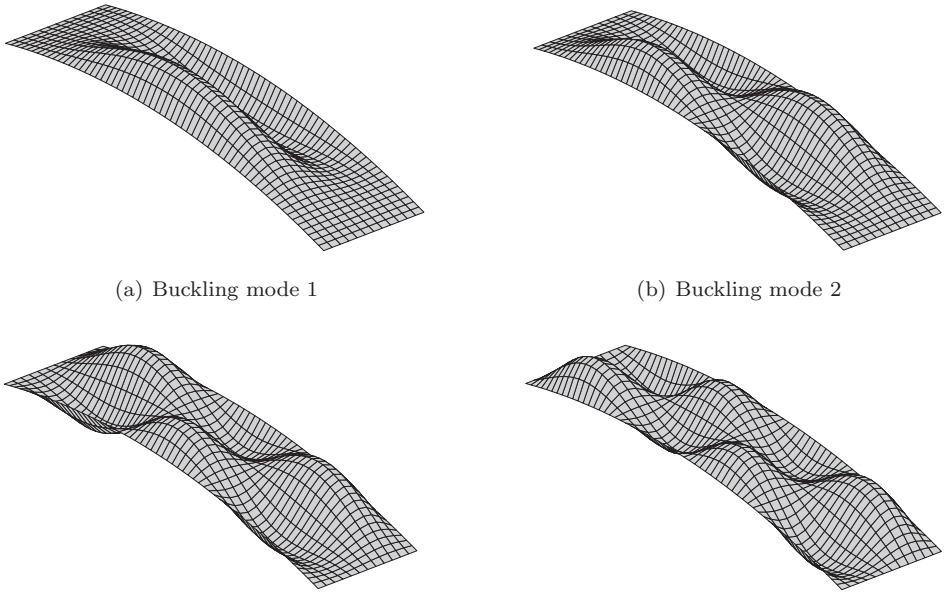

(a) Buckling mode 1

(b) Buckling mode 2

(c) Buckling mode 3

(d) Buckling mode 4

Figure 4.18: The first four buckling modes of the cylindrical panel

Nonlinear analysis of the perfect panel

The load parameter ϕ_2 related to the imperfection load is set to be zero for the perfect structure. The nonlinear response curves, end shortening vs. load, are plotted in Fig. 4.19. The dotted curve is the response curve obtained using ABAQUS which adopts the full nonlinear FEM analysis. The dash-dotted curve is obtained by just one expansion step on the undeformed configuration using the Koiter-Newton approach. This dash-dotted curve begins to deviate from the true response when the load is larger than 1000N and will overestimate the limit point later, since the structural nonlinearity of the prebuckling is very serious. According to the discussion in section 2.6, an automated technique based on the residual force is adopted to judge when the reduced order model obtained by the first expansion step loses the numerical accuracy. Then, a Newton correction is applied to find out a true equilibrium point and the second expansion step is carried out at this corrected equilibrium point. The solid curve in Fig. 4.19 is the nonlinear response curve from the second expansion step. It can be seen that this solid curve matches the curve obtained using ABAQUS near the limit point very well.

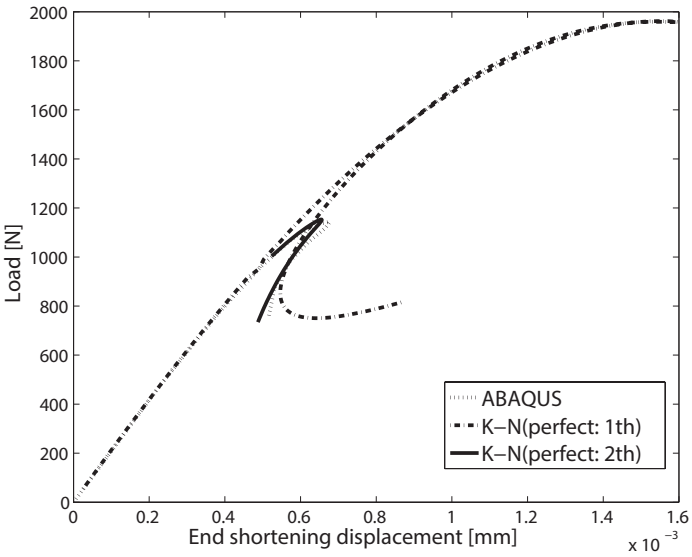

Figure 4.19: Response curves of the perfect panel

Imperfection analysis of the panel

As mentioned above, a lateral imperfection load applied in the center of the panel was considered in the Koiter-Newton approach. In the imperfection analysis, 10 different amplitudes of the imperfection loads are implemented by changing the value of the imperfection load parameter ϕ_2 in the right hand side of the ROM.

If a lateral imperfection load is applied on the panel, it will produce a corresponding lateral deformation as an initial geometric imperfection. Hence, the different amplitudes of the imperfection loads can be represented by the different maximum lateral deformations which can be scaled by using the shell thickness t. The nonlinear response curves for these ten different imperfections are shown in Fig. 4.20. The limit buckling load sharply decreases with increasing lateral imperfection load, which indicates that this panel structure is very sensitive to the imperfections.

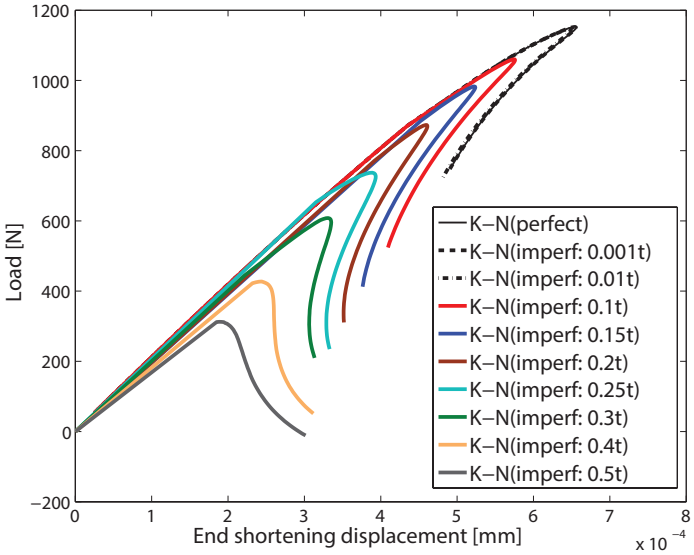

Figure 4.20: Response curves of the cylindrical panel for ten different imperfection loads

The values of the limit buckling loads for 12 different lateral imperfection loads are compared with results obtained using ABAQUS, see Fig. 4.21, from it it can be seen that the imperfection analysis obtained using the Koiter-Newton approach is accurate enough when the lateral imperfection load is smaller than 0.8N which is

equivalent to an initial geometric imperfection of $0.5t$. The deformations of the panel with the imperfection $0.1t$ near the limit point are compared in Fig. 4.22.

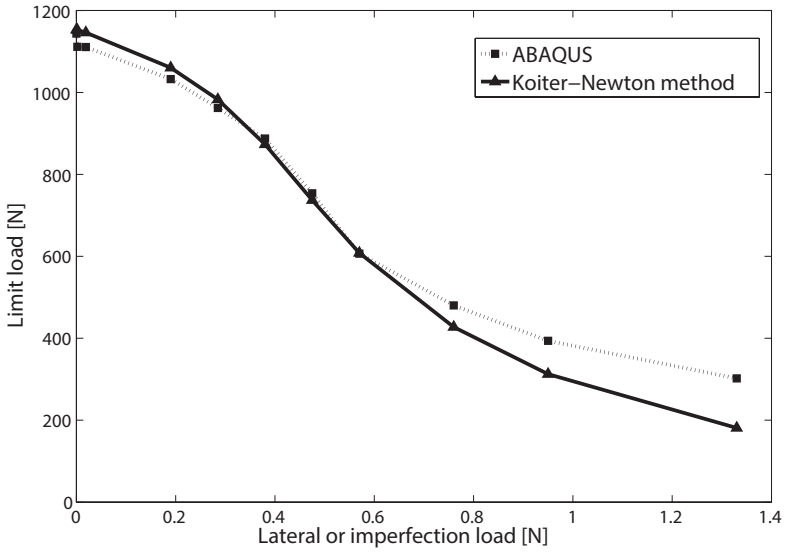

Figure 4.21: Comparison of the limit loads of the panel

The computational cost of the imperfection analysis using the Koiter-Newton approach is compared with results obtained using ABAQUS. To obtain the results shown in Fig. 4.20, ABAQUS needs to recalculate the entire FEM model ten times and each time it needs to solve approximate 156 FEM linear systems, that is ABAQUS needs to solve in total 156×10 FEM linear systems. However, since the reduced order model does not need to be reconstructed for different imperfection loads, the Koiter-Newton approach only needs to solve 8 linear FEM systems to generate the reduced order model twice and to correct the results once. This demonstrates clearly that the Koiter-Newton approach is more computational efficient when used for an imperfection analysis.

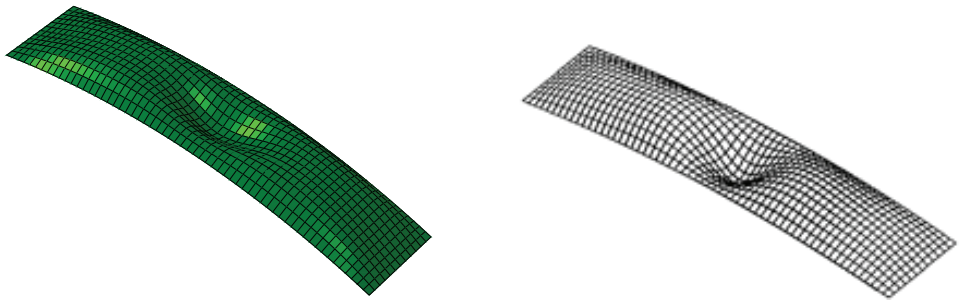

(a) ABAQUS (b) Koiter-Newton approach

Figure 4.22: Deformations of the cylindrical panel near the limit point, imperfection $0.1t$

4.7 Conclusions

The focus of this chapter is the implementation of the Koiter-Newton approach into a shell element based on the co-rotational frame. The finite rotation theory is introduced. Then, descriptions of the proposed three configurations are presented, and the material coordinate system is defined for the composite shell. Next, the strain energy is differentiated to the fourth order with respect to the global degrees of freedom. In the Matlab codes, the automatic differentiation is adopted to find the derivatives of the co-rotational frame with respect to element degrees of freedom.

Various numerical examples of the shell model are used to evaluate the performance of the Koiter-Newton approach. Compared with the results produced for the same problems using ABAQUS, it is demonstrated that the Koiter-Newton approach is an accurate and efficient reduced basis path-following technique for nonlinear structural analysis. The high computational efficiency of the Koiter-Newton approach is most obvious when it is used for an imperfection analysis, since reanalyses for the different imperfections require only a small fraction of that required for the first analysis time.

Chapter 5

Koiter-Newton analysis using Von Kármán kinematics

5.1 Introduction

The Koiter-Newton analyses using co-rotational kinematics were introduced in chapters 3 and 4. Achieving equilibrium equations of a third order form (2.8), especially the forms $\mathcal{L}$, $\mathcal{Q}$ and $\mathcal{C}$, is the main task of FE implementations. Elements in a co-rotational frame consider the fully geometric nonlinearities in the element, hence the FE implementation is complicated and time consuming. In engineering, some structures under the loading can neglect the nonlinear in-plane rotations while the rotations of the normals to the mid-surface are finitely large. In this case, the Von Karman kinematics which ignore some nonlinear terms in the Green's stain-displacement relations are also available in the analysis. The membrane part of von Kármán's strain-displacement relationships for moderately large-deflection analysis can be considered as a special case of the Green strain [112]. The expression of the Von Kármán membrane strain for a plate is given by:

$$\begin{cases} \epsilon_x = \dfrac{\partial u}{\partial x} + \dfrac{1}{2}\left(\dfrac{\partial w}{\partial x}\right)^2 \\ \epsilon_y = \dfrac{\partial v}{\partial y} + \dfrac{1}{2}\left(\dfrac{\partial w}{\partial y}\right)^2 \\ \epsilon_{xy} = \dfrac{1}{2}\dfrac{\partial u}{\partial y}\dfrac{\partial v}{\partial x} + \dfrac{1}{2}\dfrac{\partial w}{\partial x}\dfrac{\partial w}{\partial y} \end{cases} \tag{5.1}$$

where the u, v and w are the three translations of the element.

In this chapter, a Koiter-Newton analysis using Von Kármán kinematics is achieved as follows. We adopt the two-node planar beam element and the triangular three-node plat element with six degrees of freedom per node discussed in chapter 4 to obtain the forms $\mathcal{L}$, $\mathcal{Q}$ and $\mathcal{C}$ in the equilibrium equations. Then, a four-node quadrilateral element is assembled by four triangular elements using a different assembly technique compared with the technique used in chapter 4. Finally, some numerical examples are used to assess the accuracy of a Koiter-Newton analysis using Von Kármán kinematics.

5.2 Von Kármán beam kinematics

In this section, a two-node planar beam element with three degrees of freedom per node is considered in the Koiter-Newton approach. This beam element was used by Tiso [7] for Koiter analysis, and here we report how the entities necessary for the forms $\mathcal{L}$, $\mathcal{Q}$ and $\mathcal{C}$ in the equilibrium equations (2.8) are calculated.

5.2.1 Strain energy of the beam element

The beam element mentioned in Tiso's thesis [7] is described using an isoparametric formulation. A sketch of the beam is shown in Fig. 5.1.

The element nodal displacement vector is given by:

$$\mathbf{q} = [u_1 \; w_1 \; \theta_1 \; u_2 \; w_2 \; \theta_2]^t \tag{5.2}$$

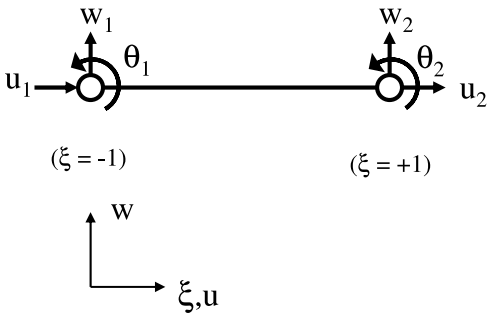

Figure 5.1: Two-node planar beam element [7]

In the isoparametric coordinate system, the relation between the isoparametric and the cartesian coordinate system is given as:

$$\xi = \frac{2}{L}x - 1 \tag{5.3}$$

where L is the length of the beam.

The in-plane and out-of-plane displacement components u and w are interpolated as:

$$\begin{bmatrix} u(\xi) \\ w(\xi) \end{bmatrix} = \begin{bmatrix} N_{u_1} & 0 & 0 & N_{u_2} & 0 & 0 \\ 0 & N_{w_1} & N_{\theta_1} & 0 & N_{w_2} & N_{\theta_2} \end{bmatrix} \mathbf{q} \tag{5.4}$$

where the specific expressions of the interpolation functions can refer to [7, 127].

Here, a compact notation is adopted to denote the strain vector $\boldsymbol{\varepsilon}$ that contains the axial strain ϵ and the curvature χ, as given by:

$$\boldsymbol{\varepsilon} = \begin{Bmatrix} \epsilon \\ \chi \end{Bmatrix} \tag{5.5}$$

where the axial strain ϵ in the Von Kármán model for a planar beam element is :

$$\epsilon = \frac{du}{dx} + \frac{1}{2}\left(\frac{dw}{dx}\right)^2 \tag{5.6}$$

and the curvature χ is:

$$\chi = \frac{d^2w}{dx^2} \tag{5.7}$$

Introducing the displacements (5.4) into Eqs. (5.6) $\sim$ (5.7) and then into Eq. (5.5), the strain vector $\boldsymbol{\varepsilon}$ is represented by the displacements. Then, the strain can be divided into the linear part and the nonlinear part with respect to the displacements, resulting in:

$$\boldsymbol{\varepsilon} = \left\{ \begin{array}{c} \epsilon \\ \chi \end{array} \right\} = \boldsymbol{\varepsilon}_l + \boldsymbol{\varepsilon}_{nl} \tag{5.8}$$

where the linear part $\boldsymbol{\varepsilon}_l$ is:

$$\boldsymbol{\varepsilon}_l = \frac{1}{L}\left\{ \begin{array}{c} -u_1 + u_2 \\ \frac{3}{2}\xi w_1 + \left(-\frac{1}{4}L + \frac{3}{4}L\xi\right)\theta_1 - \frac{3}{2}\xi w_2 + \left(\frac{1}{4}L + \frac{3}{4}L\xi\right)\theta_2 \end{array} \right\} \tag{5.9}$$

and the nonlinear part $\boldsymbol{\varepsilon}_{nl}$ is:

$$\boldsymbol{\varepsilon}_{nl} = \frac{1}{2}\left\{ \begin{array}{c} \frac{6}{5L^2}(w_1 - w_2)^2 + \frac{2}{15}(\theta_1 - \theta_2)^2 + \frac{1}{5}\theta_1\theta_2 + \frac{1}{5L}(\theta_1 + \theta_2)(w_1 - w_2) \\ 0 \end{array} \right\} \tag{5.10}$$

According to Eqs. (5.8) $\sim$ (5.10), the axial strain ϵ and the curvature χ are:

$$\begin{aligned}\epsilon =& \frac{1}{L}\left(-u_1+u_2\right) \\ &+\frac{1}{2}\left[\frac{6}{5L^2}\left(w_1-w_2\right)^2+\frac{2}{15}\left(\theta_1-\theta_2\right)^2+\frac{1}{5}\theta_1\theta_2+\frac{1}{5L}\left(\theta_1+\theta_2\right)\left(w_1-w_2\right)\right]\end{aligned} \tag{5.11}$$

$$\chi = \frac{1}{L}\left[\frac{3}{2}\xi w_1+\left(-\frac{1}{4}L+\frac{3}{4}L\xi\right)\theta_1-\frac{3}{2}\xi w_2+\left(\frac{1}{4}L+\frac{3}{4}L\xi\right)\theta_2\right] \tag{5.12}$$

Eq. (5.12) demonstrates that the curvature χ is totally linear with respect to the displacements and only the axial strain ϵ contains some nonlinear terms. The linear part of the strain vector only contributes to the linear stiffness matrix which is always a constant matrix and does not contribute to the third or fourth order derivatives of the strain energy. Hence, here we only consider the axial strain ϵ (5.11) to calculate the axial strain energy, and the bending part that results from the curvature χ can be easily superposed. The axial strain energy U of a planar beam element is written as:

$$U = \frac{1}{2}EAL\epsilon^2 \tag{5.13}$$

where E is the Young's modulus of the beam, and A is the area of the cross section. In the rest of this section, we will only use the strain energy U caused by the nonlinear axial strain ϵ for calculations.

The bending part of the linear stiffness matrix, which is generated by the curvature χ, is a very familiar form, as given by:

$$\mathsf{K}_L^{bending} = \begin{bmatrix} 0 & 0 & 0 & 0 & 0 & 0 \\ 0 & \frac{12EI}{L^3} & \frac{6EI}{L^2} & 0 & -\frac{12EI}{L^3} & \frac{6EI}{L^2} \\ 0 & \frac{6EI}{L^2} & \frac{4EI}{L} & 0 & -\frac{6EI}{L^2} & \frac{2EI}{L} \\ 0 & 0 & 0 & 0 & 0 & 0 \\ 0 & -\frac{12EI}{L^3} & -\frac{6EI}{L^2} & 0 & \frac{12EI}{L^3} & -\frac{6EI}{L^2} \\ 0 & \frac{6EI}{L^2} & \frac{2EI}{L} & 0 & -\frac{6EI}{L^2} & \frac{4EI}{L} \end{bmatrix} \tag{5.14}$$

5.2.2 Equilibrium equations in a third order form

The components of the internal load vector f, tangent stiffness matrix L, three-dimensional matrix Q and four-dimensional matrix C in the equilibrium equations (2.8) for the beam element can be obtained by differentiating the axial strain energy (5.13) to the fourth order, as follows:

$$f_i = \frac{\partial U}{\partial q_i} = EAL\left(\epsilon \frac{\partial \epsilon}{\partial q_i}\right) \tag{5.15}$$

$$L_{ij} = \frac{\partial^2 U}{\partial q_i \partial q_j} = EAL\left(\frac{\partial \epsilon}{\partial q_i}\frac{\partial \epsilon}{\partial q_j} + \epsilon \frac{\partial^2 \epsilon}{\partial q_i \partial q_j}\right) \tag{5.16}$$

$$Q_{ijk} = \frac{1}{2}\frac{\partial^3 U}{\partial q_i \partial q_j \partial q_k} = \frac{EAL}{2}\left(\frac{\partial \epsilon}{\partial q_j}\frac{\partial^2 \epsilon}{\partial q_i \partial q_k} + \frac{\partial \epsilon}{\partial q_i}\frac{\partial^2 \epsilon}{\partial q_j \partial q_k} + \frac{\partial \epsilon}{\partial q_k}\frac{\partial^2 \epsilon}{\partial q_i \partial q_j}\right) \tag{5.17}$$

$$C_{ijkl} = \frac{1}{6}\frac{\partial^4 U}{\partial q_i \partial q_j \partial q_k \partial q_l} = \frac{EAL}{6}\left(\frac{\partial^2 \epsilon}{\partial q_i \partial q_l}\frac{\partial^2 \epsilon}{\partial q_j \partial q_k} + \frac{\partial^2 \epsilon}{\partial q_j \partial q_l}\frac{\partial^2 \epsilon}{\partial q_i \partial q_k} + \frac{\partial^2 \epsilon}{\partial q_k \partial q_l}\frac{\partial^2 \epsilon}{\partial q_i \partial q_j}\right) \tag{5.18}$$

where the subscripts i, j, k and l run from 1 to 18, and the unknowns are the first and second order derivatives of the axial strain ϵ with respect to the degrees of freedom.

The vector $\mathbf{b}$ is used to denote the first derivatives of the axial strain (5.11), as given by:

$$\mathbf{b} = \frac{\partial \epsilon_{in}}{\partial q} = \left\{ \begin{array}{c} -\frac{1}{L} \\ \frac{6}{5L^2}\left(w_1 - w_2\right) + \frac{1}{10L}\left(\theta_1 + \theta_2\right); \\ \frac{2}{15}\left(\theta_1 - \theta_2\right) + \frac{1}{10}\theta_2 + \frac{1}{10L}\left(w_1 - w_2\right) \\ \frac{1}{L} \\ -\frac{6}{5L^2}\left(w_1 - w_2\right) - \frac{1}{10L}\left(\theta_1 + \theta_2\right) \\ -\frac{2}{15}\left(\theta_1 - \theta_2\right) + \frac{1}{10}\theta_1 + \frac{1}{10L}\left(w_1 - w_2\right) \end{array} \right\} \tag{5.19}$$

The second derivatives of the axial strain is expressed by the matrix s, as:

$$\mathsf{s} = \frac{\partial^2 \epsilon_{in}}{\partial q^2} = \begin{bmatrix} 0 & 0 & 0 & 0 & 0 & 0 \\ 0 & \frac{6}{5L^2} & \frac{1}{10L} & 0 & -\frac{6}{5L^2} & \frac{1}{10L} \\ 0 & \frac{1}{10L} & \frac{2}{15} & 0 & -\frac{1}{10L} & -\frac{1}{30} \\ 0 & 0 & 0 & 0 & 0 & 0 \\ 0 & -\frac{6}{5L^2} & -\frac{1}{10L} & 0 & \frac{6}{5L^2} & -\frac{1}{10L} \\ 0 & \frac{1}{10L} & -\frac{1}{30} & 0 & -\frac{1}{10L} & \frac{2}{15} \end{bmatrix} \tag{5.20}$$

Then, Eqs. (5.15) $\sim$ (5.16) can be rewritten in a compact form by using the vector $\mathbf{b}$ and the matrix s as:

$$\mathbf{f} = EAL\,(\epsilon \mathbf{b}) \tag{5.21}$$

$$\mathsf{L} = EAL\left(\mathbf{b}\mathbf{b}^t + \epsilon \mathsf{s}\right) \tag{5.22}$$

The three-dimensional matrix Q and four-dimensional matrix C are not directly and separately used in the Koiter-Newton approach, and they are involved in three places during the derivations. The first one is $\mathcal{Q}(\widetilde{\mathbf{q}})$ for calculating the geometric stiffness matrix $\mathsf{K}_g = -2\mathsf{Q}\widetilde{\mathbf{q}} = -2\mathcal{Q}(\widetilde{\mathbf{q}})$ (refer to Eq. (2.41)), the second one is $\mathcal{Q}(\mathbf{u}_\alpha, \mathbf{u}_\beta)$ which is used to solve the linear system of equations (2.22) and achieve the $\bar{\mathcal{Q}}$ in the reduced order model, and the third one is $\mathcal{C}(\mathbf{u}_\alpha, \mathbf{u}_\beta, \mathbf{u}_\gamma, \mathbf{u}_\delta)$ which is in Eq. (2.34) to calculate the $\bar{\mathcal{C}}$ in the reduced order model. These three terms are achieved as follows:

- $\mathcal{Q}(\widetilde{\mathbf{q}})$ can be achieved by the multiplication of the 3D matrix Q in Eq. (5.17) and the displacement vector $\widetilde{\mathbf{q}}$ obtained by a linear static analysis, which results in a matrix:

$$\mathcal{Q}(\widetilde{\mathbf{q}}) = Q_{ijk}\widetilde{q}_k = \frac{EAL}{2}\left(\frac{\partial \epsilon}{\partial q_j}\frac{\partial^2 \epsilon}{\partial q_i \partial q_k}\widetilde{q}_k + \frac{\partial \epsilon}{\partial q_i}\frac{\partial^2 \epsilon}{\partial q_j \partial q_k}\widetilde{q}_k + \frac{\partial \epsilon}{\partial q_k}\widetilde{q}_k\frac{\partial^2 \epsilon}{\partial q_i \partial q_j}\right) \tag{5.23}$$

  where the summation convention is applied. A compact notation can be used by using $\mathbf{b}$ and s:

$$\mathcal{Q}(\widetilde{\mathbf{q}}) = \frac{EAL}{2}\left(\mathsf{s}\widetilde{\mathbf{q}}\mathbf{b}^t + \mathbf{b}\widetilde{\mathbf{q}}^t\mathsf{s} + \mathbf{b}^t\widetilde{\mathbf{q}}\mathsf{s}\right) \tag{5.24}$$

- In the same way, $\mathcal{Q}(\mathbf{u}_\alpha, \mathbf{u}_\beta)$ which is obtained by multiplying two first order displacement fields ($\mathbf{u}_\alpha$ and $\mathbf{u}_\beta$) is written as:

$$\mathcal{Q}(\mathbf{u}_\alpha, \mathbf{u}_\beta) = \frac{EAL}{2}\left[(\mathbf{b}^t\mathbf{u}^\alpha)(\mathsf{s}\mathbf{u}^\beta) + (\mathbf{b}^t\mathbf{u}^\beta)(\mathsf{s}\mathbf{u}^\alpha) + ({\mathbf{u}^\alpha}^t\mathsf{s}\mathbf{u}^\beta)\mathbf{b}\right] \tag{5.25}$$

- $\mathcal{C}(\mathbf{u}_\alpha, \mathbf{u}_\beta, \mathbf{u}_\gamma, \mathbf{u}_\delta)$ is calculated by multiplying four first order displacement fields ($\mathbf{u}_\alpha$, $\mathbf{u}_\beta$, $\mathbf{u}_\gamma$ and $\mathbf{u}_\delta$), as given by:

$$\mathcal{C}(\mathbf{u}_\alpha, \mathbf{u}_\beta, \mathbf{u}_\gamma, \mathbf{u}_\delta) = \frac{EAL}{6} \left[\begin{array}{l} \left(\mathbf{u}^{\alpha^t} \mathbf{s} \mathbf{u}^\delta\right) \left(\mathbf{u}^{\beta^t} \mathbf{s} \mathbf{u}^\gamma\right) + \left(\mathbf{u}^{\beta^t} \mathbf{s} \mathbf{u}^\delta\right) \left(\mathbf{u}^{\alpha^t} \mathbf{s} \mathbf{u}^\gamma\right) \\ + \left(\mathbf{u}^{\gamma^t} \mathbf{s} \mathbf{u}^\delta\right) \left(\mathbf{u}^{\alpha^t} \mathbf{s} \mathbf{u}^\beta\right) \end{array} \right] \tag{5.26}$$

If we introduce a new notation:

$$D_{\alpha\beta} = \mathbf{u}^{\alpha^t} \mathbf{s} \mathbf{u}^\beta \tag{5.27}$$

Eq. (5.26) becomes a more compact form:

$$\mathcal{C}(\mathbf{u}_\alpha, \mathbf{u}_\beta, \mathbf{u}_\gamma, \mathbf{u}_\delta) = \frac{EAL}{6} \left[D_{\alpha\delta} D_{\beta\gamma} + D_{\beta\delta} D_{\alpha\gamma} + D_{\gamma\delta} D_{\alpha\beta} \right] \tag{5.28}$$

At this point, the $\mathcal{L}$, $\mathcal{Q}$ and $\mathcal{C}$ in the equilibrium equations (2.8) of a Von Kármán beam element are all achieved.

5.3 Von Kármán shell kinematics

In this section, we will use a four-node quadrilateral element which is assembled by triangular elements based on Von Kármán kinematics. The triangular three-node plat element with six degrees of freedom per node, adopted in chapter 4 and Tiso's thesis [7], is used to obtain the forms $\mathcal{L}$, $\mathcal{Q}$ and $\mathcal{C}$ in the equilibrium equations (2.8), then another assembly technique, which is different from the one used in chapter 4, is introduced due to the existence of the quadratic and cubic forms $\mathcal{Q}$ and $\mathcal{C}$.

5.3.1 Strain energy of the shell element

Firstly, we will give a quick review on the basic description of the triangular element. A discussion of the linear part and some nonlinear terms of this element can be found in appendix A and Tiso's thesis [7].

As shown in Fig. 5.2, each node of the triangular element has six degrees of freedom, as given by $\mathbf{q}_a$:

$$\mathbf{q}_a = \left\{ u_a \quad v_a \quad w_a \quad \theta_{x_a} \quad \theta_{y_a} \quad \theta_{z_a} \right\}, \quad a = 1, 2, 3 \tag{5.29}$$

where the subscript a denotes the node number. The total degrees of freedom for the element is $\mathbf{q} = \{\mathbf{q}_1, \mathbf{q}_2, \mathbf{q}_3\}^t$.

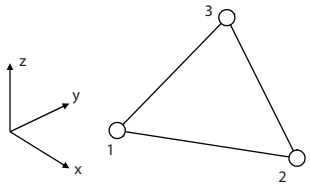

Figure 5.2: Three-node triangular element [7]

As discussed for Von Kármán beam element in section 5.2, the curvature χ is linear with respect to the displacements, hence we only consider the in-plane strain $\boldsymbol{\epsilon}$ which contains some nonlinear terms. The in-plane strain $\boldsymbol{\epsilon}$ is divided into two parts which are the linear and nonlinear parts, respectively, expressed in the following form:

$$\boldsymbol{\epsilon} = \boldsymbol{\epsilon}_l + \boldsymbol{\epsilon}_{nl} = \left(\mathsf{B}_l + \frac{1}{2}\mathsf{B}_{nl}(\mathbf{q})\right)\mathbf{q} = \mathsf{B}_l\mathbf{q} + \frac{1}{2}\mathbf{q}^t\mathsf{S}\mathbf{q} \tag{5.30}$$

where the matrix B_l can be referred to [7], $\boldsymbol{\epsilon}_{nl}$, $\mathsf{B}_{nl}(\mathbf{q})$ and S are calculated by the matrices K_{xx}, K_{yy} and K_{xy} again which are listed in reference [7], as follows:

$$\boldsymbol{\epsilon}_{nl}(\mathbf{q}, \mathbf{q}) = \left\{ \begin{array}{c} \mathbf{q}^t\mathsf{K}_{xx}\mathbf{q} \\ \\ \mathbf{q}^t\mathsf{K}_{yy}\mathbf{q} \\ \\ \mathbf{q}^t\mathsf{K}_{xy}\mathbf{q} \end{array} \right\} \tag{5.31}$$

$$\mathsf{B}_{nl}(\mathbf{q}) = \frac{\partial \boldsymbol{\epsilon}_{nl}}{\partial \mathbf{q}} = \left\{ \begin{array}{c} \mathsf{K}_{xx}\mathbf{q} \\ \\ \mathsf{K}_{yy}\mathbf{q} \\ \\ \mathsf{K}_{xy}\mathbf{q} \end{array} \right\} \tag{5.32}$$

$$\mathsf{S} = \frac{\partial^2 \boldsymbol{\epsilon}_{nl}}{\partial \mathbf{q}^2} = \left\{ \begin{array}{l} \mathsf{S}(1,:,:) = \mathsf{K}_{xx} \\ \\ \mathsf{S}(2,:,:) = \mathsf{K}_{yy} \\ \\ \mathsf{S}(3,:,:) = \mathsf{K}_{xy} \end{array} \right\} \tag{5.33}$$

where S is a $3 \times 3 \times 3$ matrix, and $\mathsf{S}(a,:,:)$ indicates the a-th 2D matrix in S.

Then, the in-plane resultant $\mathbf{N}$ is:

$$\mathbf{N} = \mathsf{A}_m \left(\mathsf{B}_l + \frac{1}{2} \mathsf{B}_{nl}(\mathbf{q}) \right) \mathbf{q} \tag{5.34}$$

where A_m is the in-plane part of the material matrix.

From Eq. (5.34), the nonlinear part $\mathbf{N}_{nl}$ of the in-plane stress is given by:

$$\mathbf{N}_{nl} = \frac{1}{2} \mathsf{A}_m \mathsf{B}_{nl} \mathbf{q} \tag{5.35}$$

5.3.2 Equilibrium equations in a third order form

According to the strain in Eq. (5.30), the in-plane strain energy can be calculated by:

$$U_{in-plane} = \frac{1}{2} \mathcal{A} A_{m_{\alpha\beta}} \left(\epsilon_{l_\alpha} + \epsilon_{nl_\alpha} \right) \left(\epsilon_{l_\beta} + \epsilon_{nl_\beta} \right) \tag{5.36}$$

where the subscripts $\alpha, \beta = 1, 2, 3$ denote the addresses of components in the tensor, and the summation convention is applied, $\mathcal{A}$ is the element area.

The nonlinear part of the in-plane strain energy (5.36), which contributes to the quadratic and cubic forms in the equilibrium equations (2.8), is expressed by U:

$$U = \frac{1}{2} \mathcal{A} A_{m_{\alpha\beta}} \left(2 \epsilon_{l_\alpha} \epsilon_{nl_\beta} + \epsilon_{nl_\alpha} \epsilon_{nl_\beta} \right) \tag{5.37}$$

In the rest of this section, we only consider the nonlinear part of the strain energy (5.37), since the linear part does not contribute to the high order differentiations. As

presented for the Von Kármán beam element in section 5.2, the components of the internal load vector $\mathbf{f}$, tangent stiffness matrix L, three-dimensional matrix Q and four-dimensional matrix C in the equilibrium equations (2.8) for the shell element are all achieved by differentiating the strain energy (5.37) to the fourth order. Firstly, the components of the $\mathbf{f}$ and L are listed:

$$f_i = \frac{\partial U}{\partial q_i} = \frac{1}{2}\mathcal{A}A_{m_{\alpha\beta}} \begin{pmatrix} 2\dfrac{\partial \epsilon_{l_\alpha}}{\partial q_i}\epsilon_{nl_\beta} + 2\dfrac{\partial \epsilon_{nl_\beta}}{\partial q_i}\epsilon_{l_\alpha} \\ + \dfrac{\partial \epsilon_{nl_\alpha}}{\partial q_i}\epsilon_{nl_\beta} + \dfrac{\partial \epsilon_{nl_\beta}}{\partial q_i}\epsilon_{nl_\alpha} \end{pmatrix} \tag{5.38}$$

$$L_{ij} = \frac{\partial^2 U}{\partial q_i \partial q_j} = \frac{1}{2}\mathcal{A}A_{m_{\alpha\beta}} \begin{pmatrix} 2\dfrac{\partial \epsilon_{l_\alpha}}{\partial q_i}\dfrac{\partial \epsilon_{nl_\beta}}{\partial q_j} + 2\dfrac{\partial \epsilon_{l_\alpha}}{\partial q_j}\dfrac{\partial \epsilon_{nl_\beta}}{\partial q_i} + 2\dfrac{\partial^2 \epsilon_{nl_\beta}}{\partial q_i \partial q_j}\epsilon_{l_\alpha} \\ +2\dfrac{\partial^2 \epsilon_{nl_\alpha}}{\partial q_i \partial q_j}\epsilon_{nl_\beta} + \dfrac{\partial \epsilon_{nl_\alpha}}{\partial q_i}\dfrac{\partial \epsilon_{nl_\beta}}{\partial q_j} \end{pmatrix} \tag{5.39}$$

where the subscripts i and j run from 1 to 18, and the summation convention is applied on α and β.

Substituting Eqs. (5.30) $\sim$ (5.33) into Eq. (5.38) and Eq. (5.39), and together with Eq. (5.34) and Eq. (5.35), the vector $\mathbf{f}$ and the matrix L can be calculated by a compact notation, as follows:

$$\mathbf{f} = \mathcal{A}\left(\mathsf{B}_l^t \mathbf{N}_{nl} + 2\mathsf{B}_{nl}^t \mathbf{N}\right) \tag{5.40}$$

$$\mathsf{L} = \mathcal{A}\left\{\left(\mathsf{B}_l^t \mathsf{B}_{nl} + \mathsf{B}_{nl}^t \mathsf{B}_l + \mathsf{B}_{nl}^t \mathsf{B}_{nl}\right) + \left(N_x \mathsf{K}_{xx} + N_y \mathsf{K}_{yy} + N_{xy}\mathsf{K}_{xy}\right)\right\} \tag{5.41}$$

where N_x, N_y and N_{xy} are the three components of the stress vector $\mathbf{N}$.

As mentioned in subsection 5.2.2, we only need to calculate the expressions of $\mathcal{Q}(\widetilde{\mathbf{q}})$, $\mathcal{Q}(\mathbf{u}_\alpha, \mathbf{u}_\beta)$ and $\mathcal{C}(\mathbf{u}_\alpha, \mathbf{u}_\beta, \mathbf{u}_\gamma, \mathbf{u}_\delta)$ for the quadratic form $\mathcal{Q}$ and cubic form $\mathcal{C}$. These three terms are achieved as follows:

- The expression of $\mathcal{Q}$ can be easily obtained by differentiating the strain energy (5.37) to a third order with respect to the degrees of freedom. Multiplying the tensor Q by a displacement vector $\widetilde{\mathbf{q}}$, $\mathcal{Q}(\widetilde{\mathbf{q}})$ is achieved and its expression

is very complicated. Hence, some notations are introduced to simplify this expression.

According to Eq. (5.32), the $\mathsf{B}_{nl}(\widetilde{\mathbf{q}})$ related to the displacement $\widetilde{\mathbf{q}}$ is given as:

$$\mathsf{B}_{nl}(\widetilde{\mathbf{q}}) = \frac{\partial \boldsymbol{\epsilon}_{nl}}{\partial \widetilde{\mathbf{q}}} = \left\{ \begin{array}{c} \mathsf{K}_{xx}\widetilde{\mathbf{q}} \\ \mathsf{K}_{yy}\widetilde{\mathbf{q}} \\ \mathsf{K}_{xy}\widetilde{\mathbf{q}} \end{array} \right\} \tag{5.42}$$

In Eq. (5.34), we assume a total matrix B related to the degrees of freedom $\mathbf{q}$ to be:

$$\mathsf{B}(\mathbf{q}) = \mathsf{B}_l + \frac{1}{2}\mathsf{B}_{nl}(\mathbf{q}) \tag{5.43}$$

Then, the stress $\overline{\mathbf{N}}(\widetilde{\mathbf{q}})$ related to the displacement $\widetilde{\mathbf{q}}$ results in:

$$\overline{\mathbf{N}}(\widetilde{\mathbf{q}}) = \mathsf{A}_m\mathsf{B}(\mathbf{q})\widetilde{\mathbf{q}} \tag{5.44}$$

Based on these notations (5.42) $\sim$ (5.44), $\mathcal{Q}(\widetilde{\mathbf{q}})$ can be rewritten to be a compact form:

$$\mathcal{Q}(\widetilde{\mathbf{q}}) = \frac{1}{2}\mathcal{A}\left\{ \begin{array}{l} \left(\mathsf{B}^t_{nl}(\widetilde{\mathbf{q}})\mathsf{A}_m\mathsf{B}(\mathbf{q}) + \mathsf{B}^t(\mathbf{q})\mathsf{A}_m\mathsf{B}_{nl}(\widetilde{\mathbf{q}})\right) \\ + \left(\overline{N}_x\mathsf{K}_{xx} + \overline{N}_y\mathsf{K}_{yy} + \overline{N}_{xy}\mathsf{K}_{xy}\right) \end{array} \right\} \tag{5.45}$$

where $\overline{N}_x$, $\overline{N}_y$ and $\overline{N}_{xy}$ are the three components of the stress vector $\overline{\mathbf{N}}(\widetilde{\mathbf{q}})$.

- Another notation is introduced for calculating $\mathcal{Q}(\mathbf{u}_\alpha, \mathbf{u}_\beta)$, as given by:

$$\overline{\overline{\mathbf{N}}}(\mathbf{u}_\alpha, \mathbf{u}_\beta) = \mathsf{A}_m\mathsf{B}(\mathbf{u}_\alpha)\mathbf{u}_\beta \tag{5.46}$$

where the stress $\overline{\overline{\mathbf{N}}}$ is related to the first order displacements, $\mathbf{u}_\alpha$ and $\mathbf{u}_\beta$.

Then, in a similar way, $\mathcal{Q}(\mathbf{u}_\alpha, \mathbf{u}_\beta)$ is expressed by:

$$\mathcal{Q}(\mathbf{u}_\alpha, \mathbf{u}_\beta) = \frac{1}{2}\mathcal{A}\left(\mathsf{B}^t_{nl}(\mathbf{u}_\beta)\overline{\mathbf{N}}(\mathbf{u}_\alpha) + \mathsf{B}^t_{nl}(\mathbf{u}_\alpha)\overline{\mathbf{N}}(\mathbf{u}_\beta) + \mathsf{B}^t\overline{\overline{\mathbf{N}}}(\mathbf{u}_\alpha, \mathbf{u}_\beta)\right) \tag{5.47}$$

- $\mathcal{C}(\mathbf{u}_\alpha, \mathbf{u}_\beta, \mathbf{u}_\gamma, \mathbf{u}_\delta)$ is achieved in the same manner, as given by:

$$\mathcal{C}(\mathbf{u}_\alpha, \mathbf{u}_\beta, \mathbf{u}_\gamma, \mathbf{u}_\delta) = \frac{1}{6}\mathcal{A}\left\{\begin{array}{l}\overline{\overline{N}}(\mathbf{u}_\alpha, \mathbf{u}_\delta)\mathbf{m}(\mathbf{u}_\beta, \mathbf{u}_\gamma) + \overline{\overline{N}}(\mathbf{u}_\beta, \mathbf{u}_\delta)\mathbf{m}(\mathbf{u}_\alpha, \mathbf{u}_\gamma) \\ + \overline{\overline{N}}(\mathbf{u}_\gamma, \mathbf{u}_\delta)\mathbf{m}(\mathbf{u}_\alpha, \mathbf{u}_\beta)\end{array}\right\} \tag{5.48}$$

where:

$$\mathbf{m}(\mathbf{u}_\alpha, \mathbf{u}_\beta) = \mathsf{B}_{nl}(\mathbf{u}_\alpha)\mathbf{u}_\beta \tag{5.49}$$

Up to this point, the $\mathcal{L}$, $\mathcal{Q}$ and $\mathcal{C}$ in the equilibrium equations (2.8) of a Von Kármán shell element are all achieved.

5.3.3 Assembling into a quadrilateral element

We need to assemble a four-node quadrilateral element using the triangular elements mentioned in this section. There are in total five terms, $\mathbf{f}$, L, $\mathcal{Q}(\tilde{\mathbf{q}})$, $\mathcal{Q}(\mathbf{u}_\alpha, \mathbf{u}_\beta)$ and $\mathcal{C}(\mathbf{u}_\alpha, \mathbf{u}_\beta, \mathbf{u}_\gamma, \mathbf{u}_\delta)$, generated from the triangular element and needed to assemble into a quadrilateral element. Due to the existence of quadratic and cubic forms of the equilibrium equations, the assembly technique presented for the co-rotational shell element in appendix A is inconvenient and too expensive to use. Hence, another assembly technique for the Von Kármán shell element is introduced here.

As shown in Fig. 5.3, there are two ways to divide a four-node quadrilateral element into two triangular elements. One is to use the main diagonal, and one is to use the secondary diagonal. In this way, four triangular elements are obtained, and a four-node quadrilateral element can be assembled by dividing the summation of these four triangular elements by two. Taking the tangent stiffness matrix L as an example, the final stiffness L_{quad} for a quadrilateral element is achieved by:

$$\mathsf{L}_{quad} = \frac{(\mathsf{L}_{123} + \mathsf{L}_{134} + \mathsf{L}_{124} + \mathsf{L}_{234})}{2} \tag{5.50}$$

where L_{abc}, $a, b, c = 1, 2, 3, 4$, is the tangent stiffness matrix of each triangular element (ijk).

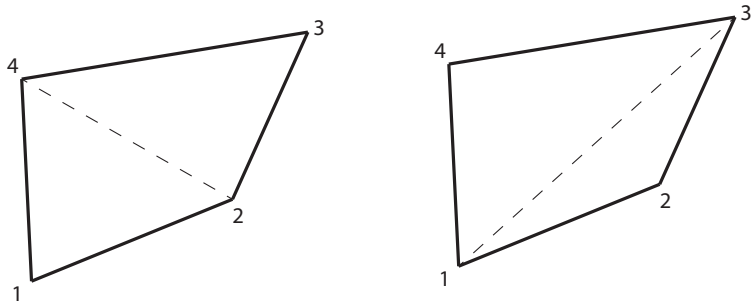

Figure 5.3: Quadrilateral element assembled by triangular elements

5.4 Numerical results

The accuracy of the Koiter-Newton approach using Von Kármán kinematics is assessed here using some numerical examples. First, some examples which were analyzed using co-rotational kinematics and discussed in chapters 3 and 4 are recalculated. Then, the Koiter-Newton analysis using Von Kármán kinematics are applied on some more complex structures where a very fine mesh is needed. The results are compared with those produced using Koiter-Newton analysis based on co-rotational kinematics and also with the results produced using ABAQUS, with the same number of elements and nodes.

5.4.1 Some examples analyzed in chapters 3 and 4

The accuracy of the Koiter-Newton analysis using Von Kármán beam kinematics is evaluated firstly. The Beam (c) in the nonlinear beam example 3.4.2 is reanalyzed here. The response curve obtained by one expansion step on the undeformed state is plotted in Fig. 5.4, and also compared with the curve obtained using ABAQUS. It demonstrates that the accuracy of the Von Kármán beam kinematics satisfies the demand.

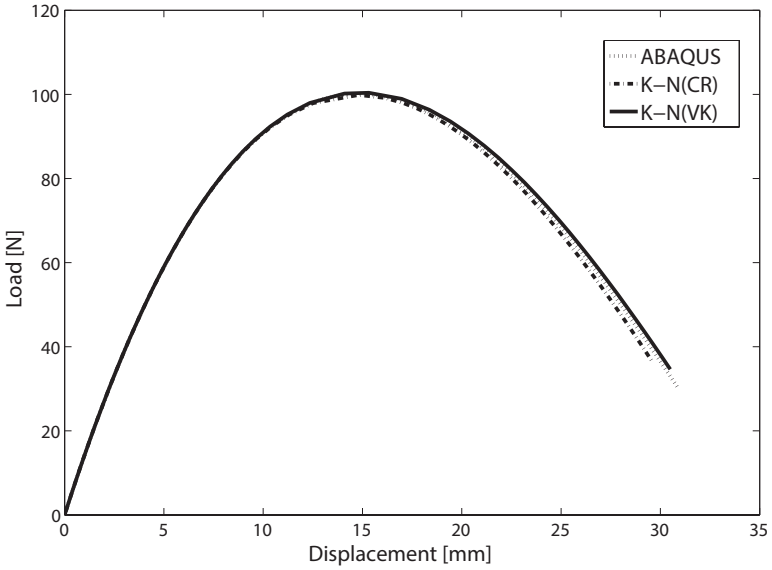

Figure 5.4: Koiter-Newton analysis of the nonlinear beam (c) using Von Kármán and co-rotational kinematical model

Then, the cylindrical shell, shallow arch and cylindrical panel, which were analyzed in examples 4.6.2, 4.6.3 and 4.6.4, respectively, are used here to evaluate the performance of the Koiter-Newton analysis using Von Kármán shell kinematics.

The response curves are shown in Figs. 5.5 $\sim$ 5.7. The results obtained using ABAQUS are plotted using black solid line. These three examples respectively adopt 3, 3 and 2 expansion steps using the Koiter-Newton approach to trace the nonlinear equilibrium path: for each expansion step, the dotted curve is obtained using the co-rotational kinematics, and the solid curve is achieved using the Von Kármán kinematics. It can be seen that the Von Kármán kinematics performs very well in the Koiter-Newton approach.

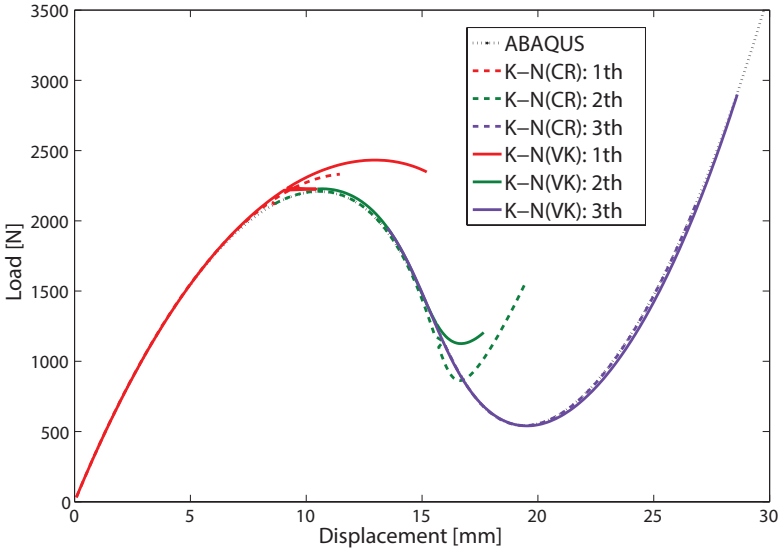

Figure 5.5: Koiter-Newton analysis of the cylindrical shell using Von Kármán and co-rotational kinematical model

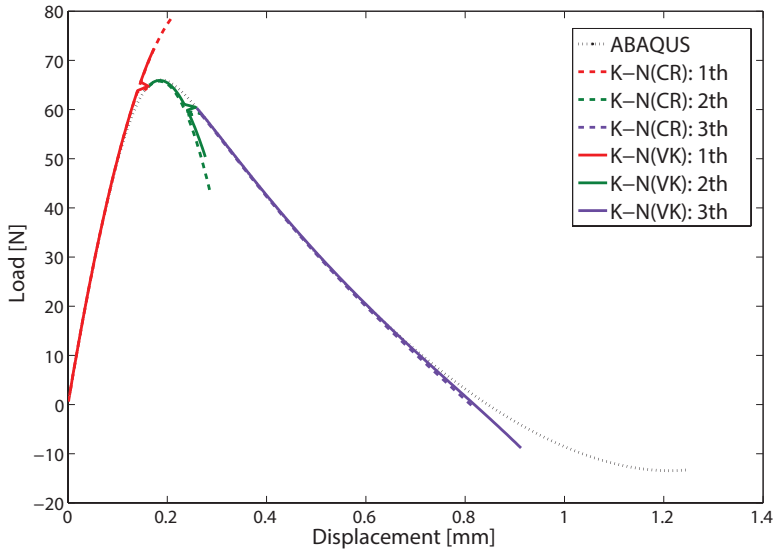

Figure 5.6: Koiter-Newton analysis of the shallow arch using Von Kármán and co-rotational kinematical model

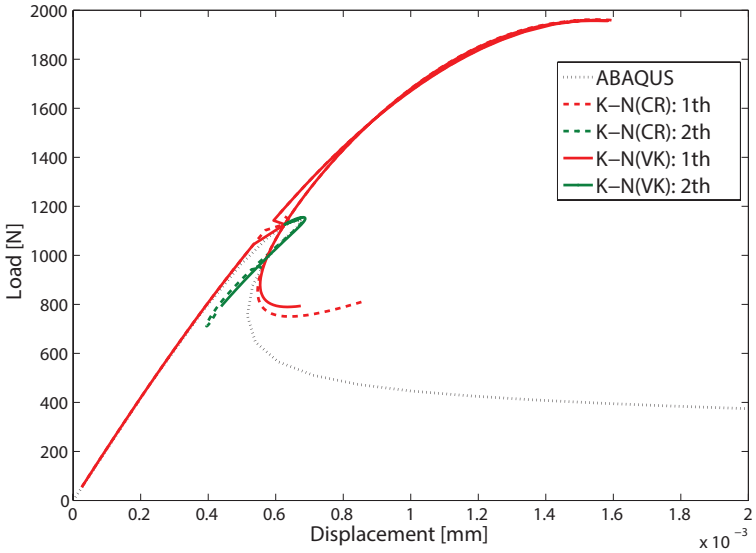

Figure 5.7: Koiter-Newton analysis of the cylindrical panel using Von Kármán and co-rotational kinematical model

5.4.2 Roorda frame

The accuracy of the proposed approach using the Von Kármán kinematics is demonstrated via a popular benchmark of the Roorda's frame. This frame was originally called the Roorda-Koiter frames in 1956 [128, 98]. In this example, the two bars are replaced by two plates with the same geometry, length $L = 20$, width $b = 10$ and thickness $t = 0.3$, as shown in Fig. 5.8. The following material properties are considered: $E = 4.444 \times 10^6$, $\nu = 0.0$, where $\nu = 0.0$ is used to avoid parasitic stress near the constrained nodes. The load, in the x direction, is distributed on the line connecting the two plates such that the total load is $\mathbf{P} = 1.0$, and the two short edges are simply supported. The Roorda frame is meshed with 1600 shell elements.

First, a linear buckling analysis is done, and the first buckling load is 3473 which is identical to the result 3473.6 obtained using ABAQUS. The first buckling mode is compared with that from ABAQUS in Fig. 5.9. Since the first buckling load is separated from the others, only the first buckling mode is used to construct the reduced order model. A small distributed imperfection load $\Delta\mathbf{P}$ is considered on the frame, as shown in Fig. 5.8. Hence, there are in total 3 degrees of freedom in the reduced order model. During generation of the reduced order model, the first order

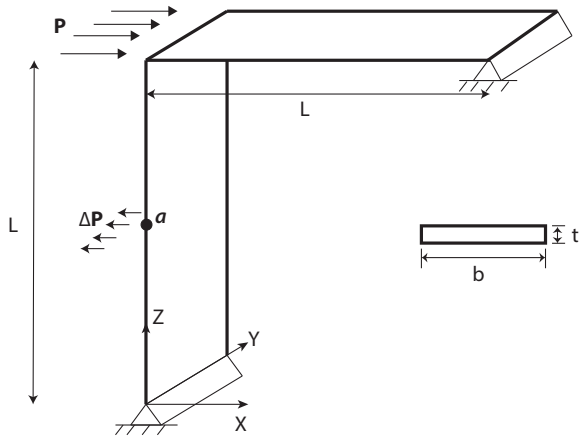

Figure 5.8: Roorda frame

displacement fields are obtained as shown in Fig. 5.10. It can be seen that $\mathbf{u}_1$ and $\mathbf{u}_2$ indicate the deformations of the frame caused by the load $\mathbf{P}$ and the imperfection load $\Delta\mathbf{P}$, respectively, and $\mathbf{u}_3$ is very similar to the first buckling mode.

The nonlinear analysis of the Roorda frame with the imperfection load $\Delta\mathbf{P} = 0.001$ is executed using the Koiter-Newton approach. One expansion step is applied on the undeformed state of the frame, and the displacement of point a, in the x direction, is plotted with the load in Fig. 5.11. The figure demonstrates that the Koiter-Newton approach can capture the buckling branch as accurately as that of ABAQUS analysis.

The Koiter-Newton approach uses 1 step to solve 1 linear FEM system to obtained the response curve in Fig. 5.11, while ABAQUS adopts 102 steps to solve 195 FEM systems. The comparison of the computational time involved in the Koiter-Newton approach and the full nonlinear analysis (ABAQUS) are summarized in Table 5.4.2. The remarkable computer time savings possible with the proposed Koiter-Newton approach are evident.

(a) ABAQUS (b) Koiter-Newton

Figure 5.9: Comparison of the first buckling mode of the Roorda frame

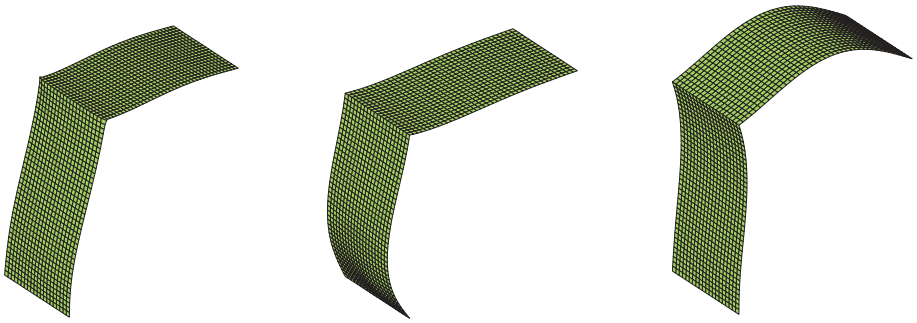

(a) $\mathbf{u}_1$ (b) $\mathbf{u}_2$ (c) $\mathbf{u}_3$

Figure 5.10: The first order displacement fields of the Roorda frame

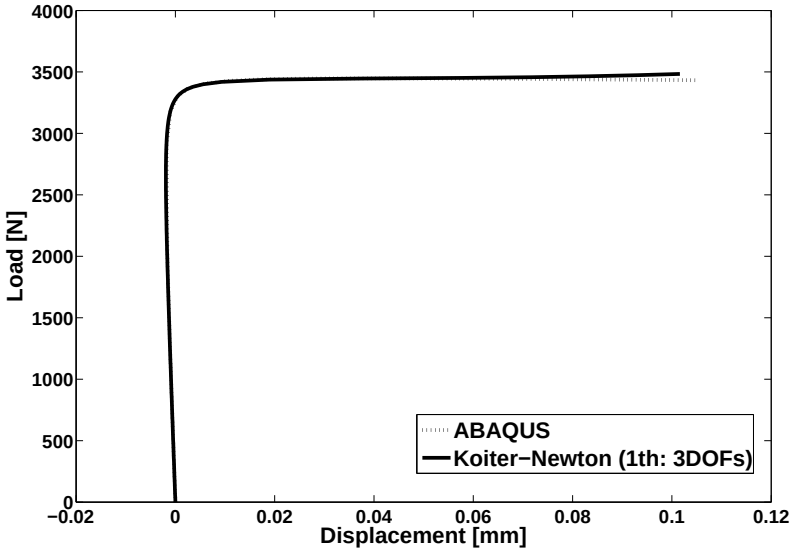

Figure 5.11: Response curves of the Roorda frame with imperfections

Table 5.1: Comparison of computational times of the Roorda frame

	Koiter-Newton approach	Full nonlinear
Linear buckling analysis	3.1278	N.A.
Construction of the ROM	5.1843	N.A.
Simulation of the ROM/full FEM model	0.0241	54.8
Total time (sec)	8.3362	54.8

5.4.3 C shaped beam

As discussed in Zagari's thesis [98], the cantilever C-shaped beam is a difficult test because it involves folding plate, interaction modes and serious nonlinear prebuckling behaviour [129, 130]. The geometry and boundary conditions of the C shaped beam are shown in Fig. 5.12. The thickness of the plate is 0.05. The elastic material properties are $E = 1 \times 10^7$ and $\nu = 0.333$. The plate is meshed with 1440 shell elements.

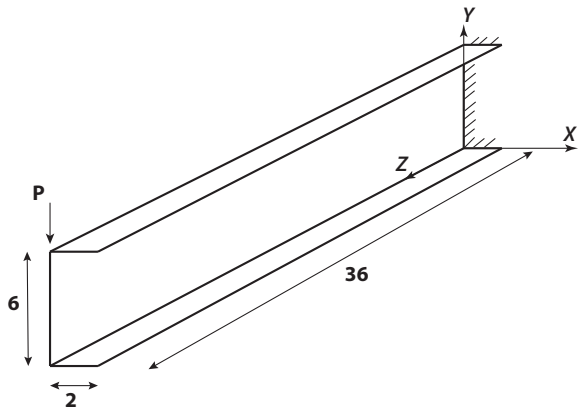

Figure 5.12: C shaped beam

The first four buckling loads are close, and the corresponding closely-spaced modes are given in Fig. 5.13. The first order displacement fields, $\mathbf{u}_1$ and $\mathbf{u}_2$, are shown in Fig. 5.14. Due to the significant prebuckling deformation, 7 expansion steps are used from the undeformed state to obtain the complete response of the structure satisfactorily up to the maximum load carrying capability. The final response curve obtained using these 7 steps are compared with the results produced by using ABAQUS in Fig. 5.15. One more expansion step is carried out on the unstable equilibrium path. To trace to the same equilibrium point on the postbuckling path, the Koiter-Newton approach uses 8 steps to solve 15 linear FEM systems, while ABAQUS uses 173 steps to solve 302 linear FEM systems.

(a) Buckling mode 1

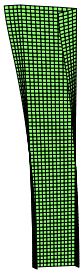

(b) Buckling mode 2

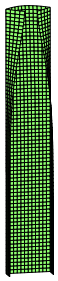

(c) Buckling mode 3

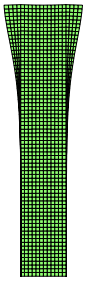

(d) Buckling mode 4

Figure 5.13: The first four buckling modes of the C shaped beam

(a) $\mathbf{u}_1$ (b) $\mathbf{u}_2$

Figure 5.14: The first order displacement fields of the C shaped beam

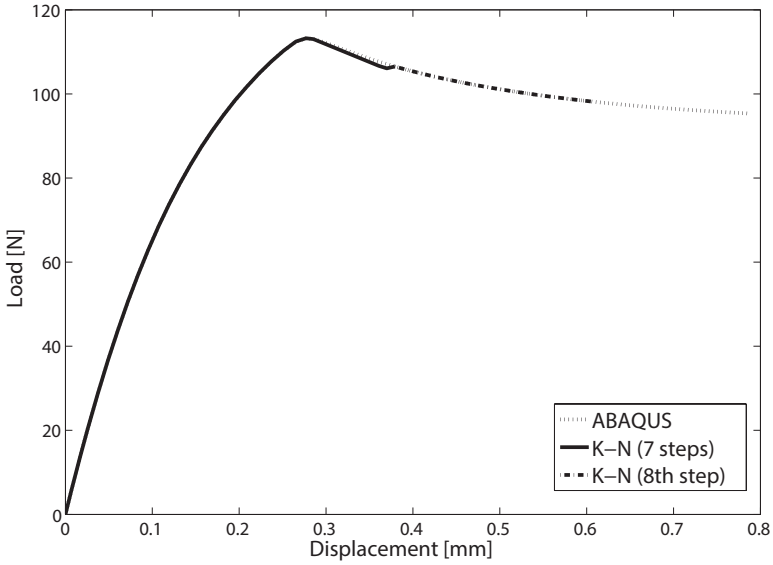

Figure 5.15: Response curves of the C shaped beam

5.4.4 Composite cylinder

In this example, a composite cylinder ($Z15$) shown in Fig. 5.16 and used by Degenhardt [2] is considered.

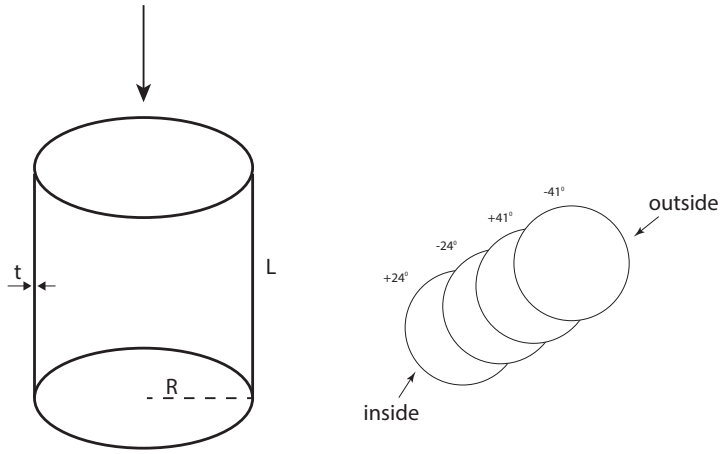

Figure 5.16: The composite cylinder

The basic information about this cylinder is presented below.

- Length L is 500mm, radius R is 250mm, thickness t is 0.5mm.
- The material properties of the ply are given in Table. 5.4.4.
- Non-symmetric laminates: $[24^o, -24^o, 41^o, -41^o]$.
- Loadings: uniform axial compression on the top.
- Constraints: all of the DOFs on both ends are fixed, excepting the axial DOF on the top.

The analysis is done using the following steps:

1. A convergence study is done for the composite cylinder.
2. An imperfection analysis is applied using the Koiter-Newton approach.

Table 5.2: Material properties of each ply of the composite cylinder

$E_{11}\ [N/mm^2]$	157362
$E_{22}\ [N/mm^2]$	10092
$G_{12}\ [N/mm^2]$	5321
ν_{11}	0.277
$\rho\ [Kg/mm^3]$	1600

Convergence study

The FE convergence of the Von Kármán kinematics is checked firstly to find a proper mesh density for the cylinder. The linear end shortening on the top and the first linear bifurcation load are used in the convergence study. The results for different element sizes are compared with those produced by ABAQUS, see Figs. 5.17 and 5.18. These two figures demonstrate that the linear end shortening and the first bifurcation load are converged when the element size is smaller than 15mm, which indicates that at least 3570 elements are needed in this cylinder. A comparison of the first buckling mode is shown in Fig. 5.19 for the Koiter-Newton approach and ABAQUS results. The first buckling mode possesses 14 full waves along the circumference, and 2 half waves along the axis.

Imperfection analysis

We then use the proposed Koiter-Newton approach to expand, once only, on the undeformed configuration of the cylinder to construct the reduced order model for the imperfection analysis. The details are as follows:

- The first 14 bifurcation loads are very close. To consider the iterations among these modes, all of these 14 closely-spaced buckling modes are considered for constructing the reduced order model.
- One lateral imperfection load (1N) is applied in the middle (1/2L) of the cylinder surface.
- There are in total 16 DOFs in the reduced order model. The first DOF is related to the primary path, the second DOF to the imperfection load, and the others are related to the 14 closely-spaced buckling modes.

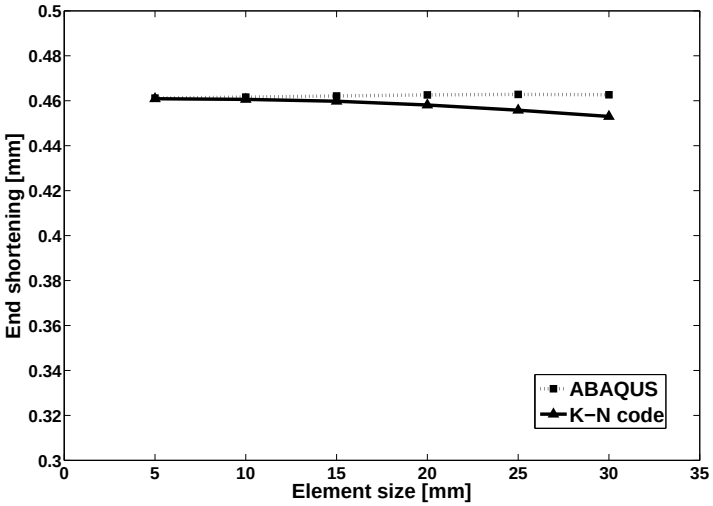

Figure 5.17: The convergence study of the end shortening of the composite cylinder

- To consider the different values of the imperfection load, we only need to change the imperfection load parameter, from 0 for the perfect structure to be any value for the imperfect structure, in the right hand side of the ROM and the ROM does not need to be reconstructed.

The nonlinear response curves are plotted in Fig. 5.20 for different values of the imperfection loads applied on the cylinder. The values of the limit loads for different imperfection loads are picked up from the curves in Fig. 5.20, and are plotted as the knock-down factor curve. In Fig. 5.21, this knock-down factor curve is compared with that obtained using ABAQUS for the same cylinder. When the imperfection load is not very large, smaller than 2.5N, the values of buckling loads match very well with the results produced using ABAQUS, while the error becomes large in the descent range of the knock-down factor curve and seems to be small again when the imperfection load is large enough. Fig. 5.21 demonstrates that the reduced order model constructed on the underformed configuration is only accurate within a certain value of the imperfection load, but it can still give us a good tendency of the buckling performance of a cylinder with different imperfections. More accurate results may be obtained by updating the reduced order model.

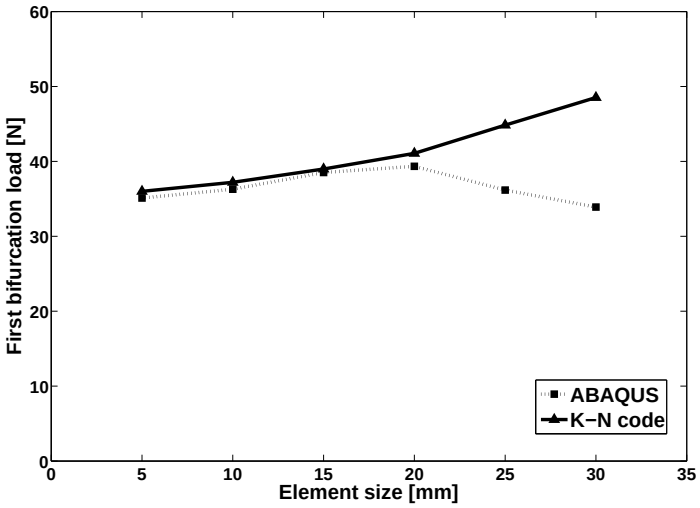

Figure 5.18: The convergence study of the first bifurcation load of the composite cylinder

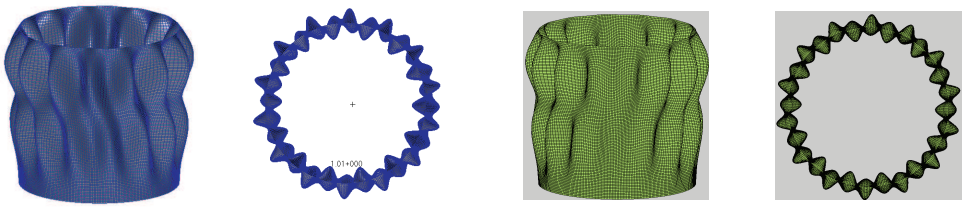

(a) ABAQUS (b) Koiter-Newton approach

Figure 5.19: Comparison of the first buckling mode of the composite cylinder

The computational cost of the imperfection analyses using the Koiter-Newton approach is compared with results obtained using ABAQUS. To obtain the response curves shown in Fig. 5.20, ABAQUS needs to recalculate the entire FEM model 9 times and each time it needs to solve approximate 136 FEM linear systems, that is ABAQUS needs to solve in total 136 $\times$ 9 FEM linear systems. However, since the reduced order model does not need to be reconstructed for different imperfection loads, the Koiter-Newton approach only needs to solve 1 linear FEM system to construct the reduced order model once for the perfect cylinder. This demonstrates again that the Koiter-Newton approach is more computational efficient if used for imperfection analyses.

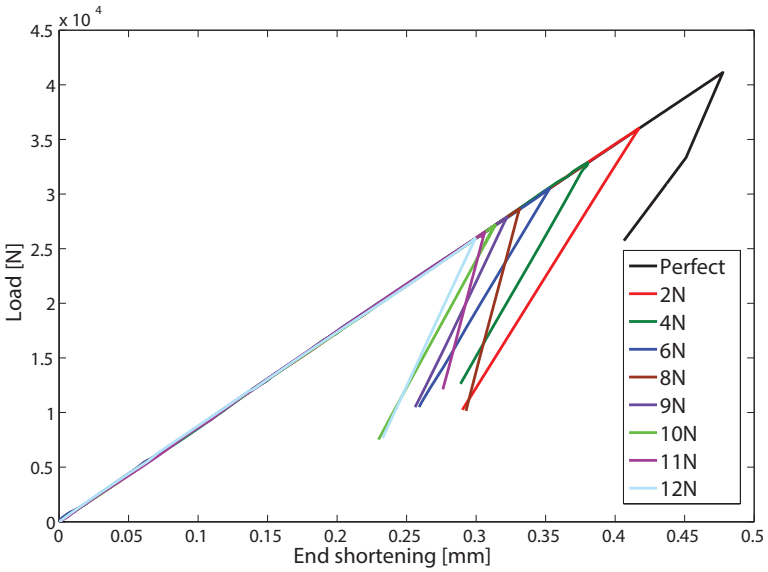

Figure 5.20: Response curves of the composite cylinder for different imperfection loads

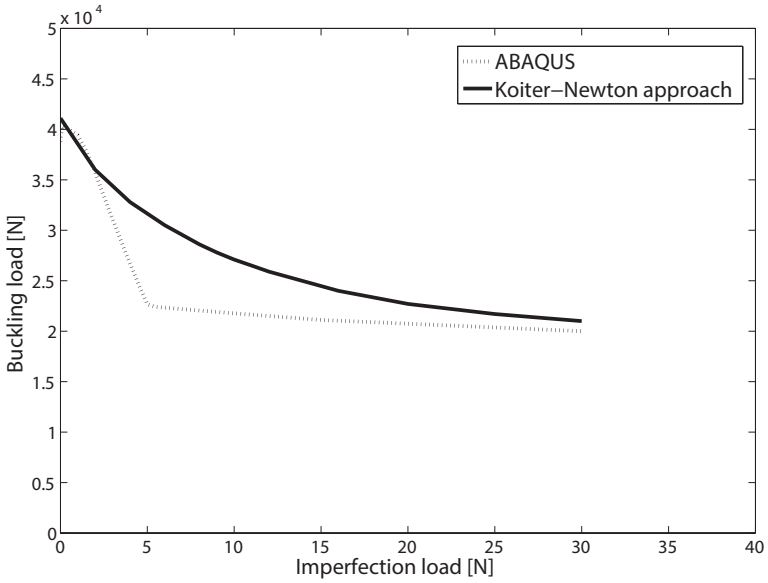

Figure 5.21: The knock-down factor curves of the composite cylinder

5.5 Conclusions

In this chapter, the Koiter-Newton approach was implemented into the beam and shell elements based on the Von Kármán kinematics which do not consider the full nonlinearities in the kinematical model. Differentiations of the strain energy to the fourth order with respect to the degrees of freedom is much easier and faster using Von Kármán kinematics. Some numerical results were used to evaluate the performance of the Koiter-Newton analysis using Von Kármán kinematics. The Koiter-Newton analysis using Von Kármán kinematics is accurate over the entire nonlinear equilibrium path and also efficient in the presence of buckling, however, at less computational cost.

Chapter 6

Concluding remarks

The nonlinear finite element method is the most frequently-used tool for the analysis of nonlinear response of structures. In spite of improvements in modern computers, a full model nonlinear analysis can still be a computationally expensive task, especially in design optimization. The present research dealt with a finite element based perturbation method, the Koiter-Newton approach, for the geometrically nonlinear analysis of structures. This new approach combines ideas from Koiter's initial post-buckling analysis and Newton arc-length methods to trace the entire nonlinear equilibrium path effectively using the reduced order model while retaining a good accuracy of the solution by the corrections.

The thesis is organized as follows. The background, motivation and literature review are introduced in chapter 1. The new proposed Koiter-Newton approach is presented in detail in chapter 2. The Koiter-Newton analyses using co-rotational beam and shell kinematics are given in chapters 3 and 4. Then, the Koiter-Newton analysis is also achieved using Von Kármán kinematics in chapter 5. Finally, some concluding remarks are discussed in the rest of this chapter.

6.1 Conclusions

The Koiter-Newton approach based on Koiter's initial post-buckling theory and Newton arc-length methods are proposed for a class of elastic nonlinear structural

analysis. In this approach Koiter's asymptotic expansion can be applied from the beginning, rather than only once at the bifurcation point, by the consideration of the primary equilibrium path in the displacement expansion. In the case of buckling and/or imperfection sensitivity, this approach also works very well due to its use of Koiter's theory. (in chapter 2)

The Koiter-Newton approach can trace the entire nonlinear equilibrium path automatically in a step by step manner using an idea taken from Newton arc-length methods. In each expansion step, a reduced order model is constructed at a known expansion equilibrium point. Then a path-following technique is adopted to simulate the ROM, and the solution is used as an initial prediction of the response of the structure. At the same time, the quality of the ROM is assessed based on the norm of the force residuals obtained using the full finite element model. If the residual exceeds the accuracy tolerance, it demonstrates that the current ROM has already lost accuracy and then the residual force can be driven to zero using the traditional Newton iterations in a corrector step. Up to this point, a whole step in the Koiter-Newton approach is finished. In the next step an updated ROM can be reconstructed at this corrected equilibrium point to reflect changes in structural stiffness. (in chapter 2)

In the presence of buckling, multiple secondary equilibrium branches may intersect with the primary path near the bifurcation points. Hence, the selection of the perturbation loads which should excite the secondary branches is very important in the Koiter-Newton approach. If the expansion point is on the stable part of the equilibrium path, an eigenvalue problem based on the tangent stiffness K_t and the geometric stiffness K_g is solved to obtain the buckling modes which can be used to construct the perturbation loads. This eigenvalue problem is unsolvable once the expansion point is on the unstable path, due to the non-positive definition of the tangent stiffness K_t. In this case, in order to capture buckling branches accurately, both the modes which are already unstable and the buckling modes which are prone to further instability must be included in the calculation to obtain the perturbation loads. An eigenvalue problem based on the material stiffness and the stress stiffness can be adopted to obtain the already unstable modes. For the buckling prone modes the eigenvalue problem, based on the tangent stiffness and the geometric stiffness required to make it, is restricted to stable modes rendering it solvable. After obtaining all the necessary modes, Koiter's asymptotic expansion can be carried out at any point to trace the entire nonlinear equilibrium path automatically, including the unstable equilibrium path. (in chapter 2)

The Koiter-Newton approach significantly improves the efficiency of nonlinear static finite element analysis. In each step, we only need to factor the augmented FE stiffness matrix once to construct the reduced order model, and do several Newton

iterations in the full finite element model to correct the results. The fairly large step sizes are possible because of the better nonlinear prediction provided by the ROM compared to linear predictors used in Newton arc-length methods. (in chapter 2)

The proposed technique is based on Koiter's theory and requires up to the third order derivatives of the element load vectors with respect to degrees of freedom which is two orders more than the first order what is traditionally needed for Newton's method. To facilitate differentiation and also consider the full nonlinear kinematics, nonlinear elements based on the element independent co-rotational frame are applied. The implementation of the Koiter-Newton approach into the co-rotational (CR) beam kinematics is first presented. Then, the Koiter-Newton analysis is extended with the co-rotational shell kinematics in greater detail. During the FE implementation, the finite rotation theory is used and the descriptions of the proposed three configurations are introduced. The material coordinate system is also defined for the composite shell. The automatic differentiation is adopted to find the derivatives of the co-rotational frame with respect to element degrees of freedom in Matlab codes. (in chapters 3 and 4)

Von Kármán kinematics, which ignore some nonlinear terms in the Green's stain-displacement relations, do not consider the full nonlinear kinematics. In the cases where the nonlinear in-plane rotations of the structure can be neglected while the rotations of the normals to the mid-surface are finitely large, Von Kármán kinematics are a good choice for the FE implementation due to the higher efficiency and acceptable accuracy. Hence, the Koiter-Newton approach is also implemented in the beam and shell elements based on Von Kármán kinematics, and the equilibrium equations of a third order form for Von Kármán kinematics are achieved. (in chapter 5)

Various numerical examples of beam and shell models are presented and used to evaluate the performance of the Koiter-Newton approach. The results are compared with results for the same problem obtained using ABAQUS based on a full nonlinear analysis, and some conclusions about the application of this new proposed approach are summarized as follows: (in chapter 3, 4 and 5)

- If the prebuckling nonlinearity or load distribution is mild, a single step is enough to obtain the complete response of the structure satisfactorily up to the maximum load carrying capability, either by buckling or a limit point instability. While more steps are needed for structures that show significant prebuckling deformation.
- The unstable equilibrium path can be obtained using the expansion steps on the unstable equilibrium points. The use of the already unstable modes and

the buckling prone modes to construct the reduced oder model is feasible and efficient. In this way, the Koiter-Newton approach can trace the entire nonlinear equilibrium path of structures.

- For the cases where one or more bifurcation points lie before the limit point, the traditional nonlinear path-following analysis (ABAQUS) usually misses these bifurcation points and overestimates the load carrying capability of a structure. While, the Koiter-Newton approach can capture these possible bifurcation branches at much less computational costs, using an eigenvalue check for the tangent matrix of the reduced order model.
- The Koiter-Newton analysis using Von Kármán kinematics shows nearly the same accuracy compared with that of co-rotational kinematics in some examples. The efficiency advantages of using Von Kármán kinematics is much more obvious for structures which need a very fine mesh.
- The number of the FEM systems of equations that need to be solved using the Koiter-Newton approach is compared with the number required using ABAQUS, with the same number of elements and nodes. To reach the same equilibrium point on the nonlinear equilibrium path, the Koiter-Newton approach is much computationally cheaper than ABAQUS as it requires fewer matrix factorizations and it uses a larger step size. In the imperfection analysis, the Koiter-Newton approach requires only a small fraction of the first analysis time, since the reduced order model does not need to be reconstructed for a different imperfection. The advantage of the proposed approach on the computational cost is much more obvious in imperfection analyses of a structure.

6.2 Recommendations

The following recommendations for future work are proposed.

1. In the current research, we only considered the geometric nonlinearity, in reality, the material may be in the plasticity range when the deformation is very large. Hence, material nonlinearity should also be taken into account in the Koiter-Newton approach for the buckling analysis.
2. We use the initial deformations caused by independent imperfection loads to model the geometric imperfections in the present work. Actually, the realistic geometric imperfections obtained by measurements can also be implemented into the proposed approach. In the reduced order model, the effect of geometric

imperfections is represented as a *load* term in the right hand side of the reduced order model. Hence, for different imperfections the reduced order model needs not be reconstructed, and the high computational efficiency in imperfection analyses also exists with the consideration of geometric imperfections.

3. The norm flow algorithm is used in the present work to simulate the nonlinear reduced order model. However, the path-following techniques which are based on the Newton arc-length method will meet difficulties in the case when there are lots of closely-spaced buckling modes around the first buckling load. The reduced order model constructed in the proposed Koiter-Newton approach is actually a system of polynomial equations, hence we can try to use the polynomial solver which is very numerically stable to obtain all the roots of the reduced order model and then plot the equilibrium path according to these points.

4. Parallel computation can be introduced into the Koiter-Newton approach to improve the efficiency of the algorithm. For example, we can divide the cylinder into 3 or 4 parts to construct the reduced order model of each part simultaneously, and then assemble them to get a total reduced order model for a whole cylinder. This may further improve the computational efficiency of the Koiter-Newton approach.

Appendix

Appendix A

Linear shell element in a co-rotational frame

In a co-rotational frame, any type of linear shell elements can be used, since the geometric nonlinearity is taken into account by the derivatives of the local co-rotational frame with respect to the global degrees of freedom. For the shell element, we adopt the four-node quadrilateral element obtained by assembling four triangular flat elements and merging the middle node. In this appendix, an introduction of the triangular flat element is presented, and then the construction of the four-node quadrilateral element is introduced.

Triangular flat shell element with the drilling DOF

A triangular three-node flat shell element with six degrees of freedom per node (three translations and three rotations) is presented in this section. This element has been implemented by Tiso and Tanvir [7, 8] in the Matlab environment to achieve Koiter's reduction methods, hence we will simply review the basics of this element following Tiso's thesis in this section.

This element seems to be the combination of a membrane element and a bending element. Figure A.1 shows the combination of the degrees of freedom for the membrane and bending part. The drilling degree of freedom θ_z is also introduced in

Appendix A

Figure A.1.

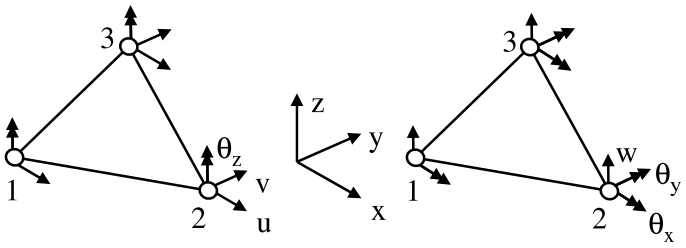

Figure A.1: The combination of the membrane (left) and bending (right) degrees of freedom in the triangle shell element [7]

In the present work, this element was extended for composite material and implemented in Matlab environment. For composite material the element material stiffness matrix K_M is given by [8]:

$$\mathsf{K}_M = \begin{bmatrix} \mathsf{K}_m & \mathsf{K}_{mb} \\ \mathsf{K}_{bm} & \mathsf{K}_b \end{bmatrix} \tag{A.1}$$

where the submatrices K_m, K_b, K_{mb}, and K_{bm} indicate the membrane, bending, membrane-bending and bending-membrane parts of element stiffness matrix respectively.

According to Tiso [7], the calculation of the linear part of the triangular element are repeated as follows.

We can assume the element degrees of freedom to be three parts:

$$\mathbf{q} = \begin{Bmatrix} \mathbf{q}_1 & \mathbf{q}_2 & \mathbf{q}_3 \end{Bmatrix}^t \tag{A.2}$$

where the degrees of freedom for each node can be written as:

$$\mathbf{q}_i = \begin{Bmatrix} u_i & v_i & w_i & \theta_{x_i} & \theta_{y_i} & \theta_{z_i} \end{Bmatrix}, \quad i = 1, 2, 3 \tag{A.3}$$

The following geometric quantities associated to the local vertex coordinates (x_1, y_1), (x_2, y_2), (x_3, y_3) are defined:

$$\begin{array}{rcll} x_{ij} & = & x_i - x_j & \\ y_{ij} & = & y_i - y_j & i, j = 1, 2, 3 \end{array} \tag{A.4}$$

According to the geometric quantities, the element area A can be calculated as:

$$A = \frac{y_{21}x_{13} - x_{21}y_{13}}{2} \tag{A.5}$$

A triangular coordinate system $(\zeta_1, \zeta_2, \zeta_3)$ is used, where the following relation holds:

$$\zeta_1 + \zeta_2 + \zeta_3 = 1 \tag{A.6}$$

The isoparametric coordinates can be linked to the cartesian coordinates through the following transformation, given by:

$$\begin{Bmatrix} 1 \\ x \\ y \end{Bmatrix} = \begin{bmatrix} 1 & 1 & 1 \\ x_1 & x_2 & x_3 \\ y_1 & y_2 & y_3 \end{bmatrix} \begin{Bmatrix} \zeta_1 \\ \zeta_2 \\ \zeta_3 \end{Bmatrix} \tag{A.7}$$

From Eq. (A.7) the link between the partial derivatives in the cartesian coordinates and those in the isoparametric coordinates can be obtained as:

$$\begin{bmatrix} \dfrac{\partial}{\partial x} \\ \\ \dfrac{\partial}{\partial y} \end{bmatrix} = \begin{bmatrix} \mathbf{T}_x \\ \\ \mathbf{T}_y \end{bmatrix} \begin{bmatrix} \dfrac{\partial}{\partial \zeta_1} \\ \\ \dfrac{\partial}{\partial \zeta_2} \end{bmatrix} \tag{A.8}$$

where the transform matrix T_x and T_y is defined as follows:

$$\mathbf{T}_x = \frac{1}{2A} \begin{bmatrix} y_{23} & y_{31} & y_{12} \end{bmatrix} \tag{A.9}$$

$$\mathbf{T}_y = \frac{1}{2A} \begin{bmatrix} x_{32} & x_{13} & x_{21} \end{bmatrix} \tag{A.10}$$

The in-plane strain components $\boldsymbol{\varepsilon}$ of the strain model can be expressed as:

$$\boldsymbol{\varepsilon} = \begin{bmatrix} \epsilon_x & \epsilon_y & \epsilon_{xy} \end{bmatrix}^T \tag{A.11}$$

The $\mathbf{B}$ matrix which gives the relationship of the in-plane strain and degrees of freedom is formed according to the formulation by Felippa [131]. The final result is listed here:

$$\mathbf{B} = [\mathbf{B}_1 \;\; \mathbf{B}_2 \;\; \mathbf{B}_3] \tag{A.12}$$

where

$$\mathbf{B}_1 = \begin{bmatrix} y_{23} & 0 & & x_{32} \\ 0 & x_{32} & \begin{bmatrix} \mathbf{0} \end{bmatrix}_{3\times 3} & y_{23} \\ \dfrac{y_{23}\,(y_{13} - y_{21})}{6} & \dfrac{x_{32}\,(x_{31} - x_{12})}{6} & & \dfrac{(x_{31}y_{13} - x_{12}y_{21})}{3} \end{bmatrix} \tag{A.13}$$

$$\mathbf{B}_2 = \begin{bmatrix} y_{31} & 0 & & x_{13} \\ 0 & x_{13} & \left[\,\mathbf{0}\,\right]_{3\times 3} & y_{31} \\ \dfrac{y_{31}\,(y_{21}-y_{32})}{6} & \dfrac{x_{13}\,(x_{12}-x_{23})}{6} & & \dfrac{(x_{12}y_{21}-x_{23}y_{32})}{3} \end{bmatrix} \tag{A.14}$$

$$\mathbf{B}_3 = \begin{bmatrix} y_{12} & 0 & & x_{21} \\ 0 & x_{21} & \left[\,\mathbf{0}\,\right]_{3\times 3} & y_{12} \\ \dfrac{y_{12}\,(y_{32}-y_{13})}{6} & \dfrac{x_{21}\,(x_{23}-x_{31})}{6} & & \dfrac{(x_{23}y_{32}-x_{31}y_{13})}{3} \end{bmatrix} \tag{A.15}$$

The bending part of the element stiffness for the triangular shell element is given in [131].

Assembling into a quadrilateral element

The four-node quadrilateral element is the most commonly used element type in engineering. Actually, one quadrilateral element can be composed of four triangular elements by splitting the quadrilateral using its two diagonals, as shown in Fig. A.2. This method will add an additional middle node which is the cross point of the two diagonals and should be merged.

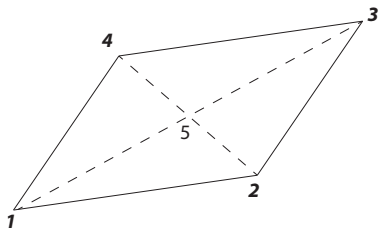

Figure A.2: Quadrilateral element assembled by four triangular elements.

In Fig. A.2 a five-node quadrilateral element $(1-2-3-4)$ with a middle node 5 is assembled using four triangular element $(1-2-5, 2-3-5, 3-4-5, 4-1-5)$.

The 18×18 linear stiffness matrices of these four triangular elements are calculated and then be assembled into a 30×30 total stiffness matrix K. K can be split into four submatrices according to the additional node 5, given by:

$$\mathsf{K} = \begin{bmatrix} \mathsf{K}_{24\times24} & \mathsf{K}_{24\times6} \\ \mathsf{K}_{6\times24} & \mathsf{K}_{6\times6} \end{bmatrix} \tag{A.16}$$

where the submatrices $\mathsf{K}_{24\times24}$ and $\mathsf{K}_{6\times6}$ are relative to nodes $1, 2, 3, 4$ and node 5 respectively, and submatrices $\mathsf{K}_{24\times6}$ and $\mathsf{K}_{6\times24}$ indicate the interaction items.

Then the corresponding equilibrium equations can be written in the form of matrix:

$$\begin{bmatrix} \mathsf{K}_{24\times24} & \mathsf{K}_{24\times6} \\ \mathsf{K}_{6\times24} & \mathsf{K}_{6\times6} \end{bmatrix} \begin{Bmatrix} \mathbf{u} \\ \mathbf{u}_5 \end{Bmatrix} = \begin{Bmatrix} \mathbf{p} \\ \mathbf{p}_5 \end{Bmatrix} \tag{A.17}$$

where the displacement and load consist of two parts, and the part without the subscript is related to the nodes $1, 2, 3, 4$ and the part with the subscript is related to node 5. Our aim is to merge the contribution of the middle node 5 and find out the relation of the displacement $\mathbf{u}$ and load $\mathbf{p}$ which are only related to the four nodes $1, 2, 3, 4$.

Since there is no load applying on the node 5, the fact $\mathbf{p}_5 = \mathbf{0}$ always exists and we can use $\mathbf{u}$ to express $\mathbf{u}_5$ from the second equation of (A.17), leading to:

$$\mathbf{u}_5 = -\frac{\mathsf{K}_{6\times24}\mathbf{u}}{\mathsf{K}_{6\times6}} \tag{A.18}$$

If substituting Eq. (A.18) into the first equation of Eq. (A.17), the relation between $\mathbf{u}$ and $\mathbf{p}$, which is just the stiffness matrix K_{quad} of the four-node quadrilateral element, can be obtained by:

$$\left(\mathsf{K}_{24\times24} - \frac{\mathsf{K}_{24\times6}\mathsf{K}_{6\times24}}{\mathsf{K}_{6\times6}}\right)\mathbf{u} = \mathbf{p} \tag{A.19}$$

where

$$\mathsf{K}_{quad} = \left(\mathsf{K}_{24\times24} - \frac{\mathsf{K}_{24\times6}\mathsf{K}_{6\times24}}{\mathsf{K}_{6\times6}}\right) \tag{A.20}$$

Bibliography

[1] B. Vermeulen and M.J.L. van Tooren. Design case study for a comparative performance analysis of aerospace materials. *Materials Design*, 27(1):10–20, 2006.

[2] R. Degenhardt, A. Kling, A. Bethge, J. Orf, L. Kärger, R. Zimmermann, K. Rohwer, and A. Calvi. Investigations on imperfection sensitivity and deduction of improved knock-down factors for unstiffened cfrp cylindrical shells. *Composite Structures*, 92(8):1939–1946, 2010.

[3] M.W. Hilburger and J.H. Starnes Jr. Buckling behavior of compression-loaded composite cylindrical shells with reinforced cutouts. *International Journal of Non-Linear Mechanics*, 40(7):1005–1021, 2005.

[4] H. Ullah. Buckling of thin-walled cylindrical shells under axial compression. *International Journal for Numerical Methods in Engineering*, 79(11):1332–1353, 2009.

[5] G.A. Maugin and A.V. Metrikine. *Mechanics of Generalized Continua*. Springer, 2010.

[6] C.A. Felippa and K.C. Park. Direct time integration methods in nonlinear structural dynamics. In *International Conference on Finite Elements in Nonlinear Mechanics*, 1978.

[7] P. Tiso. *Finite Element Based Reduction Methods for Static and Dynamic Analysis of Thin-Walled Structures*. PhD thesis, Delft University of Technology, 2006.

[8] T. Rahman. *A Perturbation Approach for Geometrically Nonlinear Structural Analysis Using a General Purpose Finite Element Code*. PhD thesis, Delft University of Technology, 2009.

[9] K. Liang, M. Abdalla, Z. Gürdal, and Q. Sun. A koiter-newton approach for nonlinear structural analysis. In *3rd Aircraft Structural Design conference, Delft, the Netherlands*, 2012.

[10] Valery V. Vasiliev. *Advanced Mechanics of Composite Materials (Second Edition): Chapter 8 - Optimal Composite Structures*. Elsevier Ltd, 2007.

[11] A. Hirahara, R. Hino, F. Yoshida, and V.V. Toropov. Numerical optimization of sheet metal forming process using new fracture criterion. *International Journal of Modern Physics B*, 22:5692–5698, 2008.

[12] H. Saffari, M.J. Fadaee, M. ASCE, and R. Tabatabaei. Nonlinear analysis of space trusses using modified normal flow algorithm. *Journal of Structural Engineering*, 134(6):998–1005, 2008.

[13] E. Ramm. Strategies for tracing the nonlinear response near limit points. In *"Nonlinear finite element analysis in structural mechanics." Proceedings of the Europe - US Workshop, Germany, July 28-31, Springer-Verlag Berlin*, pages 63–89, 1981.

[14] D.A. Pecknold, J. Ghaboussi, and T. J. Healey. snap-through and bifurcation in a simple structure. *Journal of Engineering Mechanics*, 111(7):909–922, 1985.

[15] D.S. Jagannathan, P. Christiano, and H.I. Epstein. Nonlinear analysis of reticulated space trusses. *J. Struct. Div.*, 101(12):2641–2658, 1975.

[16] R. Levy and W.R. Spillers. Analysis of geometrically nonlinear structures. In *Proceedings of the 2nd Ed., Kluwer, Dordrecht, The Netherlands.*, 2003.

[17] M. Papadrakakis. Inelastic post-buckling analysis of trusses. *Journal of Structural Engineering*, 109(9):2129–2147, 1983.

[18] G.E. Blandford. Large deformation analysis of inelastic space truss structures. *Journal of Structural Engineering*, 122(4):407–415, 1996.

[19] S.A. Ragon, Z. Gürdal, and L.T. Watson. A comparison of three algorithms for tracing nonlinear equilibrium paths of structural systems. *International Journal of Solids Structures*, 139:689–698, 2002.

[20] W.E. Haisler and J.A. Stricklin. Development and evaluation of solution procedures for geometrically nonlinear analysis. *AIAA Journal*, 10(3):164–172, 1996.

[21] E. Riks. An incremental approach to the solution of snapping and buckling problems. *International Journal of Solids and Structures*, 15:524–551, 1979.

[22] E. Riks. Buckling analysis of elastic structures: A computational approach. *Advances in Applied Mechanics*, 34:1–76, 1997.

[23] G.A. Wempner. Discrete approximation related to nonlinear theories of solids. *International Journal of Solids and Structures*, 17:1581–1599, 1971.

[24] M.A. Crisfield. A fast incremental/iterative solution procedure that handles snap-through. *Computers & Structures*, 13:55–62, 1981.

[25] B.W.R. Forde and S.F. Stiemer. Improved arc-length orthogonality methods for nonlinear finite element analysis. *Computers & Structures*, 27(5):625–630, 1987.

[26] S.N. Al-Rasby. Solution techniques in nonlinear structural analysis. *Computers & Structures*, 40(4):985–993, 1991.

[27] M. Bashir-Ahmad and S. Xiao-zu. Arc-length technique for nonlinear finite element analysis. *J. Zhejiang Univ.*, 5(5):618–628, 2004.

[28] K. Georg. Numerical integration of the davidenko equation. In *Lecture Notes in Math. Springer, Berlin*, 1981.

[29] L.T. Watson, M. Sosonkina, R.C. Melville, A.P. Morgan, and H.F. Walker. Algorithm 777: Hompack90: A suite of fortran 90 codes for globally convergent homotopy algorithms. *ACM Transactions on Mathematical Software*, 23(4):514–549, 1997.

[30] I. Fried. Orthogonal trajectory accession to the nonlinear equilibrium curve. *Computer Methods in Applied Mechanics and Engineering*, 47:283–298, 1984.

[31] L.T. Watson, S.C. Billups, and A.P. Morgan. Algorithm 652: Hompack: A suite of codes for globally convergent homotopy algorithms. *ACM Transactions on Mathematical Software*, 13(3):281–310, 1987.

[32] J.F. Besseling. Nonlinear analysis of structures by the finite element method as a supplement to a linear analysis. *Comp. Meth. Appl. Mech. Engng*, 3(2):173–194, 1974.

[33] B.O. Almroth, P. Stern, and F.A. Brogan. Automatic choice of global shape functions in structural analysis. *AIAA Journal*, 16(5):525–528, 1978.

[34] D.A. Nagy. Modal representation of geometrically nonlinear behavior by the finite element method. *Composite Structures*, 10(4):683–688, 1979.

[35] A.K. Noor and J.M. Peters. Reduced basis technique for nonlinear analysis of structures. *AIAA Journal*, 18:455–462, 1980.

[36] A.K. Noor, C.M. Andersen, and J.M. Peters. Global-local approach for nonlinear shell analysis. In *Proc. 7th ASCE Conf. on Electronic Computation, Washington University, St. Louis, Missouri, August 6-8*, pages 634–657, 1979.

[37] A.K. Noor. Recent advances in reduction methods for nonlinear problems. *Computers & Structures*, 13(1-3):31–44, 19801.

[38] D.A. Nagy and M. Konig. Geometrically nonlinear finite element behaviour using buckling mode superposition. *Computer Methods in Applied Mechanics and Engineering*, 19:447–484, 1979.

[39] B.O. Almroth, P. Stern, and F-A. Brogan. Automatic choice of globai shape functions in structural analysis. *AIAA Journal*, 16(5):525–528, 1978.

[40] A.S.L. Chan and KM. Hsiao. Nonlinear analysis using a reduced number of variables. *Computer Methods in Applied Mechanics and Engineering*, 52:899–913, 1985.

[41] B. Cochelin. A path-following technique via an asymptotic-numerical method. *Computers & Structures*, 53(5):1181–1192, 1994.

[42] B. Cochelin, N. Damil, and M. Potier-Ferry. Asymptotic-numerical methods and padé approximants for non-linear elastic structures. *International Journal for Numerical Methods in Engineering*, 37:1187–1213, 1994.

[43] W.T. Koiter. *On the stability of the elastic equilibrium*. PhD thesis, Delft University of Technology, 1945.

[44] J.M.T. Thompson and A.C. Walker. The nonlinear perturbation analysis of discrete structural systems. *International Journal of Solids and Structures*, 4:151–168, 1968.

[45] R.H. Gallagher. Perburbation procedures in nonlinear finite element structural analysis. In *Conf on Comp. Method in Nonlinear Mech., Austin, Texas*, pages 634–657, 1974.

[46] E. Riks. Some computational aspect of the stability analysis of nonlinear structures. *Computer Methods in Applied Mechanics and Engineering*, 47:219–259, 1984.

[47] M. Jamal, H. Elasmar, and B. Braikat. Bifurcation indicators. *Acta Mechanica*, 139:129–142, 2000.

[48] N. Damil and M. Potier-Ferry. A new method to compute perturbed bifurcations: application to the buckling of imperfect elastic structures. *International Journal of Engineering Science*, 9:943–957, 1990.

[49] B. Cochelin, N. Damil, and M. Potier-Ferry. Asymptotic-numerical methods and padé approximants for nonlinear elastic structures. *International Journal for Numerical Methods in Engineering*, 37(7):1187–1213, 1994.

[50] L. Azrar, B. Cochelin, N. Damil, and M. Potier-Ferry. An asymptoticnumerical method to compute the postbuckling behaviour of elastic plates and shells. *International Journal for Numerical Methods in Engineering*, 36:1251–1277, 1993.

[51] E.H. Boutyour, H. Zahrouni, M. Potier-Ferry, and M. Boudi. Bifurcation points and bifurcated branches by an asymptotic numerical method and padé approximants. *International Journal for Numerical Methods in Engineering*, 60(12):1987–2012, 2004.

[52] S. Lopez. An effective parametrization for asymptotic extrapolations. *Computer Methods in Applied Mechanics and Engineering*, 189(1):297–311, 2000.

[53] H. Mottaqui, B. Braikat, and N. Damil. Discussion about parameterization in the asymptotic numerical method: Application to nonlinear elastic shells. *Computer Methods in Applied Mechanics and Engineering*, 199:1701–1709, 2010.

[54] J.C. Amazigo, B. Budiansky, and G.F. Carrier. Asymptotic analysis of the buckling of imperfect columns on nonlinear elastic foundations. *International Journal of Solids Structures*, 6:1341–1356, 1970.

[55] B. Budiansky. Theory of buckling and postbuckling behavior of elastic structures. *Advances in Applied Mechanics*, 14:1–65, 1974.

[56] G.A. Cohen. Effect of a nonlinear prebuckling state on the postbuckling behavior and imperfection sensitivity of elastic structures. *AIAA Journal*, 6:1616–1619, 1968.

[57] J.R. Fitch. The buckling and postbukling behavior of spherical caps under concentrated loads. *International Journal of Solids and Structures*, 4:421–446, 1968.

[58] N. Rizzi and A. Tatone. Symbolic manipulation in buckling and postbuckling analysis. *Computers & Structures*, 21:691–700, 1985.

[59] D. Hui and I.H.Y. Du. Initial postbuckling behavior of imperfect, antisymmetric crossply cylindrical shells under torsion. *Journal of Applied Mechanics*, 54:174–180, 1987.

[60] J. Arbocz and J.M.A.M. Hol. Koiters stability theory in a computer-aided engineering (cae) environment. *International Journal of Solids Structures*, 26:945–975, 1990.

[61] R.H. Gallagher. Perturbation procedures in nonlinear finite element structural analysis, in computational mechanics. In *Lecture Notes in Mathematics. Vol. 461, Springer Verlag, Berlin*, 1975.

[62] S.S. Antman. Bifurcation problems in non-linearly elastic structures. *Academic Press*, 1977.

[63] U. Eckstein, R.K. Jürcke, and W.B. Krẗzig. Imperfection sensitivity of elastic structures a numerical postbuckling approach. In *In 8th International Conference on Structural Mechanics in Reactor Technology, Brussels, Belgium, August*, pages 634–657, 1985.

[64] C. Pacoste and A. Eriksson. Beam elements in instability problems. *Computer Methods in Applied Mechanics and Engineering*, 144:163–197, 1997.

[65] B. Wu and Z. Wang. A perturbation method for the determination of the buckling strength of imperfection-sensitive structures. *Computer Methods in Applied Mechanics and Engineering*, 145:203–215, 1997.

[66] B. Geier. A method to compute koiters b-factor of anisotropic panels. *International Journal of Non-Linear Mechanics*, 37:699–707, 2002.

[67] G. Garcea, A. Madeo, G. Zagari, and R. Casciaro. Asymptotic postbuckling fem analysis using co-rotational formulation. *International Journal of Solids and Structures*, 46:377–397, 2009.

[68] J.F. Olesen and E. Byskov. Accurate determination of asymptotic postbuckling stresses by the finite element method. *Computers & Structures*, 15:157–163, 1982.

[69] E. Byskov. Smooth postbuckling stresses by a modified finite element method. *International Journal for Numerical Methods in Engineering*, 28:2877–2888, 1989.

[70] P.N. Poulsen and L. Damkilde. Direct determination of asymptotic structural postbuckling behavior by the finite element method. *International Journal for Numerical Methods in Engineering*, 42:685–702, 1998.

[71] R.T. Haftka, R.H. Mallett, and W. Nachbar. Adaption of koiter's method to finite element analysis of snap-through buckling behavior. *International Journal of Solids and Structures*, 7:1427–1445, 1971.

[72] E.G. Carnoy. Asymptotic study of the elastic postbuckling behavior of structures by the finite element method. *Computer Methods in Applied Mechanics and Engineering*, 29:147–173, 1981.

[73] G. Salerno, R. Casciaro, and A.D. Lanzo. Finite element asymptotic analysis of slender elastic structures: A simple approach. *International Journal for Numerical Methods in Engineering*, 35:1397–1426, 1992.

[74] W.T. Koiter and G.D.C. Kuiken. The interaction between local buckling and overall buckling on the behavior of built-up columns. In *Technical Report WTHD-23, Delft University of Technology, Delft, The Netherlands*, 1971.

[75] W.T. Koiter. General theory of mode interaction in stiffened plate and shell structures. In *Technical Report WTHD-91, Delft University of Technology, Delft, The Netherlands*, 1976.

[76] E. Byskov and J.W. Hutchinson. Mode interaction in axially stiffened cylindrical shells. *AIAA Journal*, 15:941–948, 1977.

[77] R. Peek and M. Kheyrkhahan. Postbuckling behavior and imperfection sensitivity of elastic structures by the lyapunov-schmidt-koiter approach. *Computer Methods in Applied Mechanics and Engineering*, 108:261–279, 1993.

[78] G. Salerno and R. Casciaro. Mode jumping and attractive paths in multi-mode elastic buckling. *International Journal for Numerical Methods in Engineering*, 40:833–861, 1997.

[79] A.D. Lanzo and G. Garceai. Koiter's analysis of thin-walled structures by a finite element approach. *International Journal for Numerical Methods in Engineering*, 39:3007–3031, 1996.

[80] G. Garcea, R. Casciaro, G. Attanasio, and F. Giordano. Perturbation approach to elastic post-buckling analysis. *Computers & Structures*, 66:585–595, 1998.

[81] G. Garcea. Mixed formulation in koiter analysis of thin-walled beams. *Computers & Structures*, 190:3369–3399, 2001.

[82] A.D. Lanzo, G. Garcea, and R. Casciaro. Asymptotic post-buckling analysis of rectangular plates by hc finite elements. *International Journal for Numerical Methods in Engineering*, 38:2325–2345, 1995.

[83] M. Aristodemo. A high-continuity finite element method for two-dimensional elastic problems. *Computers & Structures*, 21:987–993, 1985.

[84] D. Ho. Buckling load of non-linear systems with multiple eigenvalues. *International Journal of Solids Structures*, 10:1315–1330, 1974.

[85] W.T. Koiter. Current trend in the theory of buckling. In *In Buckling of structures, Proc. IUTAM Symp., Springer, Berlin*, pages 1–13, 1976.

[86] A. Bilotta, A.D. Lanzo, and R. Casciaro. A finite element model for the koiter nonlinear analysis of composite thin-walled structures. In *In Congress ECCOMAS 2000, Barcellona*, 2000.

[87] G. Garcea, G.A. Trunfio, and R. Casicaro. Path-following analysis of thin-walled structures and comparison with asymptotic post-critical solutions. *International Journal for Numerical Methods in Engineering*, 55:73–100, 2002.

[88] C.M. Menken, G.M.A. Schreppers, W.J. Groot, and R. Petterson. Analyzing buckling mode interactions in elastic structures using an asymptotic approach; theory and experiment. *Computers & Structures*, 64:473–480, 1997.

[89] C.M. Menken, R. Couhia, and W.J. Groot. An investigation into non-linear interaction between buckling modes. *Thin-walled structures*, 19:129–145, 1994.

[90] G.M. van Erp and C.M. Menken. Initial post-buckling analysis with the finitestrip method. *Computers & Structures*, 40(5):1193–1201, 1991.

[91] C.M. Menken and G.M. van Erp. The spline finite-strip method in the buckling analyses of thin walled structures. *Communications in Applied Numerical Methods*, 6:477–484, 1990.

[92] G.M.A. Schreppers and C.M. Menken. Mode-reduction applied to initial post-buckling behavior. In *In DIANA computational mechanics: 1st international conference on computational mechanics, Delft, Netherlands*, pages 287–296, 1994.

[93] M. Kheyrkhahan and R. Peek. Postbuckling analysis and imperfection sensitivity of general shells by the finite element method. *International Journal of Solids and Structures*, 36:2641–2681, 1999.

[94] E. Byskov. Mode interactions in structures - an overview. In *In WCCM VI in conjunction with APCOM, Beijing, China, September*, 2004.

[95] R. Kouhia and M. Mikkola. Tracing the equilibrium path beyond compound critical points. *International Journal for Numerical Methods in Engineering*, 46:1049–1074, 1999.

[96] B.Z. Huang and S.N. Atluri. A simple method to follow post-buckling paths in finite element analysis. *Computers & Structures*, 57:477–489, 1995.

[97] A. Magnusson. Treatment of bifurcation points with asymptotic expansion. *Computers & structures*, 77:475–484, 2000.

[98] G. Zagari. *Koiter's asymptotic numerical methods for shell structures using a corotational formulation*. PhD thesis, Universita Della Calabria, 2009.

[99] C.C. Rankin and B.N. Omid. The use of projectors to improve finite element performance. *Computers & Structures*, 30(1-2):257–267, 1988.

[100] C.C. Rankin, F.A. Brogan, and E. Riks. Some computational tools for the analysis of through cracks in stiffened fuselage shells. *Computational Mechanics*, 13(3):143–156, 1993.

[101] G. Zagari, A. Madeoa, R. Casciaro, S. de Mirandab, and F. Ubertini. Koiter analysis of folded structures using a corotational approach. *International Journal of Solids and Structures*, 50(5):755–765, 2013.

[102] B. Budiansky and J.W. Hutchinson. Dynamic buckling of imperfection sensitive structures. In *In Proceedings of the 11th IUTAM congress, pages 636651.Springer-Verlag, Berlin/Gottingen/Heidelberg/Newyork*, pages 636–651, 1964.

[103] J. Arbocz and J.M.A.M. Hol. Anilisa - computational module for koiters imperfection sensitivity theory. In *Technical Report LR-582, Delft University of Technology*, 1989.

[104] T. Rahman and E.L. Jansen. Finite element based initial post-buckling analysis of shells of revolution. In *In 49th AIAA/ASME/ASCE/AHS/ASC Structures, Structural Dynamics and Materials Conference, Schaumburg, Illinois*, 2008.

[105] T. Rahman and E.L. Jansen. Finite element based multi-mode initial post-buckling analysis of composite cylindrical shells. In *In 50th AIAA/ASME/ASCE/AHS/ASC Structures, Structural Dynamics and Materials Conference*, 2009.

[106] K. Liang, M. Abdalla, and Z. Gürdal. A koiter-newton approach for tracing the entire structural nonlinear equilibrium path. In *International Conference on Computational Mechanics (CM13), Durham, UK*, 2013.

[107] J.G. Teng and Y.F. Lou. Post-collapse bifurcation analysis of shells of revolution by the accumulated arc-length method. *International Journal for Numerical Methods in Engineering*, 40(13):2369–2383, 1997.

[108] K. Liang, M. Abdalla, and Z. Gürdal. Buckling imperfection-sensitivity analysis using a koiter-newton approach. In *In 54th AIAA/ASME/ASCE/AHS/ASC Structures, Structural Dynamics and Materials Conference, Boston, Massachusetts, US*, 2013.

[109] E.L. Allgower and K. Georg. Homotopy methods for approximating several solutions to nonlinear systems of equations. In *Numerical solution of highly*

nonlinear problems, W. Forster, ed., North-Holland, Amsterdam, The Netherlands, pages 253–270, 1980.

[110] Hong Hu Chen, Wen Yi Lin, and Kuo Mo Hsiao. Co-rotational finite element formulation for thin-walled beams with generic open section. *Computer Methods in Applied Mechanics and Engineering*, 195(19-22):2334–2370, 2006.

[111] C.A. Felippa. *Nonlinear Finite Element Methods.* Course materials for the Department of Aerospace Engineering Sciences University of Colorado at Boulder, 1999.

[112] M.A. Crisfield. *Nonlinear Finite Element Analysis of Solids and Structures, Vol. 1.* Wiley, Chichester, 1997.

[113] B. Fraeijs de Veubeke. The dynamics of flexible bodies. *International Journal of Engineering Science*, 14(10):895–913, 1976.

[114] C.A. Felippa and B. Haugen. A unified formulation of small-strain corotational finite elements: I. theory. *Computer Methods in Applied Mechanics and Engineering*, 194(21-24):2285–2335, 2005.

[115] P. Norachan, S. Suthasupradit, and Ki-Du Kim. A co-rotational 8-node degenerated thin-walled element with assumed natural strain and enhanced assumed strain. *Finite Elements in Analysis and Design*, 50:70–85, 2012.

[116] E. Gal, M. Zelkha, and R. Levy. A simple co-rotational geometrically non linear membrane finite element wrinkling analysis. *International Journal of Structural Stability and Dynamics*, 11(1):237–240, 2011.

[117] N.D. Cortivoa, C.A. Felippa, H. Bavestrelloc, and W.T.M. Silva. Plastic buckling and collapse of thin shell structures, using layered plastic modeling and co-rotational andes finite elements. *Computer Methods in Applied Mechanics and Engineering*, 198(5-8):785–798, 2009.

[118] S.C. Chang and J.J. Chen. Effectiveness of linear bifurcation analysis for predicting the nonlinear stability limits of structures. *International Journal for Numerical Methods in Engineering*, 23(5):831–846, 1986.

[119] J. Arbocz, M. Potier-Ferry, J. Singer, and V. Tvergaard. Post-buckling behaviour of structures numerical techniques for more complicated structures. *Buckling and Post-Buckling: Lecture Notes in Physics*, 288:83–142, 1987.

[120] A. Cardona and M. Geradin. An excursion into large rotations. *Computer Methods in Applied Mechanics and Engineering*, 32:85–155, 1982.

[121] A. Ibrahimbegovic, F. Frey, and Kozar. Computational aspects of vector-like parametrization of three-dimensional finite rotations. *International Journal for Numerical Methods in Engineering*, 38(21):3653–3673, 1995.

[122] Ibrahimbegovic. On the choice of finite rotation parameters. *Computer Methods in Applied Mechanics and Engineering*, 149(1-4):49–71, 1997.

[123] M.R. Correa and D. Camotim. On the differentiation of the rodrigues formula and its significance for the vector-like parameterization of reissner-simo beam theory. *International Journal for Numerical Methods in Engineering*, 55(9):1005–1032, 2002.

[124] M.R. Correa and D. Camotim. Work-conjugacy between rotation-dependent moments and finite rotations. *International Journal of Solids and Structures*, 40(11):2851–2873, 2003.

[125] A. Cardona and M. Geradin. Beam finite element non-linear theory with finite rotations. *International Journal for Numerical Methods in Engineering*, 26(11):2403–2438, 1988.

[126] I. Tsukanov and M. Hall. Data structure and algorithms for fast automatic differentiation. *International Journal for Numerical Methods in Engineering*, 56:1949–1792, 2003.

[127] Robert D. Cook, David S. Malkus, Michael E. Plesha, and Robert J. Witt. *Concepts and Applications of Finite Element Analysis, 4th Edition*. Wiley, 2001.

[128] I. Elishakoff, Y.W. Li, and J.H. Starnes Jr. Imperfection sensitivity due to the elastic moduli in the roorda-koiter frame. *Chaos, Solitons Fractals*, 7(8):1179–1186, 1996.

[129] A. Ibrahimbegovic. Stress resultant geometrically nonlinear shell theory with drilling rotations: Part i. a consistent formulation. *Computer Methods in Applied Mechanics and Engineering*, 118(3-4):265–284, 1994.

[130] J. Chroscielewski, J. Makowski, and H. Stumpf. Genuinely resultant shell finite elements accounting for geometric and material non-linearity. *International Journal for Numerical Methods in Engineering*, 35(1):63–94, 1992.

[131] C.A. Felippa. A study of optimal membrane triangles with drilling freedoms. In *Technical Report CU-CAS-03-02, Center for Aerospace Structures - College of Engineering - University of Colorado*, 2003.

Curriculum Vitae

Ke Liang was born on November 3th, 1984 in Luoyang, China. He enrolled in Northwestern Polytechnical University of China after graduating from high school in 2003. His major was aircraft designing and engineering. After obtaining a bachelor's degree with high honors, he was asked to enter the Ph.D program at NPU directly to work with Prof. Qin Sun. In October 2010, he came to the Netherlands to become a Ph.D researcher in the Aerospace Structure group, at the faculty of Aerospace Engineering, Delft University of Technology. Under the guidance of Prof. Zafer Gürdal and Dr. Mostafa Abdalla, he worked on reduction methods for the nonlinear analysis of structures. The results of his Ph.D work are presented in this thesis.